# LABYRINTH SEAL LEAKAGE EQUATION

A Thesis

by

SAIKISHAN SURYANARAYANAN

Submitted to the Office of Graduate Studies of
Texas A&M University
in partial fulfillment of the requirements for the degree of

MASTER OF SCIENCE

May 2009

Major Subject: Mechanical Engineering

# LABYRINTH SEAL LEAKAGE EQUATION

A Thesis

by

SAIKISHAN SURYANARAYANAN

Submitted to the Office of Graduate Studies of
Texas A&M University
in partial fulfillment of the requirements for the degree of

MASTER OF SCIENCE

Approved by

Chair of Committee,    Gerald L. Morrison
Committee Members,    Je C. Han
                       Robert E. Randall
Head of Department,    Dennis O'Neal

May 2009

Major Subject: Mechanical Engineering

# ABSTRACT

Labyrinth Seal Leakage Equation.

(May 2009)

Saikishan Suryanarayanan, B.E., Anna University, India

Chair of Advisory Committee:  Dr. Gerald L. Morrison

A seal is a component used in a turbomachine to reduce internal leakage of the working fluid and to increase the machine's efficiency. The stability of a turbomachine partially depends upon the rotodynamic coefficients of the seal. The integral control volume based rotodynamic coefficient prediction programs are no more accurate than the accuracy of the leakage mass flow rate estimation. Thus an accurate prediction of the mass flow rate through seals is extremely important, especially for rotodynamic analysis of turbomachinery.

For labyrinth seals, which are widely used, the energy dissipation is achieved by a series of constrictions and cavities. When the fluid flows through the constriction (under each tooth), a part of the pressure head is converted into kinetic energy, which is dissipated through small scale turbulence-viscosity interaction in the cavity that follows. Therefore, a leakage flow rate prediction equation can be developed by comparing the seal to a series of orifices and cavities. Using this analogy, the mass flow rate is modeled as a function of the flow coefficient under each tooth and the carry over coefficient, which accounts for the turbulent dissipation of kinetic energy in a cavity.

This work, based upon FLUENT CFD simulations, initially studies the influence of flow parameters, in addition to geometry, on the carry over coefficient of a cavity, developing a better model for the same. It is found that the Reynolds number and clearance to pitch ratios have a major influence and tooth width has a secondary influence on the carry over coefficient and models for the same were developed for a generic rectangular tooth on stator labyrinth seal.

The discharge coefficient of the labyrinth seal tooth (with the preceding cavity) was found to be a function of the discharge coefficient of a single tooth (with no preceding cavity) and the carry over coefficient. The discharge coefficient of a single tooth is established as a function of the Reynolds number and width to clearance ratio of the tooth and a model for the same is developed. It is also verified that this model describes the discharge coefficient of the first tooth in the labyrinth seal. By comparing the coefficients of discharge of compressible flow to that of incompressible flow at the same Reynolds number, the expansion factor was found to depend only upon the pressure ratio and ratio of specific heats. A model for the same was developed. Thus using the developed models, it is possible to compute the leakage mass flow rate as well as the axial distribution of cavity pressure across the seal for known inlet and exit pressures. The model is validated against prior experimental data.

# DEDICATION

*Dedicated to Gayathri, who stimulates my mind to learn, who motivates my spirit to seek the truth and who guides my intellect towards understanding the reality*

# ACKNOWLEDGEMENTS

Firstly I am deeply grateful to my advisor Dr. Gerald Morrison for providing me with the fundamental ideas and inspiration to take up this research. Dr. Morrison has been of great help throughout this thesis. He has provided me with the right inputs at the right times and has been a constant source of motivation. He has not only been a research guide, but also has been my academic advisor and well wisher.

I am also greatly thankful to Dr. Je Han and Dr. Robert Randall for serving on my committee and for their valuable input. I am grateful to all the professors who have taught me for enabling me to gain the necessary knowledge to pursue this research.

I express my sincere gratitude to the Turbomachinery Research Consortium for partially funding this research. I am indeed proud to have been a part of the Turbomachinery Laboratory and would like to extend my warm regards to the faculty, staff and fellow researchers of the Turbolab.

I thank my mom, dad and my uncle Muthukumar for their constant moral support and belief in me. I believe that the blessings of my grandparents, whom I dearly miss, have been a force behind all the success I have had and will have in my life.

Anto John, Satish, Prakash, Hemanth, Sylvia, Varuna and Aarthi, who have been my best friends in College Station, deserve a special mention for the wonderful time I have had with them. I also thank my friends Gurunarayana Ravi and Balaraman Rajan for their support.

I would also like to express my appreciation for the tradition and spirit of Aggieland and to the Aggie family as a whole for making my journey a memorable one.

# NOMENCLATURE

A - Clearance area, $\pi Dc$

c - Radial clearance, m

$C_d^{1tooth}$ - Discharge coefficient for seal with single tooth

$C_d$ - Discharge coefficient for a given tooth of a multi tooth labyrinth seal

D – Shaft diameter, m

h – Tooth height, m

k – Ratio of specific heats , $C_p/C_v$

L - Axial length of the seal, m

$\dot{m}$ - Mass flow rate of leakage flow (kg/s)

$P_i$ – Seal inlet pressure, Pa

$P_e$ - Seal exit pressure, Pa

$p_i$ – Tooth inlet pressure, Pa

$p_e$ - Tooth exit pressure, Pa

Pr – Pressure ratio, $p_e/p_i$

Re – Reynolds number based on clearance, $\dfrac{\dot{m}}{\pi D \mu}$

s - Tooth pitch, m

w - Tooth width, m

x - Axial distance along seal, m

z – Ratio of discharge coefficient of a tooth following a cavity to the discharge coefficient of a single tooth with same tooth width and clearance with no preceding cavity at the same Reynolds number

viii

α - Flow coefficient

β – Divergence angle of jet , radians

γ - Kinetic energy carry over coefficient

ε – Dissipation of turbulent kinetic energy

κ – Turbulent Kinetic energy

μ– Dynamic viscosity, Pa/s

$\rho_i$ – Fluid density at seal inlet, kg/m$^3$

ρ – Fluid density at tooth inlet, kg/m$^3$

χ- Percentage of kinetic energy carried over

ψ - Expansion Factor

# TABLE OF CONTENTS

# LIST OF FIGURES

# LIST OF TABLES

**CHAPTER I**

**INTRODUCTION**

A seal is a component used in a turbomachine to reduce internal leakage of the working fluid and increase the machine's efficiency. The stability of a turbomachine partially depends upon the rotodynamic coefficients of the seal. The integral control volume based rotodynamic coefficient prediction programs are no more accurate than the accuracy of the leakage mass flow rate estimation. Thus an accurate prediction of the mass flow rate through seals is extremely important, especially for rotodynamic analysis of turbomachinery. With recent advancements in turbomachinery increasing the need for more precise rotodynamic analyses, there is a necessity for more accurate prediction of leakage rate.

The labyrinth seal is one of the popular seal designs and is widely used in a variety of turbomachinery. As for any seal, the purpose of the labyrinth seal is to reduce the internal fluid leakage by increasing the friction to fluid flow in the leakage path by dissipating as much of the kinetic energy of the leakage flow as possible. For labyrinth seals, the energy dissipation is achieved by a series of constrictions and cavities. When the fluid flows through the constriction (under each tooth), a part of the pressure head is converted into kinetic energy, which is dissipated through small scale turbulence-viscosity interaction in the cavity that follows. This increases the resistance to flow compared to a smooth seal.

_____

This thesis follows the style of Journal of Turbomachinery.
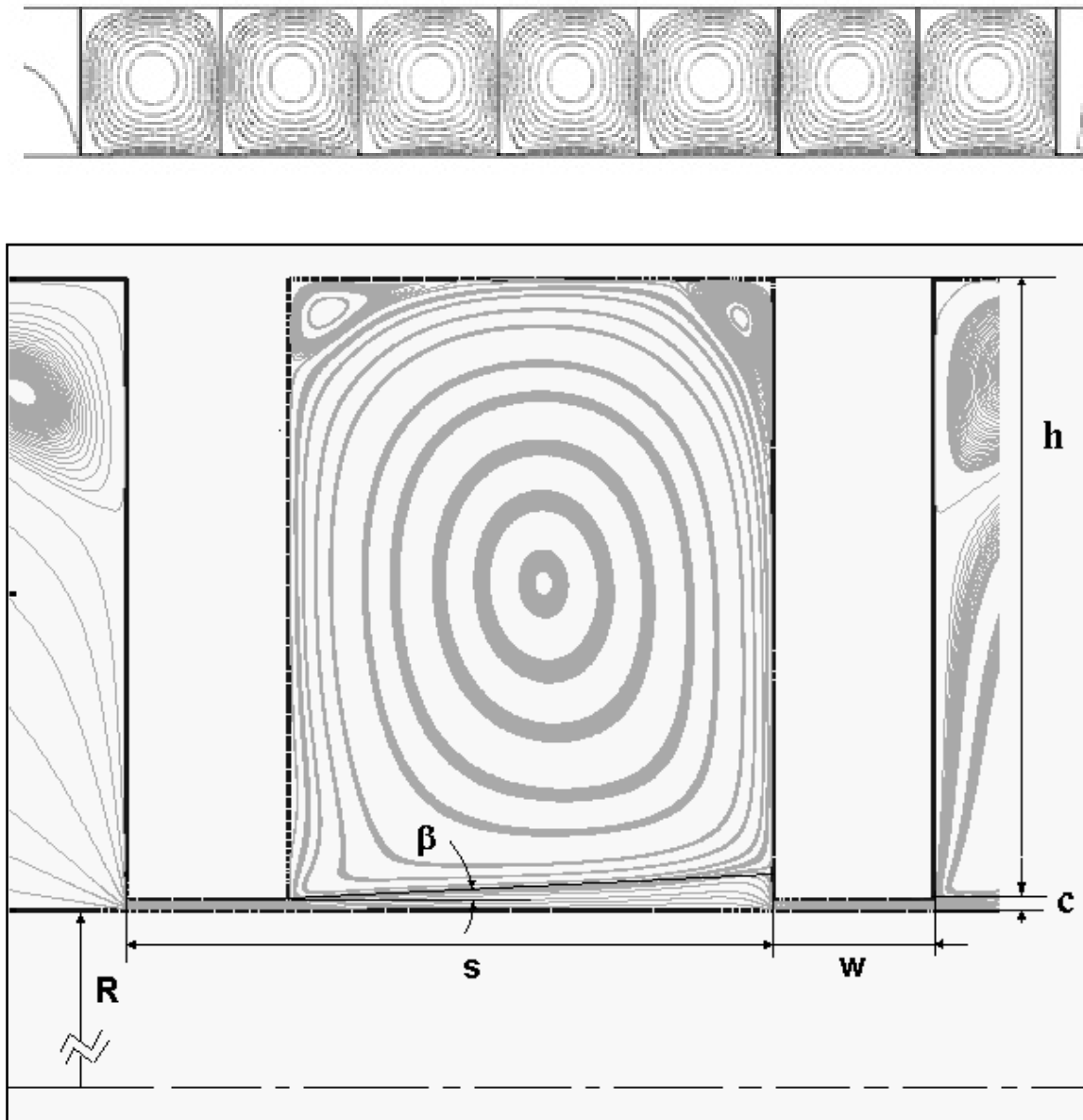
**Figure 1.1.  Flow pattern within a labyrinth seal cavity.**

A straight through labyrinth seal is commonly used for turbines primarily due to ease of manufacture and assembly. This design, however, has a greater kinetic energy carry over compared to stepped or staggered designs. Hence it becomes extremely

important to study the carry over coefficient of straight through labyrinth seals in order to improve the accuracy of leakage prediction.

Figure 1.1. shows the typical flow pattern within a labyrinth seal. It can be observed from the streamlines, a part of the jet goes under the next tooth, while the remaining portion recirculates within the cavity. The portion of the kinetic energy that is not dissipated in the cavity is indicated by the carry over coefficient which can be measured in terms of the angle β .

The carry over coefficient accounts for the turbulent dissipation of kinetic energy occurring inside each individual cavity. The relationship between the carry over coefficient, γ, and the percentage of kinetic energy carried over into the next cavity , $\chi$, is given by

$$\gamma^2 = \frac{1}{1-\chi} \quad [1] \tag{1.1}$$

This relationship is illustrated in Figure 1.2. When $\gamma = 1$ , $= 0$ , indicating that all kinetic energy entering into the cavity is dissipated. The kinetic energy carry over increases with an increase in the carry over coefficient. In other words, a higher value of $\gamma$ indicates that the cavity is less effective in dissipating kinetic energy.
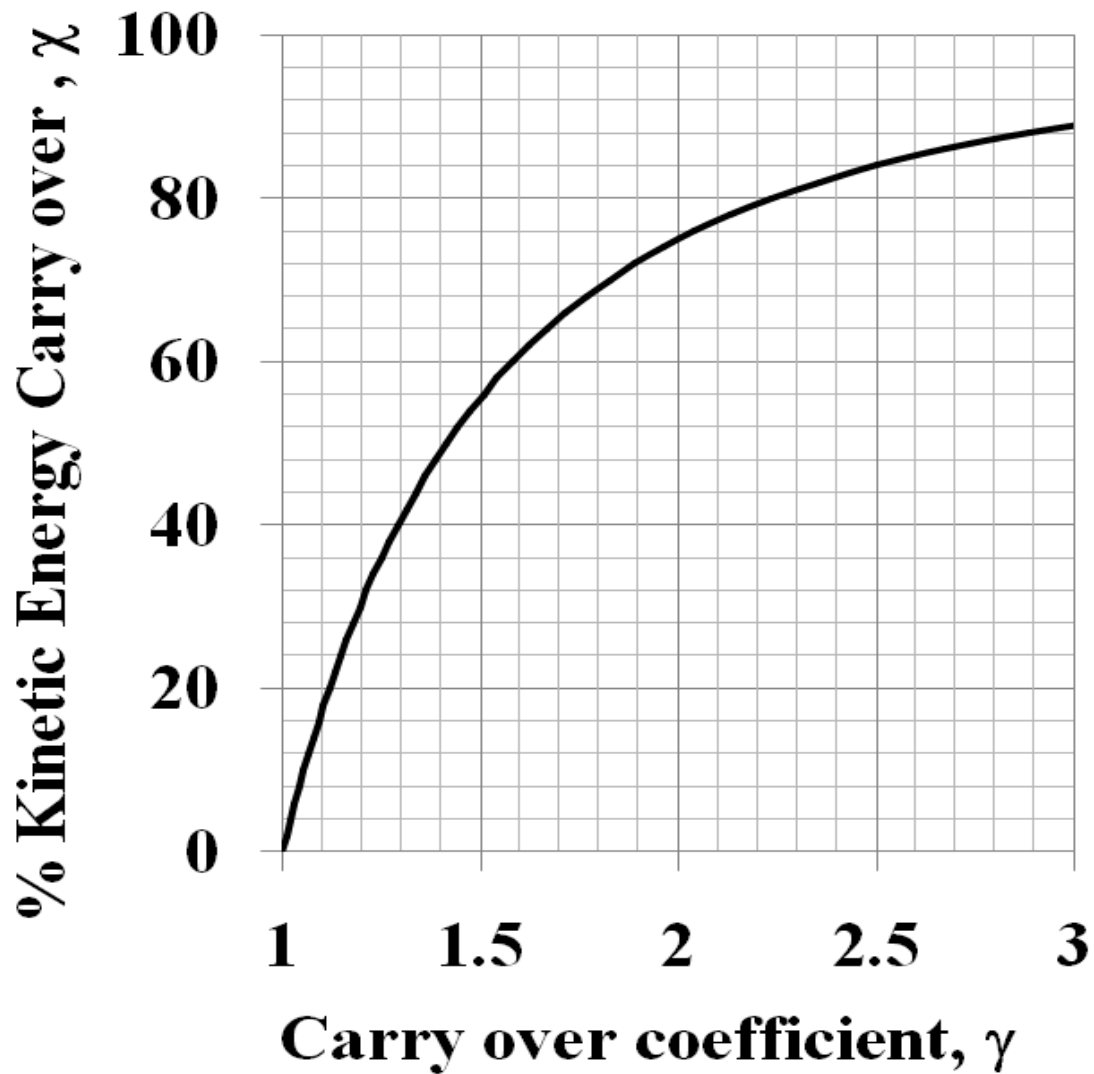
**Figure 1.2. Relationship between $\gamma$ and $\chi$.**

This work, based on FLUENT CFD simulations, attempts to arrive at a more accurate leakage model for labyrinth seals by making extensive study of the parameters affecting the kinetic energy carry over as well as the discharge coefficient.

# CHAPTER II

# PRIOR WORK AND REVIEW OF EXISTING LEAKAGE MODELS

The prior work in labyrinth seals has been discussed in detail by Cogan [2] and Gamal [3]. Gamal's dissertation also provides a detailed discussion on all the existing leakage models and evaluates them against experimental data. Hence only a concise account of the literature pertinent to the present study is presented in this section.

A leakage flow rate prediction equation can be developed by considering the seal as a series of orifices and cavities. The mass flow rate is represented as a function of the discharge coefficient under each tooth and the carry over coefficient inside each cavity.

Labyrinth seal leakage rate prediction equations have been of interest as early as 1908 when Martin [4] presented a model. This simple equation models the leakage flow rate based on the work done to achieve the required pressure drop. He neglected the effect of kinetic energy carry over (assumed $\gamma = 1$). This equation, which is applicable only to incompressible flows, was purely based on an analytical approach and did not compare its results to experimental data. Even though this model, shown in equation 2.1 is not very accurate, it is widely used even today. It also forms the basis for several following models.

$$\dot{m} = \frac{A\,P_i}{\sqrt{RT_i}}\sqrt{\frac{1-\left(\frac{P_e}{P_i}\right)^2}{n-\ln\left(\frac{P_e}{P_i}\right)}} \qquad (2.1)$$

Stoloda [5] was another early researcher of labyrinth seal leakage. He analyzed compressible flow and provided separate equations for subsonic and choked flows. He

mentioned that the mass flow rate is inversely proportional to the square root of the number of teeth. Like Martin, he neglected the effect of kinetic energy carry over.

Gerke [6], in deriving the equation for labyrinth seal leakage, considered the effects of variable areas through the seal. But he also did not consider the kinetic energy carry over.

Egli [7] provided a rational theoretical treatment of the labyrinth problem based on the flow characteristics typical for a sharp edged orifice. He identified the need for a kinetic energy carry-over coefficient His description of the flow through the constrictions of a labyrinth seal "as the steam flows through the labyrinth, a pressure drop occurs across each throttling. After each throttling, a small part of the kinetic energy of the steam jet will be reconverted into pressure energy, a second part will be destroyed and transferred into heat, and the remaining kinetic energy will enter the following throttling". Egli modified the basic equation put forth by Martin by including an experimentally determined flow coefficient to account for the kinetic energy carry over. His model is shown in equation 2.2. Egli also reasoned that the carry over coefficient should increase with increase in clearance and decrease as the axial distance between blades (tooth pitch) increases.

$$\dot{m} = \gamma_{emperical} \frac{A\,P_i}{\sqrt{RT_i}} \sqrt{\frac{1-\left(\frac{P_e}{P_i}\right)^2}{n-\ln\left(\frac{P_e}{P_i}\right)}} \qquad (2.2)$$

Hodkinson [8] modified Egli's approach to provide a semi empirical relation that was based on assumptions of a gas jet's geometry. His assumption was as follows. The

fluid jet expands conically from the tip of an upstream tooth at a small angle, $\beta$. A part of the jet impinges on the downstream tooth to recirculate in the cavity, dissipating the kinetic energy associated with it, while a portion of the jet travels under the downstream tooth and carries over the kinetic energy to the next cavity. He assumed the angle $\beta$ to be only a function of seal geometry.

He presented the following relation for seal leakage

$$\dot{m} = A\, \alpha\, \psi\, \gamma\, \sqrt{\rho_i\, P_i} \tag{2.3}$$

Where the expansion coefficient, which accounts for compressibility effects, is defined as

$$\psi = \sqrt{\frac{1 - \left(\frac{P_e}{P_i}\right)^2}{n - \ln\left(\frac{P_e}{P_i}\right)}} \tag{2.4}$$

The kinetic energy carry over coefficient, $\gamma$, is modeled as a function of seal geometry as

$$\gamma = \sqrt{\frac{1}{1 - \frac{n-1}{n}\frac{\frac{c}{s}}{\frac{c}{s}+0.02}}} \tag{2.5}$$

The last factor, $\alpha$, is an experimentally determined flow coefficient, similar to a discharge coefficient.

Vermes [9] developed an expression for the kinetic energy carry over based upon boundary layer theory to modify Martin's equation which is shown in equation 2.6.

$$\gamma = \sqrt{\frac{1}{1-\alpha}} \tag{2.6}$$

Where, $\alpha$, the relative amount of kinetic energy present upstream of tooth is given by

$$\alpha = \frac{8.52}{\frac{s-w}{c} + 7.23} \qquad (2.7)$$

The model developed by Neumann [10], shown in equations 2.8-2.12 incorporates a carry over coefficient, which is expressed as a function of radial clearance and tooth pitch. He used Chaplygin's formula, as defined by Gurevich [11], as flow coefficient which also accounts for compressibility effects. Neumann treats each throttle individually and hence his model represents leakage as a function of upstream and downstream pressures of a tooth. Therefore, when this model is used, it does not provide the leakage in a single step, but results in a set of N equations which can be solved to obtain both leakage and the pressure distribution.

$$\dot{m} = Cf_i \, \gamma_i \, A \sqrt{\frac{p_i^2 - p_{i+1}^2}{RT}} \qquad (2.8)$$

$$Cf_i = \frac{\pi}{\pi + 2 - 5\beta_i + 2\beta_i^2} \qquad (2.9)$$

$$\beta_i = \left(\frac{p_i}{p_{i+1}}\right)^{\frac{k-1}{k}} - 1 \qquad (2.10)$$

$$\gamma_i = \sqrt{\frac{N}{N\,(1-\alpha_i) + \alpha_i}} \qquad (2.11)$$

$$\alpha_i = 1 - \frac{1}{\left(1 + 16.6\left(\frac{c}{s}\right)\right)^2} \qquad (2.12)$$

Zimmerman and Wolf [12] took into account that the flow through the first tooth is different as there is no kinetic energy carry over. Hence they suggested using

St. Venant's equation [13] for the first constriction and Martin's equation with a carry over coefficient for the downstream teeth. Their model is shown in equation 2.13.

$$\dot{m} = \frac{A\,P_i}{\sqrt{kRT_i}}\sqrt{\frac{2k^2}{k-1}\left(\left(\frac{P_{i+1}}{P_i}\right)^{\frac{2}{k}} - \left(\frac{P_{i+1}}{P_i}\right)^{\frac{k+1}{k}}\right)} \quad \text{for i =1} \qquad (2.13)$$

$$\dot{m} = \gamma_i\,\frac{A\,P_i}{\sqrt{RT_i}}\sqrt{\frac{1-\left(\frac{P_{i+1}}{P_i}\right)^2}{n-\ln\left(\frac{P_{i+1}}{P_i}\right)}} \qquad \text{for i >1}$$

Scharrer's model [14] was based on Neumann's equation but used Vermes' carry over coefficient. Esser and Kazakia [15] also used the Neumann's equation, but used a constant flow coefficient of 0.716 instead of Chaplygin's formula.

Gamal [3] carried out an evaluation of leakage models by comparing the respective leakage predictions to experimental data. His analyses reveal that certain models perform well under high pressure ratios while others are more suited for low pressure labyrinth seals. Gamal also attempted to create hybrid models using different combinations of base equation, model for carry over coefficient and model for flow coefficient found in literature.

The above models have considered the carry over coefficient purely as a function of seal geometry and neglect the possibility of the effect of flow parameters.

From Gamal's analyses, it was observed that the models that perform well under certain flow conditions fail under other flow conditions. This perhaps reveals that the underlying assumption of flow independent carry over coefficient may not be correct. G.L. Morrison and Adnan Al- Ghasem [1] studied the leakage flow through windback seals. Under the suspicion that Hodkinson's model for the carry over coefficient may not

be applicable for windback seals, $\gamma$ was obtained by CFD analysis of the flow pattern within the seal cavity. It was found that $\gamma$ was not a constant for a given seal geometry as proposed by Hodkinson, but varied with pressure ratio. This observation of the flow dependence of $\gamma$ has been the primary motivation for the current study, as it was felt that $\gamma$ might be dependent upon flow parameters for labyrinth seals as well. This is in contrast to the existing models that describe carry over coefficient purely based upon geometric parameters. If the flow dependence of the carry over coefficient can be analyzed and modeled, it will result in significantly improving the accuracy of the leakage flow rate predictions. Ultimately, using an improved seal leakage flow rate prediction equation, designers can improve turbomachinery efficiency and stability.

# CHAPTER III

# RESEARCH OBJECTIVES

The objective of this project is to develop a simple empirical model for the leakage flow rate in straight through annular labyrinth seals with simple rectangular cavities. The model will allow designers of turbomachines to quickly estimate seal leakage allowing more design options to be considered compared to experimental methods or CFD simulations. This objective will be attained by the following:

1. Perform simulations of leakage flow through a labyrinth seal cavity using FLUENT for a matrix of different geometry and flow conditions.

2. Study the flow dependence of the carry over coefficient upon flow conditions and geometry to develop a model for the same.

3. Analyze, at different flow conditions, the effect of geometric factors such as tooth width, cavity depth and shaft diameter in addition to clearance and pitch. Incorporate these results into the above developed model.

4. Extend the above results obtained for a single generic cavity to a labyrinth seal with multiple cavities.

5. Research the effect of various geometrical and flow parameters on the discharge coefficient for a tooth and develop a model for the same. This may be related to the discharge coefficient of a single tooth and the carry over coefficient.

6. Obtain a model for the expansion factor computed by comparing the discharge coefficients of incompressible and compressible flows of the same Reynolds number.

7. Obtain an improved leakage flow rate prediction equation by utilizing the models that were developed for the discharge coefficient. Develop a model that can predict the mass flow rate and the pressure distribution across the different cavities of the seal for a given seal geometry, inlet and exit pressures.

8. Evaluate the model against earlier experimental findings and compare the accuracy against existing leakage equations.

# CHAPTER IV

# COMPUTATIONAL METHOD

This study is based upon CFD simulations performed using the commercial CFD code FLUENT 6.3.26. The effects of flow and geometric parameters on the carry over and discharge coefficients are to be investigated for a generic rectangular cavity, tooth on stator, labyrinth seal, as depicted in Figure 1.1. An extensive study, which is prohibitively expensive and time consuming if done experimentally, can be performed using CFD.

The commercial code FLUENT 6.3.26 is used as the Navier Stokes solver for this work. It uses the finite volume method for discretization. Initially simulations are performed with water. The standard k – $\varepsilon$ turbulence model has been proven to accurately simulate the flow through seals based on comparisons to experiments conducted by Morrison and Al-Ghasem [1]. The standard k – $\varepsilon$ turbulence model and finite volume method are explained in FLUENT Manual [16]. Brief descriptions of the same are included in Appendix A for the convenience of the reader.

A single cavity (two tooth) labyrinth seal was considered for the initial study. The geometry and initial mesh are created using GAMBIT 2.3.16. The geometry and flow are assumed to be axisymmetric and hence a two dimensional (axial – radial) simulation is utilized. The rotor is represented by the line along the bottom of the domain. The long entrance and exit regions before and after the seal are present to allow

the assumed inlet and exit conditions to equilibrate before the flow field enters the first cavity. A sample mesh (for case 1 in Appendix B) is shown in Figure 4.1.
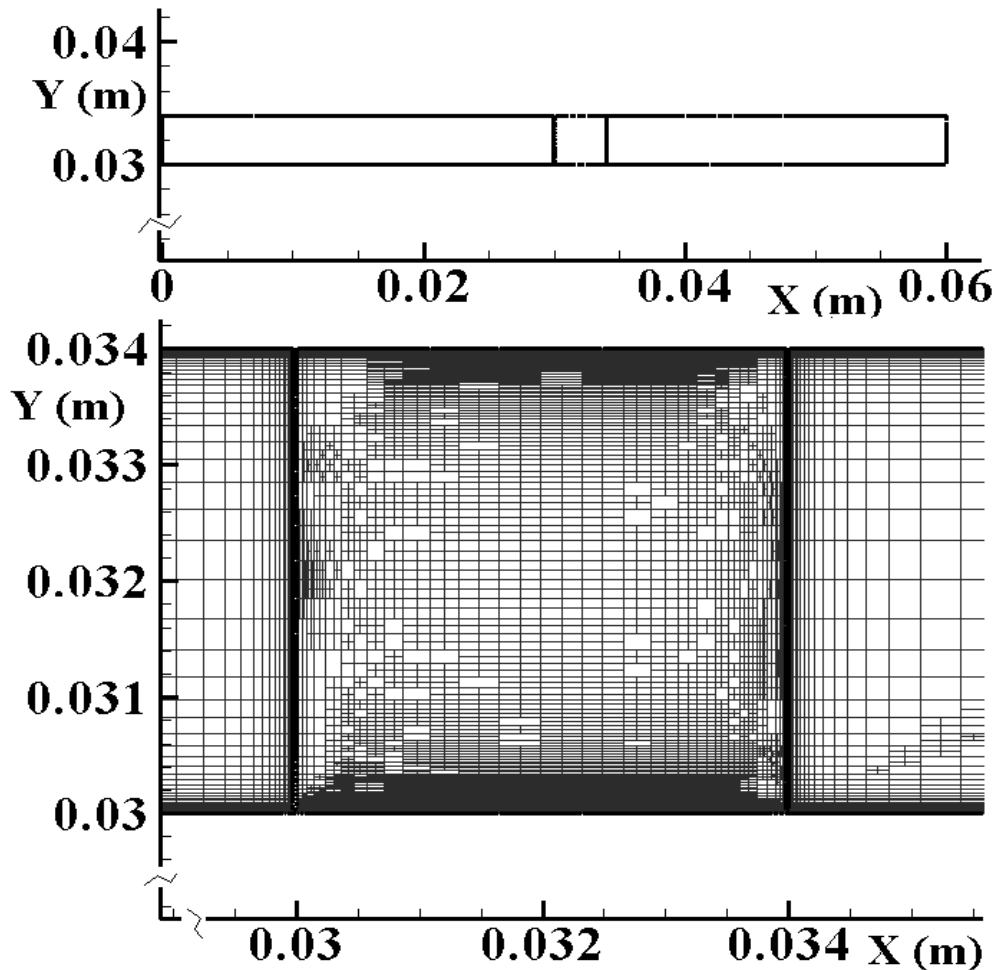


**Figure 4.1. Seal geometry and mesh.**

The computational mesh is much finer in the regions near the stator walls, in the seal clearance region, and near the rotor surface. Morrison and Al-Ghasem [1] showed that for seal analyses, the enhanced wall treatment (available in FLUENT) must be used to obtain accurate leakage prediction. It is also necessary to place nodes closest to the walls at $Y^+$ values less than 5 in order to resolve the laminar sublayer.

Another reason for choosing standard k – $\varepsilon$ turbulence model were the comparison of flow patterns obtained with different turbulence models with the experimental LDA data obtained by Johnson [17]. It is also noted that the standard k – $\varepsilon$ model was the one that has been widely used for computational analysis of labyrinth seals in earlier studies [18-21].
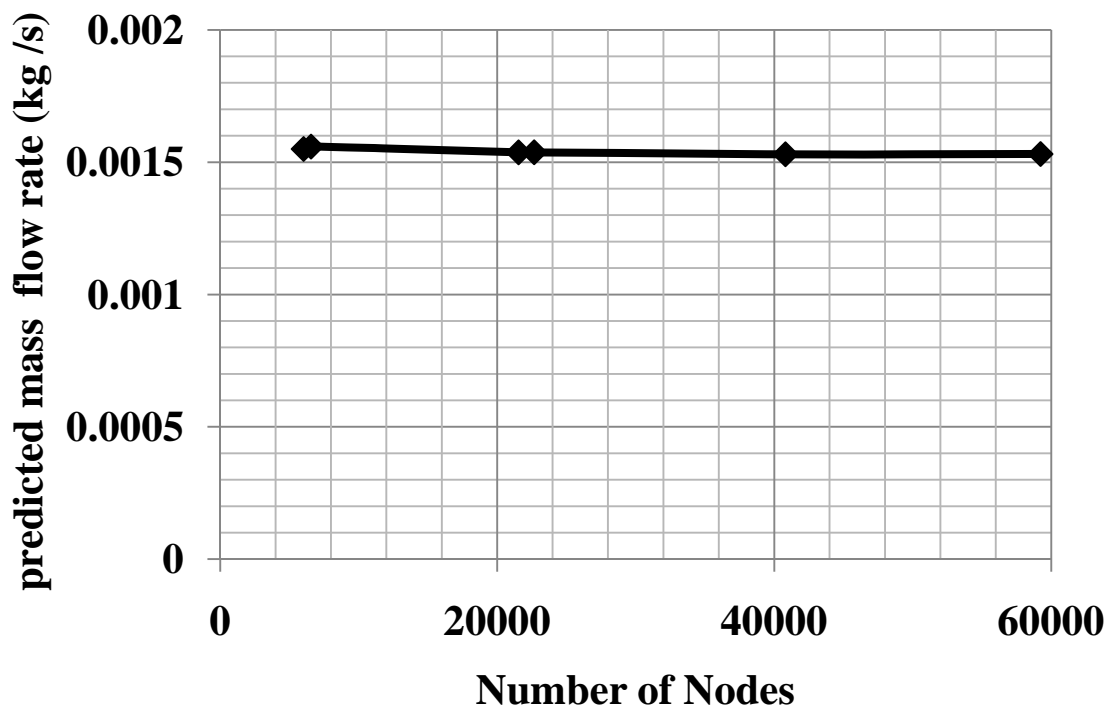


**Figure 4.2. Accuracy of mass flow rate prediction with number of nodes.**

A grid independence study was performed by observing the mass flow rates predicted for a given pressure ratio for various levels of grid refinement (shown in Figure 4.2). Initial work has found that the change in mass flow rate was less than 0.5% when more than 20000 nodes are employed. Adaptation based on pressure gradient, maximum set to 0.1 and $Y^+$ set to 3 was employed to refine the grid.

# CHAPTER V

# CARRY OVER COEFFICIENT

**CALCULATION OF CARRY OVER COEFFICIENT**

Following the definition presented by Hodkinson [8], $\gamma$ is calculated as a function of the divergence angle, $\beta$, measured from the streamline separating the fluid recirculating in the seal cavity and that passing under the tooth, using the following relationships provided by Hodkinson

$$\gamma^2 = \frac{1}{1-\chi} \tag{5.1}$$

and

$$\tan\beta = c\frac{(1-\chi)}{\chi\, s} \tag{5.2}$$

The divergence angle, $\beta$, is the angle made between the line connecting the lip of the upstream tooth to the point of impingement of the jet onto the downstream tooth and a line parallel to the rotor surface. The latter is found by examining the position on the downstream tooth where the radial velocity is zero as indicated in Figure 5.1. Tecplot 360 is used for this analysis.

A number of simulations are performed for a fixed the seal geometry with varying flow conditions. The carry over coefficient is measured for each case. Thus, the effect of flow parameters such as Reynolds number and pressure ratio on kinetic energy carry over are isolated and studied. Once the behavior of kinetic energy carry over based on flow parameters is studied, the seal geometry is varied (again, a single geometrical parameter is varied while others are fixed) and the model developed based

on flow parameters is modified to include the geometry effects. Effect of shaft rotation on the carry over coefficient is studied by respective simulations. The initial cases considered are for a single cavity (two teeth) seal. Multiple cavities will be considered later.
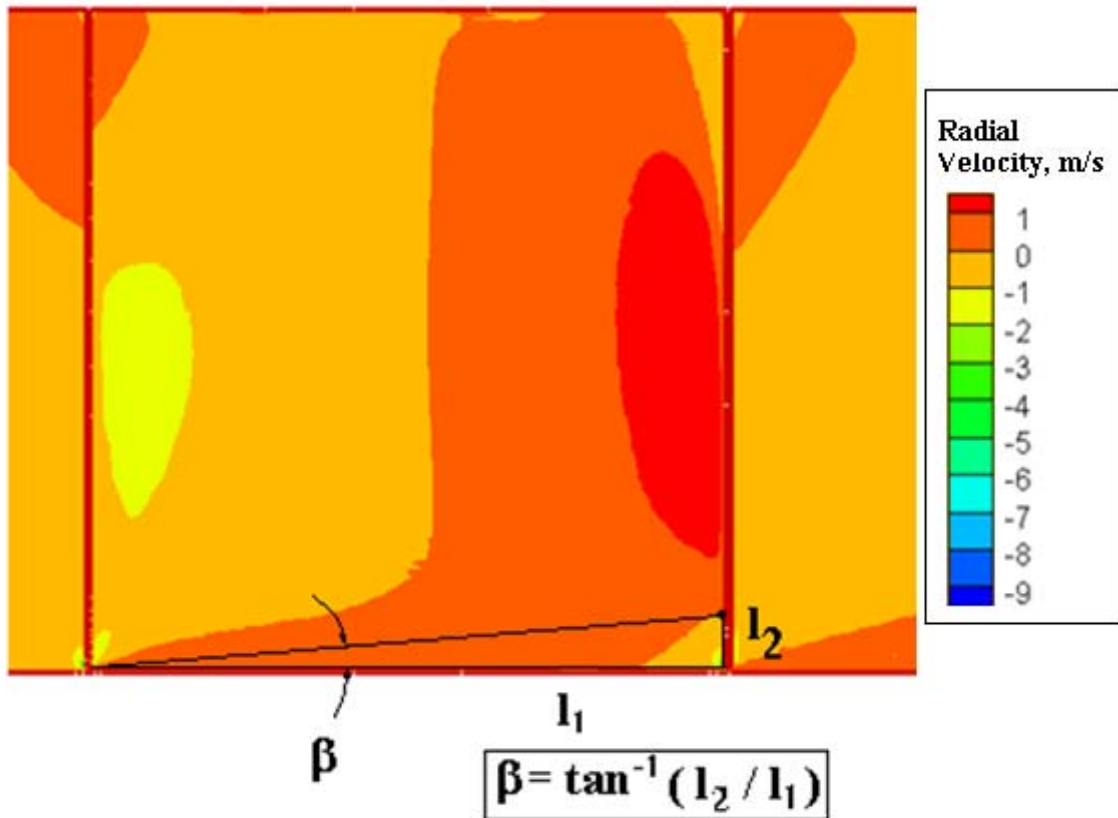


**Figure 5.1. Contour plots of radial velocity and measurement of β.**

**EFFECT OF FLOW PARAMETERS (FOR INCOMPRESSIBLE FLOW)**

The seal geometry is fixed so as to consider only the effect of flow parameters. The initial analysis utilizes water to eliminate compressibility effects and considers a stationary shaft. These results are compared with air flows operating under incompressible conditions.

For a given seal geometry, the carry over coefficient, $\gamma$, was calculated for different mass flow rates. The Reynolds number based on clearance, $\frac{\dot{m}}{\pi D \mu}$, was found to be the dominant non-dimensional parameter. Figure 5.2 illustrates the variation of $\gamma$ for air and water as a function of Reynolds number for the same geometric configuration (case 1 in Appendix B). It has to be noted that, for this analysis, the pressure ratios for air have been kept small enough to ensure incompressible flow. It can be seen that the variation of $\gamma$ with Reynolds number collapses onto a single relationship. This is a very important finding in that the relationship is the same for fluids possessing very different densities and viscosities. It clearly indicates that the carry over coefficient is not only a function of seal geometry (as assumed by Hodkinson [8]) but also is Reynolds number dependent. At low Reynolds numbers, $\gamma$ tends to nearly 1.0 which indicates that all of the kinetic energy is dissipated. As the Reynolds number increases, the carry over coefficient increases indicating ever increasing amounts of kinetic energy are not being dissipated in the seal cavity but convected out of the cavity. This indicates a reduced effectiveness of the seal with increasing Reynolds number. For comparison, the carry over coefficient for this seal geometry as predicted by Hodkinson's model is 1.076, about mid-span of the values computed in this study.

The increase in γ with Reynolds number can be explained as follows. The Reynolds number based on clearance is the ratio of the inertia of the jet issuing from under a tooth to the viscous forces. Therefore, at higher values of Reynolds number, higher inertia of the jet and lower viscous forces result in a smaller divergence of the jet, resulting in a larger portion of the jet's kinetic energy traversing the seal cavity and passing under the downstream tooth without being dissipated by the turbulence viscosity interactions in the cavity. Hence a smaller portion of the kinetic energy is dissipated in the cavity leading to a larger carry over coefficient. These results are valid for both air and water, provided the flow is incompressible.
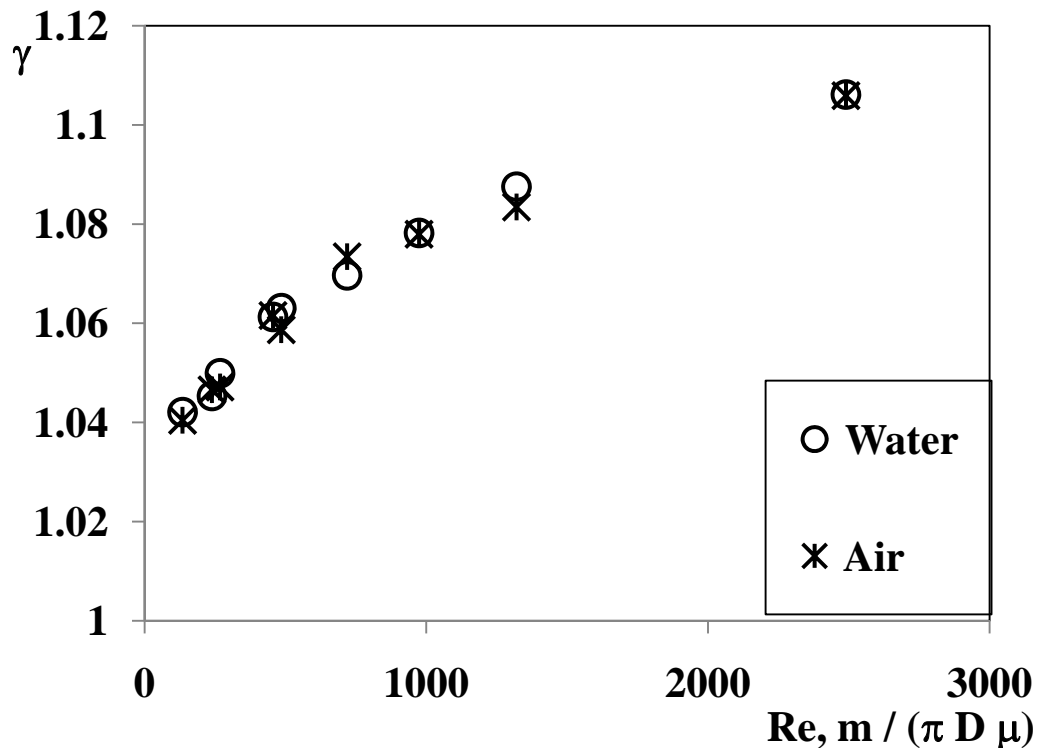


**Figure 5.2. γ vs. Re for water and air.**

To examine the effects of pressure, the $\gamma$ - Re relationship for different pressure ratios and seal exit pressures are compared ( for case 1 in Appendix B). Water is used as the fluid in this study to assure the flow is incompressible. As it can be observed from Figures 5.3 and 5.4, changing the ratio of the seal inlet pressure to exit pressure ( Pr) or the seal exit pressure ($p_e$) does not change the relationship between the carry over coefficient and Reynolds number for a given seal geometry for incompressible flow.
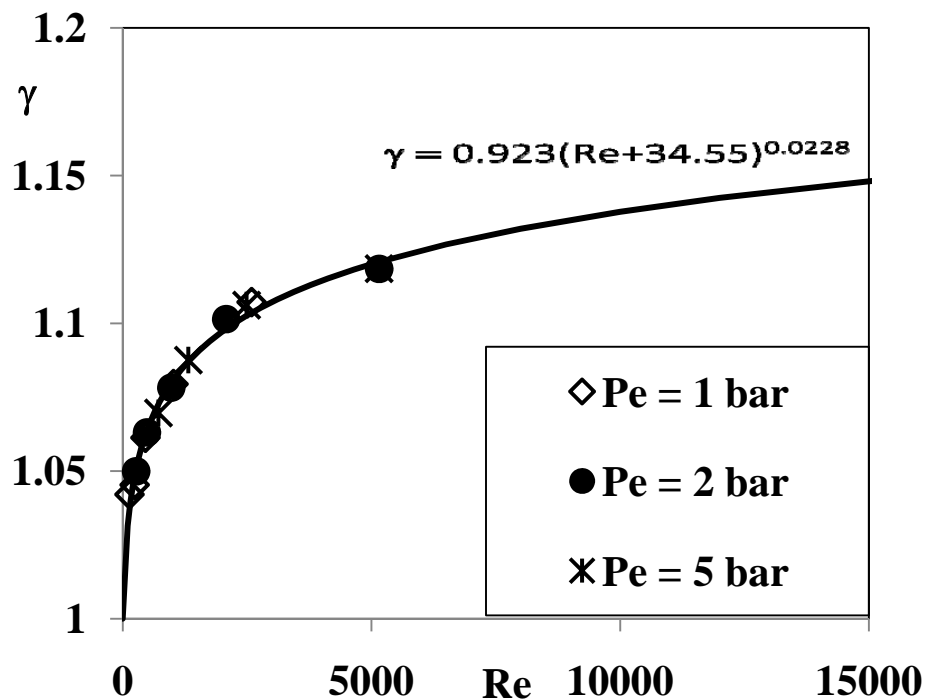


**Figure 5.3. $\gamma$ vs. Re for water at different exit pressures.**
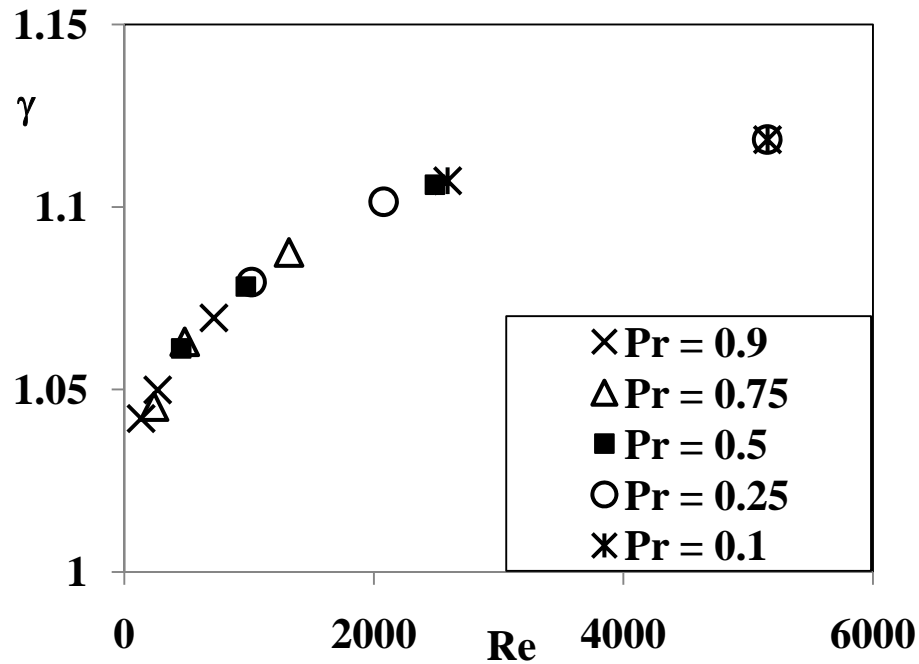
**Figure 5.4. γ vs. Re for water operating under different pressure ratios.**

These data illustrate that an increase in the Reynolds number increases γ. The influence of the Reynolds number is effectively modeled using a power law curve fit as shown in Figure 5.3. The curve fit is of the form:

$$\gamma = C_1 \left( \mathrm{Re} + C_1^{-\frac{1}{C_2}} \right)^{C_2}$$

(5.3)

Where $C_1$ and $C_2$ are possibly functions of seal geometry and other flow parameters yet to be determined. The presence of $C_1^{-\frac{1}{C_2}}$ in the model ensures that γ becomes 1 when the Reynolds number is 0. This is essential as the minimum value of γ is 1. For this baseline geometry (case 1 in Appendix B), $C_1$=0.923 and $C_2$=0.0228.

**EFFECT OF CLEARANCE**

It was found that clearance is one of the major geometric parameters that influences the carry over coefficient. Hence the constants $C_1$ and $C_2$ in equation 5.3 must depend upon clearance. Since both $\gamma$ and Re are dimensionless, $C_1$ and $C_2$ should depend on a dimensionless length parameter. In Hodkinson's model [8], the clearance over pitch is used as the non dimensional parameter. Therefore the current study also adopts c/s as the non dimensional parameter describing seal geometry. Hence $C_1$ and $C_2$ in equation 7 are assumed to be functions of the clearance to pitch ratio, provided all other geometric parameters are fixed. In order to assess the effect of c/s ratio, seals with four different clearances are simulated for a range of Reynolds numbers for a fixed pitch, which corresponded to cases 1- 4 presented in Appendix B. The variation of $\gamma$ for each of the cases is calculated and the results are presented in Figure 5.5. The power law given by equation 5.3 is applied to each data series and constants $C_1$ and $C_2$ are found for the best fit.

Figure 5.5. shows a dramatic increase in the carry over coefficient as the clearance increases. Reducing the clearance to pitch ratio from 0.015 to 0.0075 (factor of two) reduces the values of $\gamma$ by about 10% (percentage of carry over reduced from 30% to 17% at higher Reynolds numbers). Increasing the clearance by a factor of 2.5 increases the carry over coefficient by 30 to 50 % depending upon the Reynolds number. It is also observed that the simulation results in a larger deviation from the curve fit at higher Reynolds numbers and clearances.

From the curve fits it is observed that $C_1$ decreases with increasing c/s ratio while $C_2$ increases with increasing c/s. The relationships are found to be linear and are shown in Figure 5.6. It has to be noted that, in order to make physical sense, the carry over coefficient approaches 1 as Re approaches 0. In order to satisfy this, $C_1$ has to become 1 and $C_2$ should become zero at c/s = 0 (as zero clearance implies no flow and zero Re). Considering the above observation, $C_1$ and $C_2$ in equation 5.3 are expressed in the form

$$C_1 = 1 - k_1 \left( \frac{c}{s} \right)$$

(5.4)

$$C_2 = k_2 \left( \frac{c}{s} \right)$$

(5.5)

The constants $k_1$ and $k_2$ are determined as 6.5 and 2.454 for the least RMS of relative error. $C_1$ represents the effect of Reynolds number on the carry over coefficient, in other words the deviation from Hodkinson's model (in which $C_2 = 0$ , as γ is assumed to be independent of Reynolds number). Therefore higher clearances imply a greater effect of Reynolds number on carry over coefficient.

For a given Reynolds number, a higher value of c/s results in a higher carry over coefficient. The physics behind this observation follows Hodkinson's theory. For a given divergence of the jet, more fluid flows under the tooth when the clearance is higher. Therefore an increase in c increases γ. Also, for a given divergence angle, a higher value of pitch results in a higher impingement point of the jet, on the downstream tooth. Hence a smaller portion of the kinetic energy of the jet flows under the downstream tooth, reducing the carry over coefficient. Hence an increase in s decreases γ.
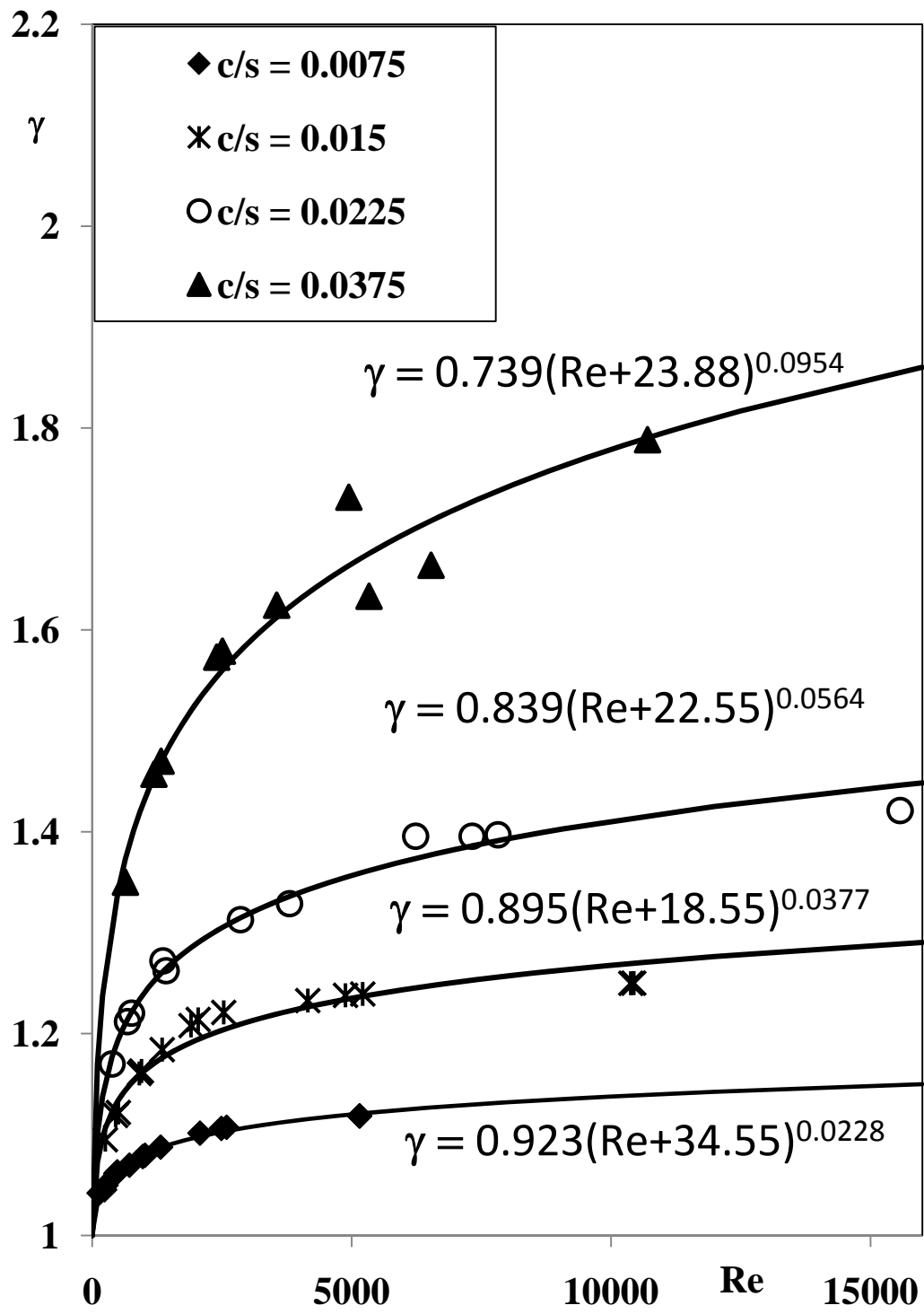
**Figure 5.5. γ vs. Re for different c/s ratios.**
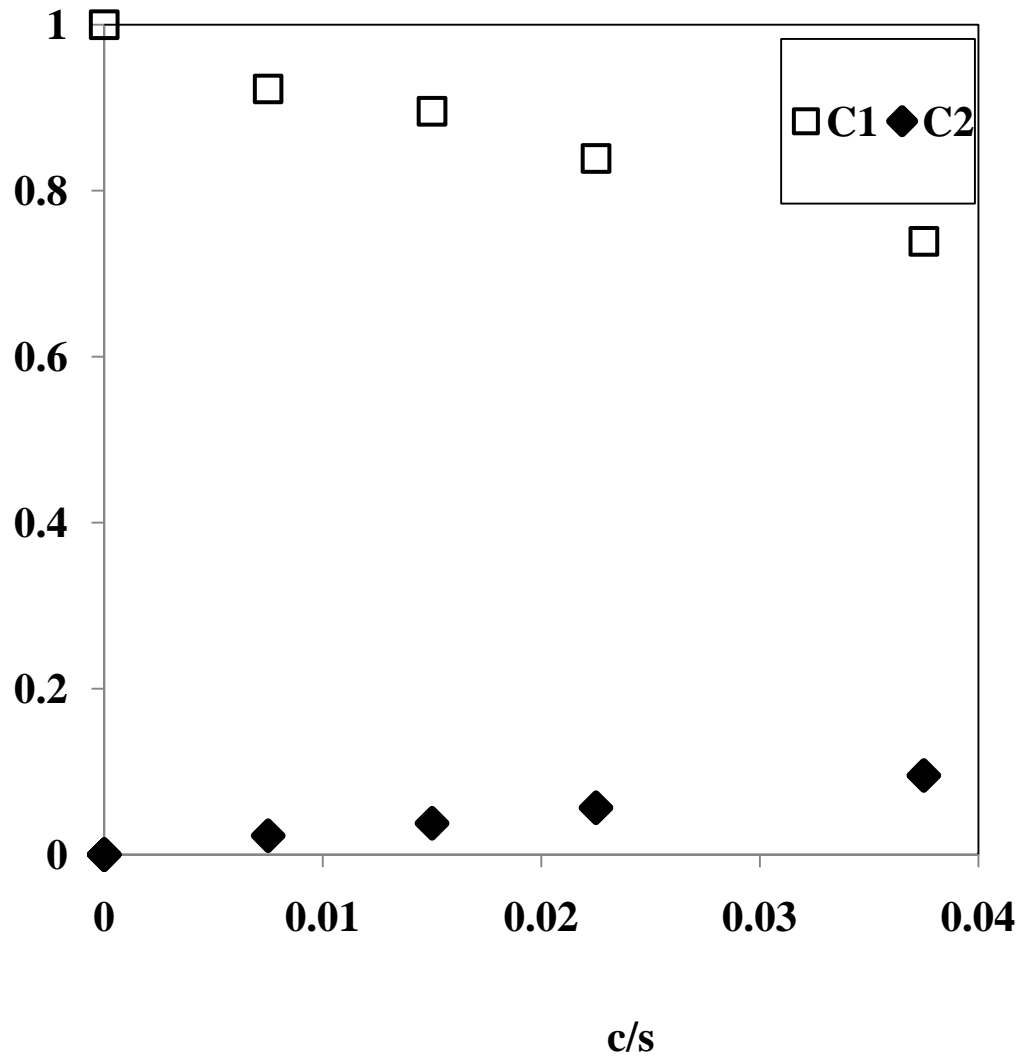
**Figure 5.6. Variation of $C_1$ and $C_2$ with c/s ratio.**

On substitution of (5.4) and (5.5) into (5.3), we obtain a model for the carry over coefficient as

$$\gamma = \left(1 - 6.5\left(\frac{c}{s}\right)\right)\left(\text{Re} + \left(1 - 6.5\left(\frac{c}{s}\right)\right)^{-\frac{1}{2.454\left(\frac{c}{s}\right)}}\right)^{2.454\left(\frac{c}{s}\right)} \tag{5.6}$$

**EFFECT OF PITCH**

  Pitch has been traditionally chosen as the geometric parameter to non-dimensonalize clearance [7, 8]. Hence, this idea was adopted in arriving at equation 5.6. It was felt that a detailed verification whether the effect of changing pitch was the exact reverse of changing clearance was warranted. This would verify the selection of pitch as the non dimensionalizing variable used with clearance.

  The validity of this assumption was investigated by comparing the carry over coefficients of two thin teeth seal geometries with the second geometry having twice the clearance and twice the pitch of the first geometry so that c/s remains the same. The tooth height is also doubled so that (h/s) is identical for both cases, to avoid the effect of tooth height (if any).
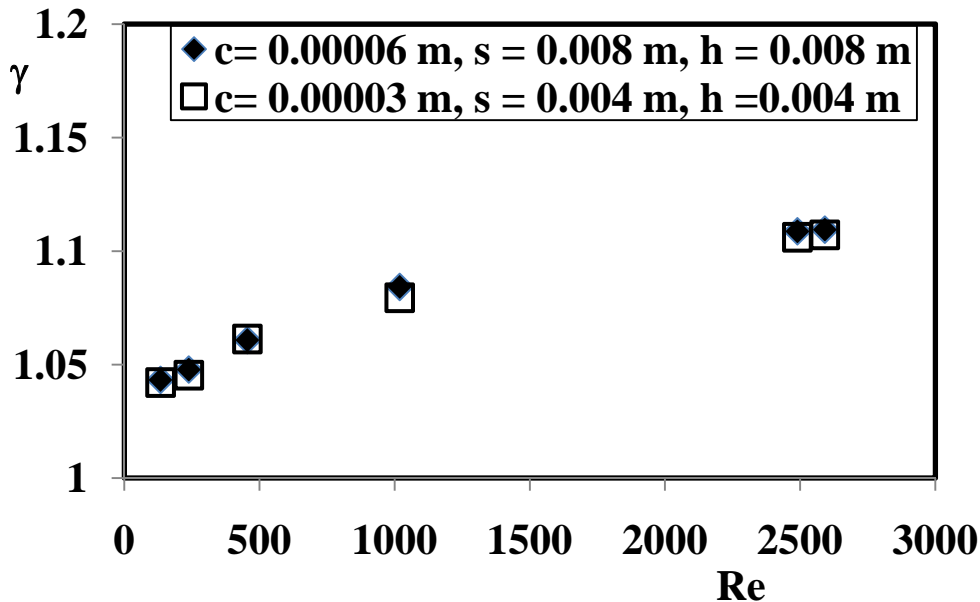
**Figure 5.7. Effect of changing pitch when c/s is held fixed (cases 2 and 5 in Appendix B).**

The results shown in Figure 5.7 illustrate that the kinetic energy carry over coefficient is the same for both geometries provided c/s is held constant even if the clearance and pitch are changed.  This validates the use of c/s as the non dimensional parameter.

**EFFECT OF TOOTH HEIGHT**

Another geometric parameter that could possibly affect kinetic energy carry over is the tooth height (or cavity depth). Changing the non dimensional tooth height (h/s) changes the aspect ratio of the cavity and hence the pattern of recirculation inside the seal cavity. Therefore it is possible that altering tooth height may have some effect on the kinetic energy carry over even though its effect is ignored by all earlier leakage models.

The h/s ratio was varied from 0.75 to 4 (cases 2, 6, 7 and 8 in Appendix B). The simulation results for carry over coefficient are presented in Figure 5.8. It can be seen that the carry over coefficient is fairly independent of h/s for h/s > 0.75 except at very high Reynolds numbers where deep cavities show a small decrease in kinetic energy carry over. In other words, the assumption that tooth height has no effect on kinetic energy coefficient is reasonably valid when the aspect ratio of the cavity is close to or greater than unity.
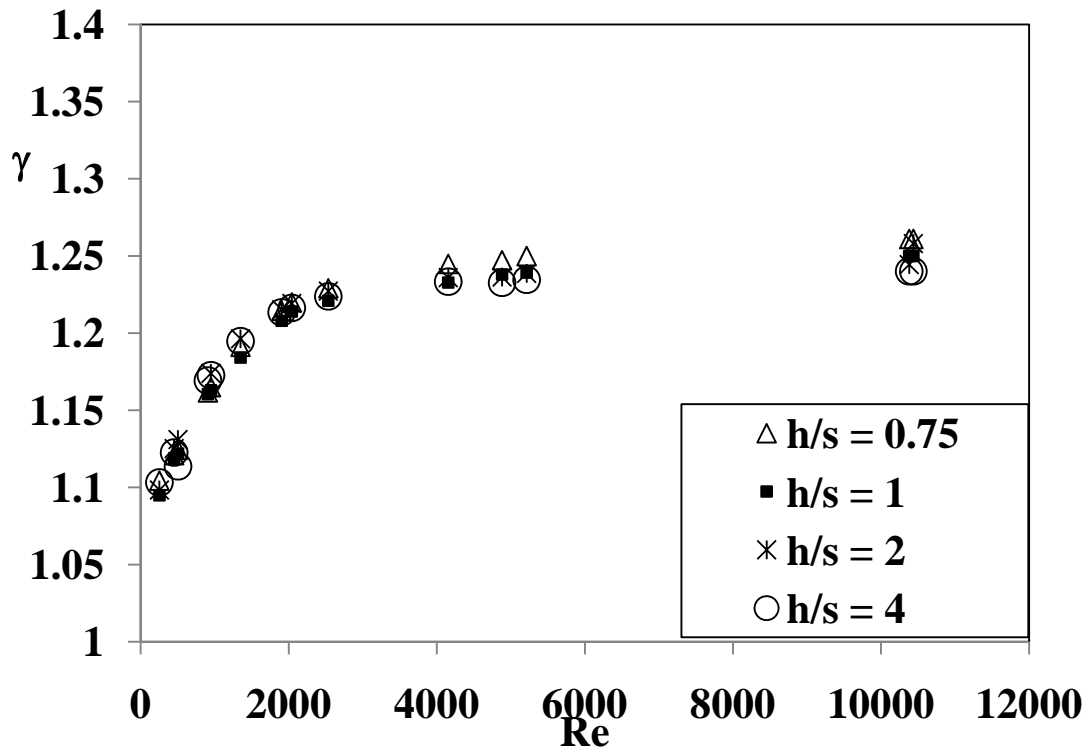
**Figure 5.8. Effect of tooth height on carry over coefficient.**

**EFFECT OF TOOTH WIDTH**

In the earlier section, the effect of Reynolds number on carry over coefficient is studied for a seal with very thin teeth. This was a first order approximation which involved considering the flow under the teeth similar to a flow through an orifice. However, any real world labyrinth seal has significantly larger tooth widths than used in that study. Therefore, while the Reynolds number dependence of the carry over coefficient was presented, it becomes essential to extend those results to different tooth widths. In order to model the effect of tooth width, the relationship between $\gamma$ and Re was studied for different tooth widths while fixing all other geometrical parameters. The

results for a fixed clearance to pitch ratio, c/s = 0.015 (cases 2, 11, 13, 14 in Appendix

B), are presented in Figure 5.9.
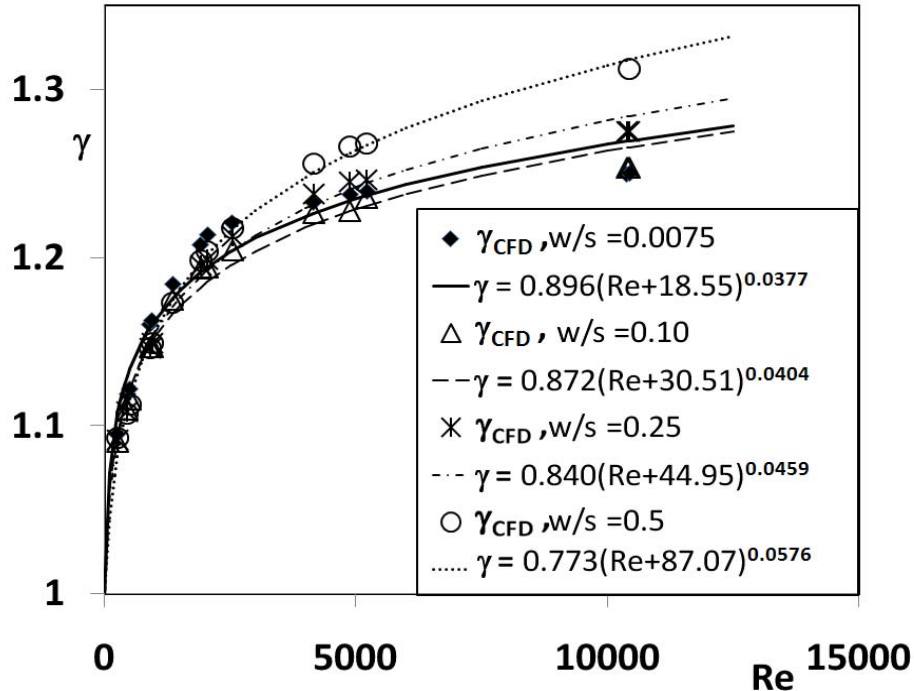


**Figure 5.9. Relationship between carry over coefficient and Reynolds number for different tooth widths (for c/s = 0.015).**

It can be observed that the functional relationship between the carry over coefficient and Reynolds number for different tooth widths retain the same characteristics whilst showing a small variation with tooth width. It can also be seen that the power law, $\gamma = C_1\left(\text{Re} + R_o\right)^{C_2}$, which was used to describe the γ- Re relationship for the very thin tooth in the earlier section, can be used to model the relationship for the other tooth widths by altering the coefficients $C_1$ and $C_2$. Figures 5.10 and 5.11 show the variation in $C_1$ and $C_2$ with respect to tooth width for c/s = 0.015 respectively. Tooth

width is non-dimensionalized based on tooth pitch, as clearance is also non-dimensionalized with tooth pitch.
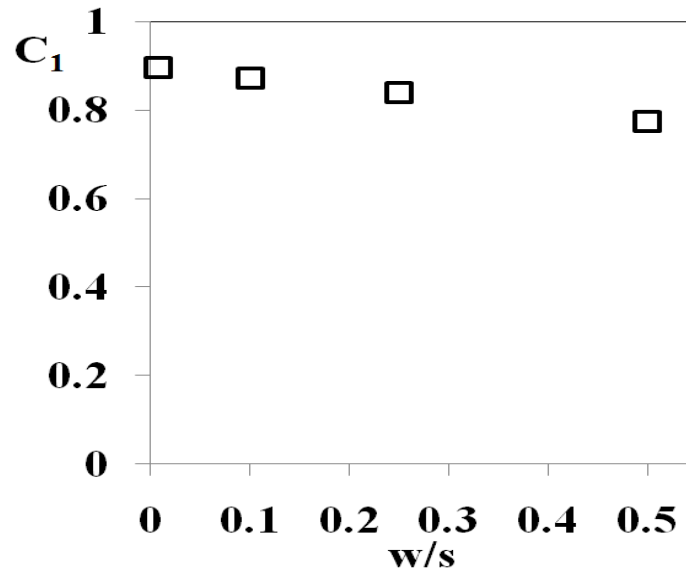


**Figure 5.10. Variation of $C_1$ with tooth width (for c/s = 0.015).**
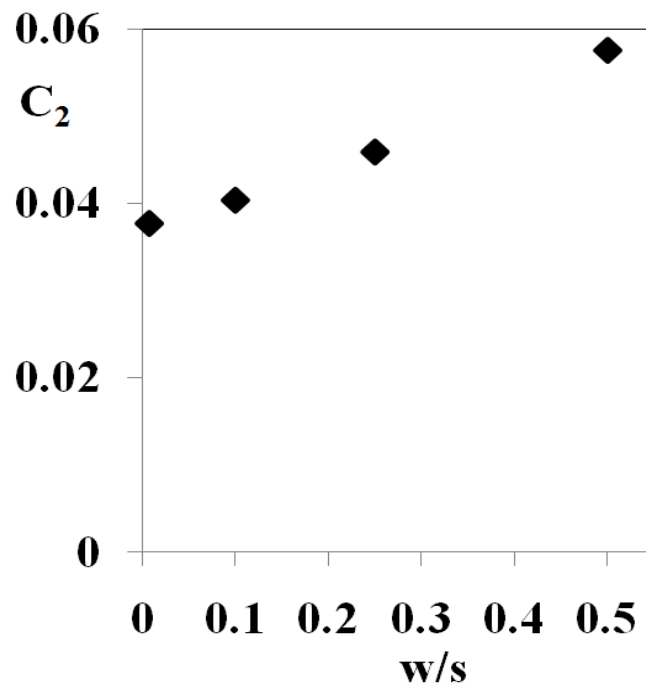


**Figure 5.11. Variation of $C_2$ with tooth width (for c/s = 0.015).**

This effect of tooth width can be incorporated into the earlier model as

$$\gamma = \left(1 - 6.5\left(\frac{c}{s}\right) - k_3 f_1\right)(\text{Re} + R_o)^{\left(2.454\left(\frac{c}{s}\right) + k_4 f_2\right)}$$

(5.7)

with $R_0 = \left(1 - 6.5\left(\frac{c}{s}\right) - k_3 f_1\right)^{-\frac{1}{\left(2.454\left(\frac{c}{s}\right) + k_4 f_2\right)}}$

where $f_1$ and $f_2$ are functions of w/s. $k_3$ and $k_4$ are constants for a given c/s, but are possibly functions of c/s. In order to determine the effect of clearance on the dependence of $C_1$ and $C_2$ on w/s, the above study was conducted for other values of c/s (cases 15 - 18 in Appendix B).
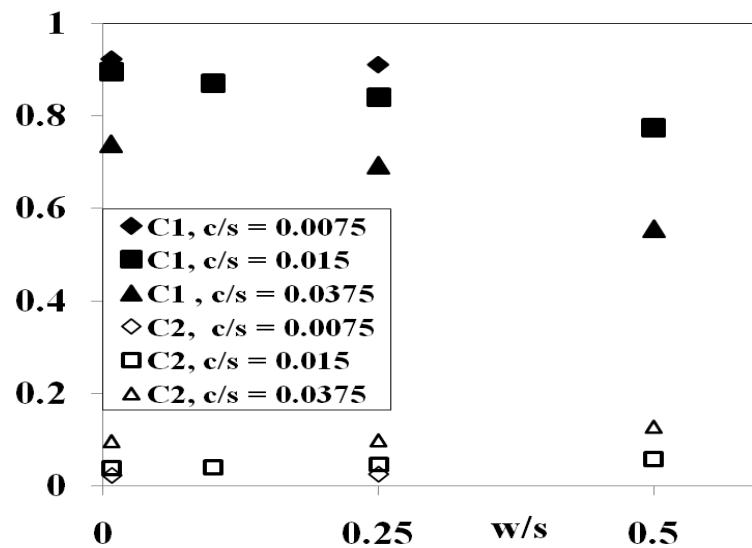


Figure 5.12 Variation of $C_1$ and $C_2$ with tooth width for different values of c/s.

It can be observed from Figure 5.12 that the effect of tooth width has a greater effect on the carry over coefficient at higher clearance to pitch ratios.

Based on the above results, the earlier model for thin teeth is modified as

$$\gamma = \left(1 - 6.5\left(\frac{c}{s}\right) - C_3\left(\frac{c}{s}\right)^a\left(\frac{w}{s}\right)^b\right)(\text{Re} + R0)^{\left(2.454\left(\frac{c}{s}\right) + C_4\left(\frac{c}{s}\right)^c\left(\frac{w}{s}\right)^d\right)}$$

(5.8)

Analysis of various linear, polynomial, and power law fits showed that the power law function is still the best fit for these data. The constants in eqn. 5.8 are determined as to reduce the RMS of relative error. The maximum value of w/s used in the data set is 0.5, above which the CFD predictions deviate from the model. However w/s > 0.5 is generally not common in real world labyrinth seals and is not considered for this study.

$$\gamma = \left(1 - 6.5\left(\tfrac{c}{s}\right) - 8.638\left(\tfrac{c}{s}\right)\left(\tfrac{w}{s}\right)\right)(Re + R_0)^{\left(2.454\left(\tfrac{c}{s}\right)+2.268\left(\tfrac{c}{s}\right)\left(\tfrac{w}{s}\right)^{1.673}\right)} \quad (5.9)$$

$$R_0 = \left(1 - 6.5\left(\tfrac{c}{s}\right) - 8.638\left(\tfrac{c}{s}\right)\left(\tfrac{w}{s}\right)\right)^{\left(-\frac{1}{2.454\left(\tfrac{c}{s}\right)+2.268\left(\tfrac{c}{s}\right)\left(\tfrac{w}{s}\right)^{1.673}}\right)}$$

The RMS error of this model was 1.49 % from the CFD data. If the effect of tooth width is neglected and the earlier model for thin teeth is used for the same data set, the RMS error is 2.3 %. The values of γ predicted by eqn. 5.6 and eqn. 5.9 are compared with those calculated directly from the CFD simulations are shown in Figure 5.13.
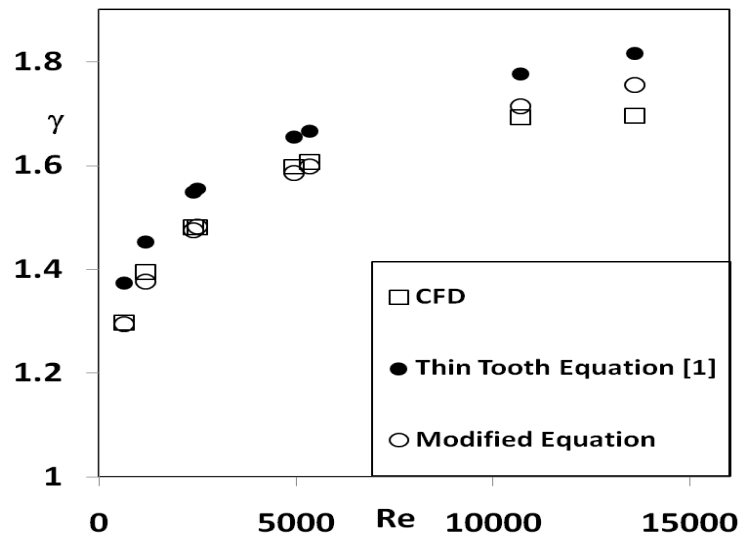


**Figure 5.13. Improvement in carry over coefficient prediction accuracy after considering effect of tooth width (case 17 in Appendix B: c/s = 0.0375, w/s = 0.25).**

**EFFECT OF SHAFT DIAMETER**
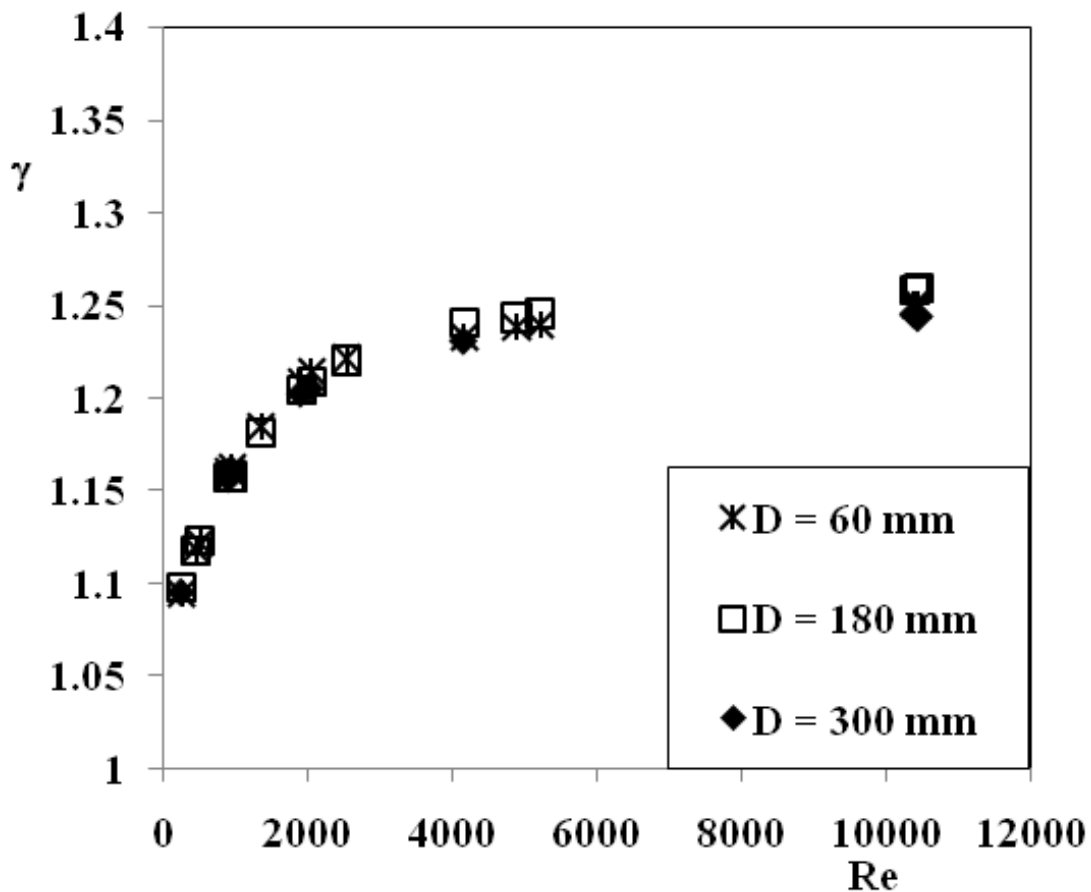


**Figure 5.14. Effect of shaft diameter on carry over coefficient.**

All prior work neglect the effect of changing shaft diameter on carry over coefficient of the labyrinth seals [4, 7 - 10]. However, none of them present a verification of the assumption. It was felt that in order to develop a more accurate model for carry over coefficient, secondary effects (if any) should be addressed. Hence, a study into the effect of shaft diameter on kinetic energy carry over is conducted. Simulations are carried out on three cases with shaft diameters of 60 mm, 180 mm and 300 mm (cases 2, 19 and 20 in Appendix B), while all other geometric parameters are fixed. The

results of the analysis are shown in Figure 5.14. It can be seen that even for this wide variation in shaft diameter, the functional relationship between the carry over coefficient and the Reynolds number remains the same. Therefore this study validates the earlier assumption that carry over coefficient is independent of shaft diameter.

**EFFECT OF NUMBER OF TEETH**

All the studies in the previous sections have been carried out by analyzing flow through a labyrinth seal with two teeth. It is necessary to determine how the single cavity simulation may compare with a labyrinth seal with multiple cavities. To investigate the possible differences, the carry over coefficient in each cavity of a labyrinth seal with 8 teeth operating over the same range of Reynolds number as an earlier case (case 21 in Appendix B) is compared to the single cavity (two teeth) results presented earlier.

From the results presented in Figure 5.15, it can be observed that the carry over coefficient does not vary for the different cavities of a multiple cavity seal for a given Reynolds number. It can also be seen that the carry over coefficient observed in a multiple cavity labyrinth seal is nearly identical to that of the single cavity (two teeth) cases used throughout this study across all Reynolds numbers. Hence it can be concluded that the carry over coefficient results obtained for a single cavity are valid for multiple tooth labyrinth seal and is independent of the number of cavities (teeth) for incompressible flow.
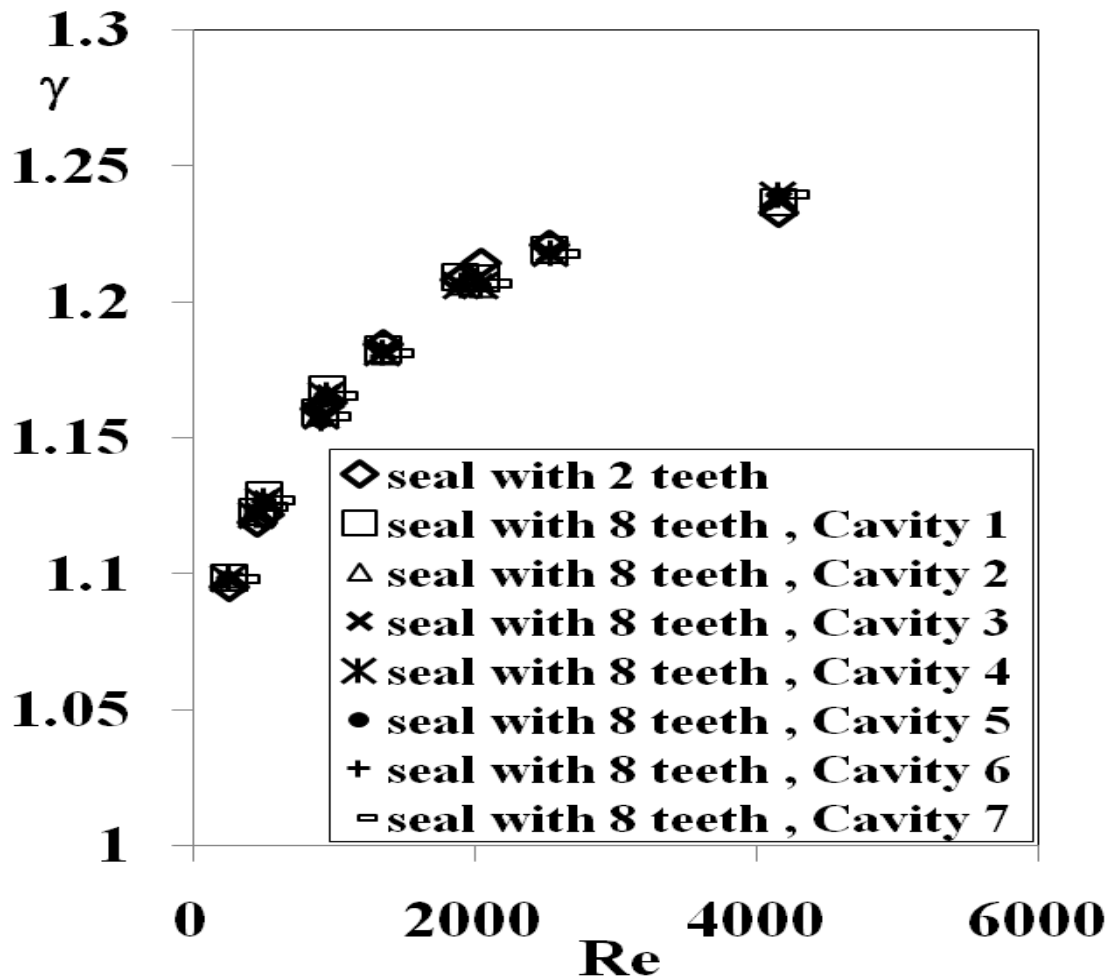
**Figure 5.15. Comparison of carry over coefficient across different cavities of a multiple cavity labyrinth seal with that of a single cavity labyrinth seal (case 21).**
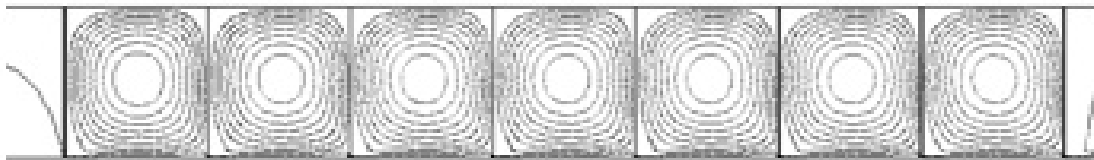


**Figure 5.16. Flow pattern within different cavities of a multiple cavity labyrinth seal (case 21 in Appendix B, Re = 2043).**

Further inspection reveals that not only the carry over coefficient, but the entire flow pattern is independent of cavity as seen in Figure 5.16. This reasserts the earlier conclusion that for incompressible flow, the Reynolds number defined by $\frac{\dot{m}}{\pi D \mu}$ is the only flow parameter that influences carry over coefficient, as it is the only parameter that remains constant across all the cavities. For deeper understanding, the pressure distribution across the seal is shown in Figure 5.17 for the same Reynolds number corresponding to the streamlines shown in Figure 5.16 . It can be seen that the pressure drop across each tooth remains constant except for the first tooth (Figure 5.18) where there is an entrance effect due to the flow upstream of the first tooth being different from the flow inside each cavity upstream of each subsequent tooth.  The pressure ratio decreases with each downstream tooth (Figure 5.19).  The last few teeth have significantly lower pressure ratios, however there is no deviation in the carry over coefficient across the different cavities. This result once again reasserts the earlier observation that the Reynolds number is the only flow parameter governing the kinetic energy carry over, when the flow is incompressible.
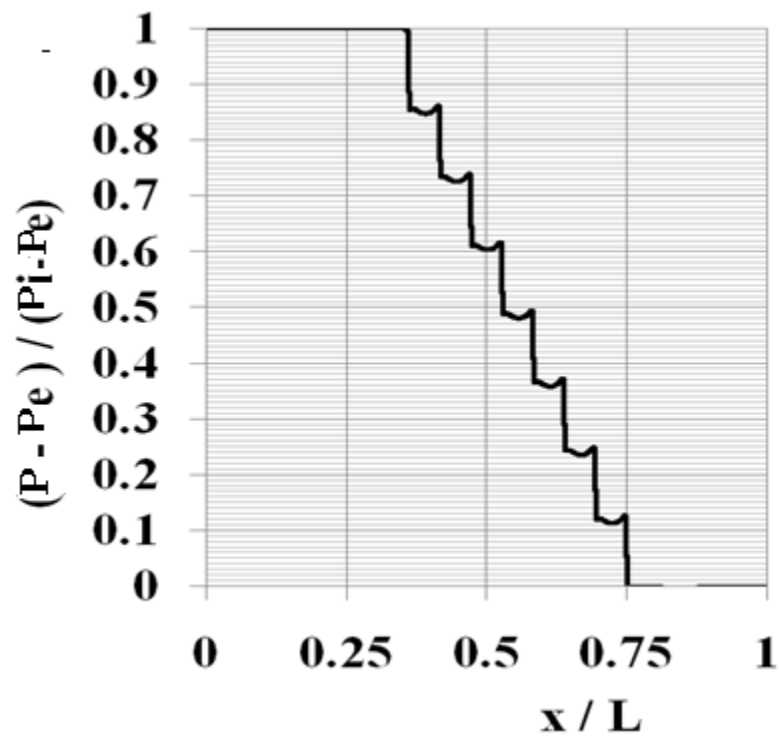
**Figure 5.17. Axial pressure distribution (case 21 in Appendix B, Re = 2043).**
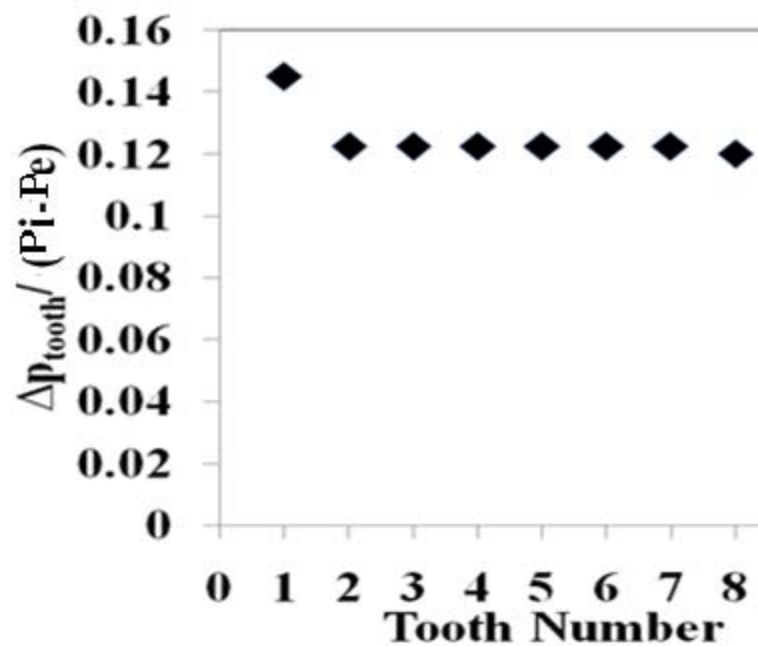


**Figure 5.18 . Comparison of pressure drop across each tooth (case 21, Re = 2043).**
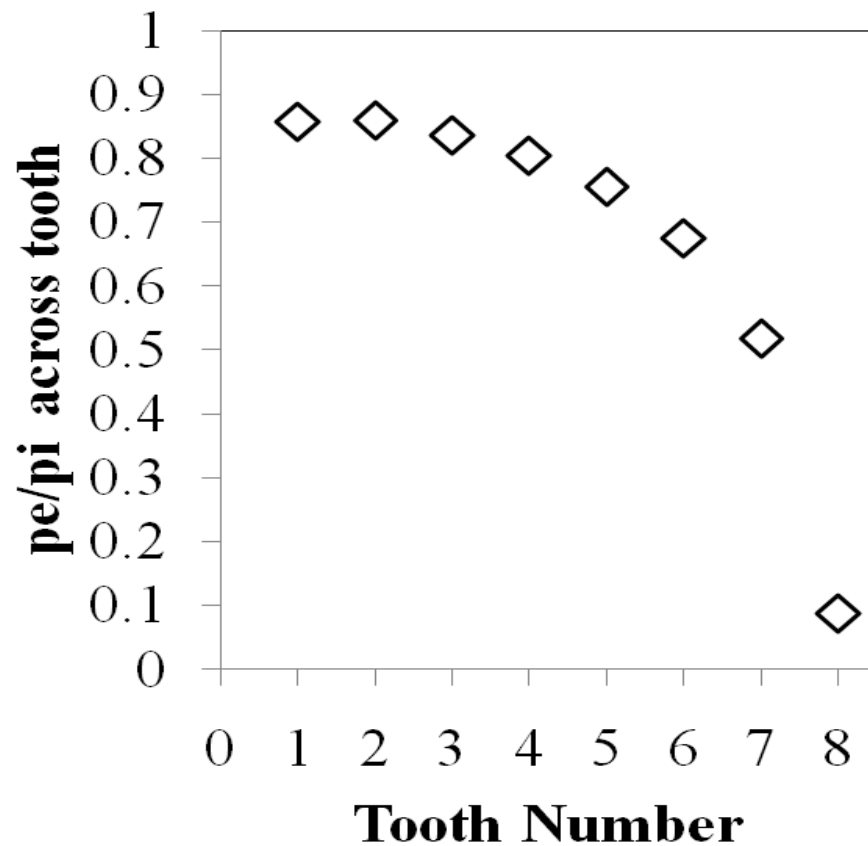
**Figure 5.19. Individual tooth pressure ratios (case 21 in Appendix B, Re = 2043).**

**EFFECT OF SHAFT ROTATION**

A rotating shaft may change the flow pattern within the seal as it introduces swirl velocity. Hence the speed of the shaft might influence the carry over coefficient. To analyze this effect, simulations are performed for a given flow condition and seal geometry at different shaft speeds. The results, as seen from Figure 5.20, show that the carry over coefficient is independent of shaft speed. However, it has to be noted that this study deals teeth on stator seals. The results might differ for seals with teeth on rotor.
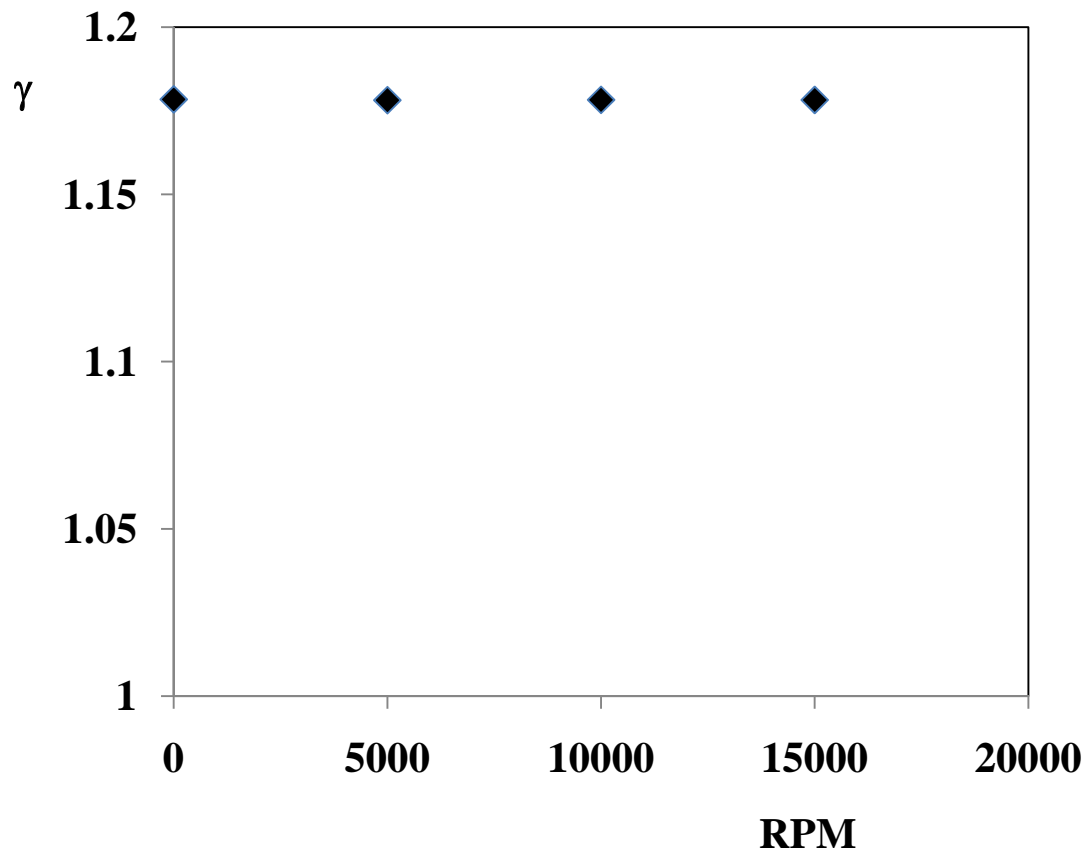
**Figure 5.20. Variation of $\gamma$ with shaft speed (for case 2 in Appendix B, Re = 1348.87).**

# CHAPTER VI

# DISCHARGE COEFFICIENT

On obtaining an understanding of the influence of flow and geometry on the carry over coefficient and developing a model for the same, focus is shifted to the study of the discharge coefficient. Throughout this thesis, the term 'discharge coefficient' describes the total losses that occur as the fluid flows through the cavity and under the tooth. Thus it is the representation of the combined effects of the dissipation in the cavity and the frictional losses that occur at the tooth and is defined as

$$C_d = \frac{\dot{m}}{A\sqrt{2\,\rho\,(p_1 - p_e)}} \qquad\qquad (6.1)$$

Where $p_i$ and $p_e$ are the inlet and exit pressures across a tooth. Hence if the discharge coefficients of all the teeth in a labyrinth seal are known, it is possible to calculate the leakage mass flow rate based on the overall pressure difference across the seal. It is also possible to calculate the pressure distribution across the seal using the same. Thus, this work attempts to develop a labyrinth seal leakage equation by developing a model for the discharge coefficient.

The effect of geometry and flow parameters on discharge coefficient is to be studied in a similar manner to the carry over coefficient. It is expected that the discharge coefficient for the first tooth will be different to that of the subsequent teeth and hence a separate model may need to be developed for the same.

**DISCHARGE COEFFICIENT OF SEAL WITH A SINGLE TOOTH**

Many previous studies represent the discharge coefficient as a product of the carry over coefficient and a flow coefficient [3, 7]. The flow coefficient represents the loss under the tooth and is either an experimentally determined value or modeled in using an empirical relation.

The current work follows a slightly different approach to modeling the discharge coefficient. Rather than representing the discharge coefficient of a cavity followed by a tooth as a product of the kinetic energy carry over coefficient (of the cavity) and the flow coefficient (of the tooth), this work attempts to model the discharge coefficient, which describes the net loss, as a function (not necessarily in form of a product) of the carry over coefficient.

In order to obtain a better understanding of the effect of the kinetic energy carry over, it is desired to compare the discharge coefficient of a tooth following the cavity with that of a single tooth (with no preceding cavity).  Therefore simulations are performed on a seal with a single tooth. Sample geometry and mesh (corresponding to case 24 in Appendix B) are shown in Figure 6.1.
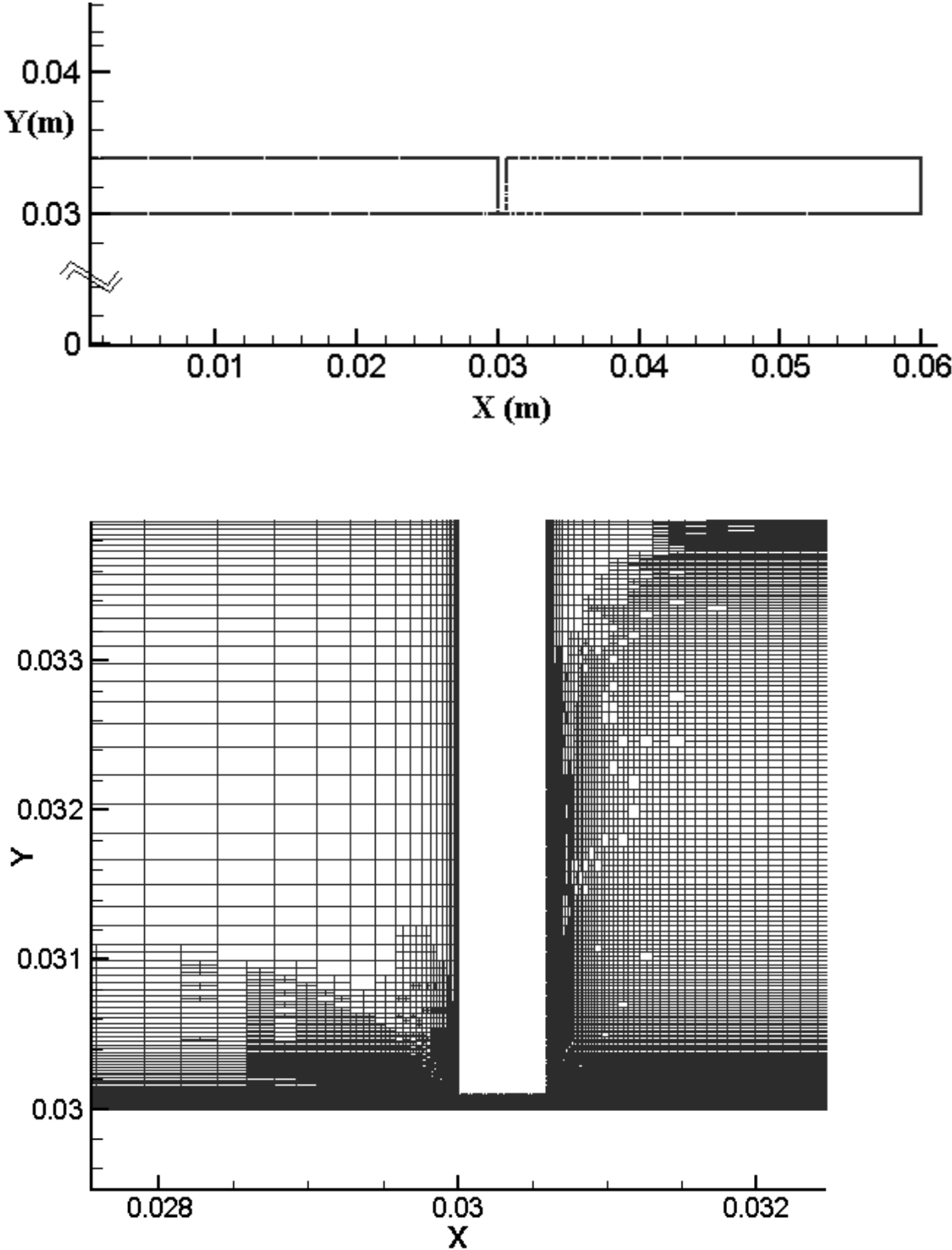
**Figure 6.1. Geometry and mesh for seal with single tooth.**

EFFECT OF REYNOLDS NUMBER

The variation of the discharge coefficient of a single tooth with Reynolds number is shown in Figure 6.2 for incompressible flow. The Reynolds number based on clearance is found to be the only flow parameter governing the discharge coefficient of the single tooth (when the flow in incompressible) .
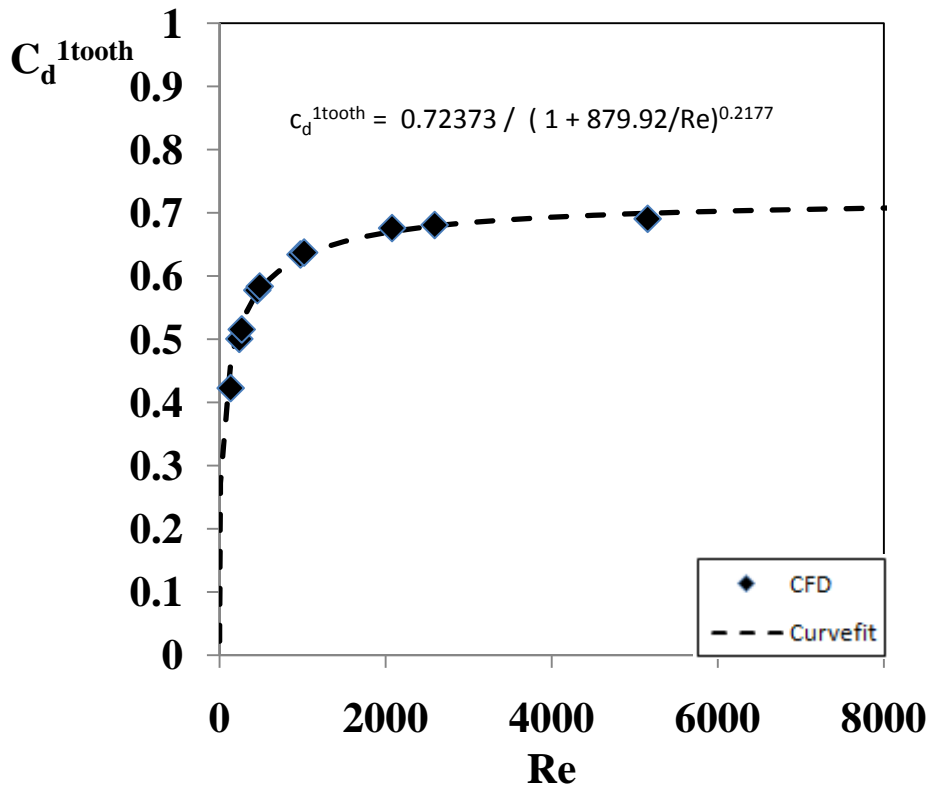


Figure 6.2. Discharge coefficient of a seal with single tooth  (c = 0.00003 m, w = 0.0006m, h = 0.004 m).

An equation of the form

$$C_d^{1tooth} = \frac{A_1}{\left(1+\frac{A_2}{Re}\right)^{A_3}}$$

(6.2)

was chosen to fit the data. The curve fit is shown along with the CFD data in Figure 6.2. It has to be understood that it is probable that the constants $A_1$, $A_2$ and $A_3$ in equation 6.2 could depend upon tooth geometry.

EFFECT OF TOOTH WIDTH AND CLEARANCE

To analyze the effects of flow geometry, simulations are performed for different tooth width, clearance, tooth height and shaft diameters for the range of Reynolds numbers (cases 22 – 34 in Appendix B). It can be concluded from Figure 6.3. that, for a given Reynolds number, the discharge coefficient of a single tooth does not change if the tooth width to clearance ratio is fixed when clearance and width are independently changed. It has to be noted that earlier study by Kearton and Keh [22] obtained experimental curves for the discharge coefficient of a single tooth for different tooth width to clearance ratios. The CFD simulations of the current work attempt to reassert the theory that the only geometrical parameter that significantly affects the discharge coefficient of a single tooth (with no preceding cavity) is the tooth width to radial clearance ratio.

Figure 6.3. shows that discharge coefficients of teeth with different clearance and width but with same w/c ratio (cases 22 and 23 in Appendix B) show the same functional relationship with Reynolds number thus verifying that w/c is the correct non-dimensional geometrical parameter that influences the discharge coefficient of a single tooth. Since the data involves simulations with different back pressures (1 bar and 2 bar), Reynolds number based on clearance is the only flow parameter that is needed to determine the discharge coefficient of a seal with a single tooth for incompressible flow.

However after a certain value of Reynolds number, the discharge coefficient of a seal with a single tooth reaches an almost constant value and does not increase further with increases in Reynolds number.
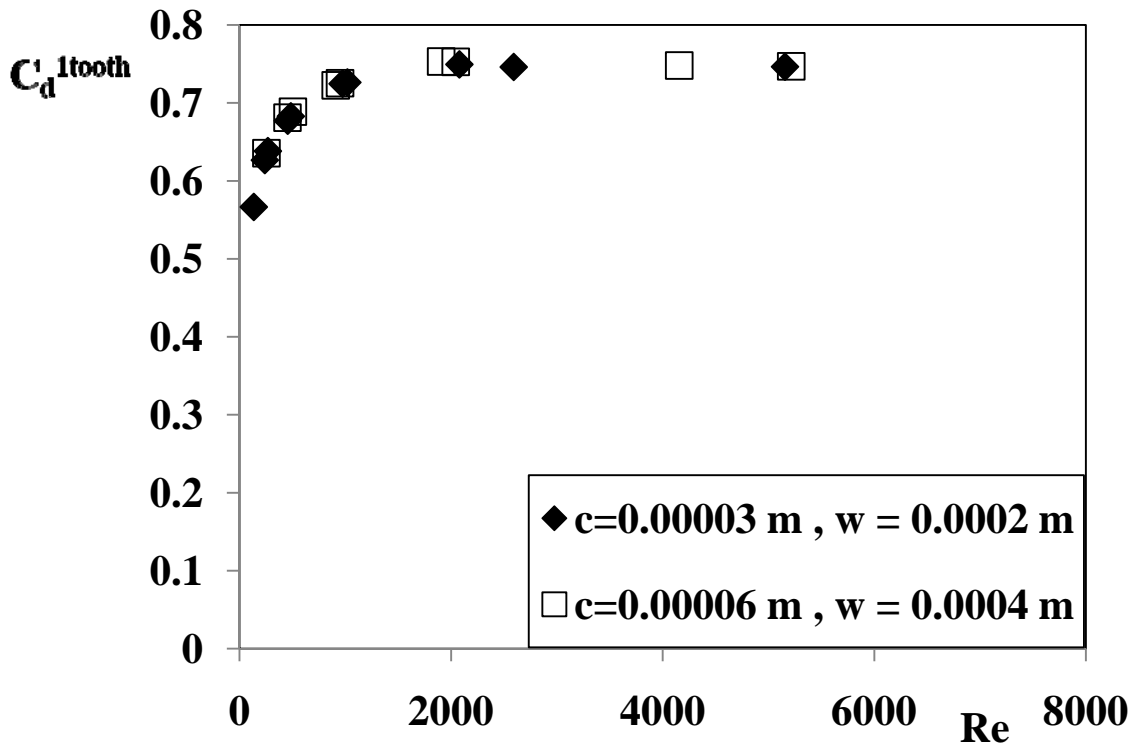


**Figure 6.3. Discharge coefficient of seals with single tooth having same w/c ratio.**

Figure 6.4. shows the relationship between the discharge coefficient and the Reynolds number for different tooth width to clearance ratios (cases 22-24, 28, 31 in Appendix B). It can been seen for smaller values of w/c (that is for thinner tooth and/or higher clearances), the discharge coefficient is higher for the entire range of Reynolds numbers. In a laminar flow through a channel, the pressure drop is proportional to the length of the channel (analogous to tooth width) to the channel width (analogous to radial clearance). While the problem in question involves a more complex geometry, is

axisymmetric, and involves turbulent flow, the finding that the discharge coefficient is directly proportional (though may not be linear) to width to clearance ratio can be understood along similar lines. It can also be observed that the value of Reynolds number at which the discharge coefficient approaches a constant value increases with increased values of the w/c ratio. However in all of the cases, equation 6.2 can be used to model the discharge coefficient provided the constants $A_1$, $A_2$ and $A_3$ are suitably varied.
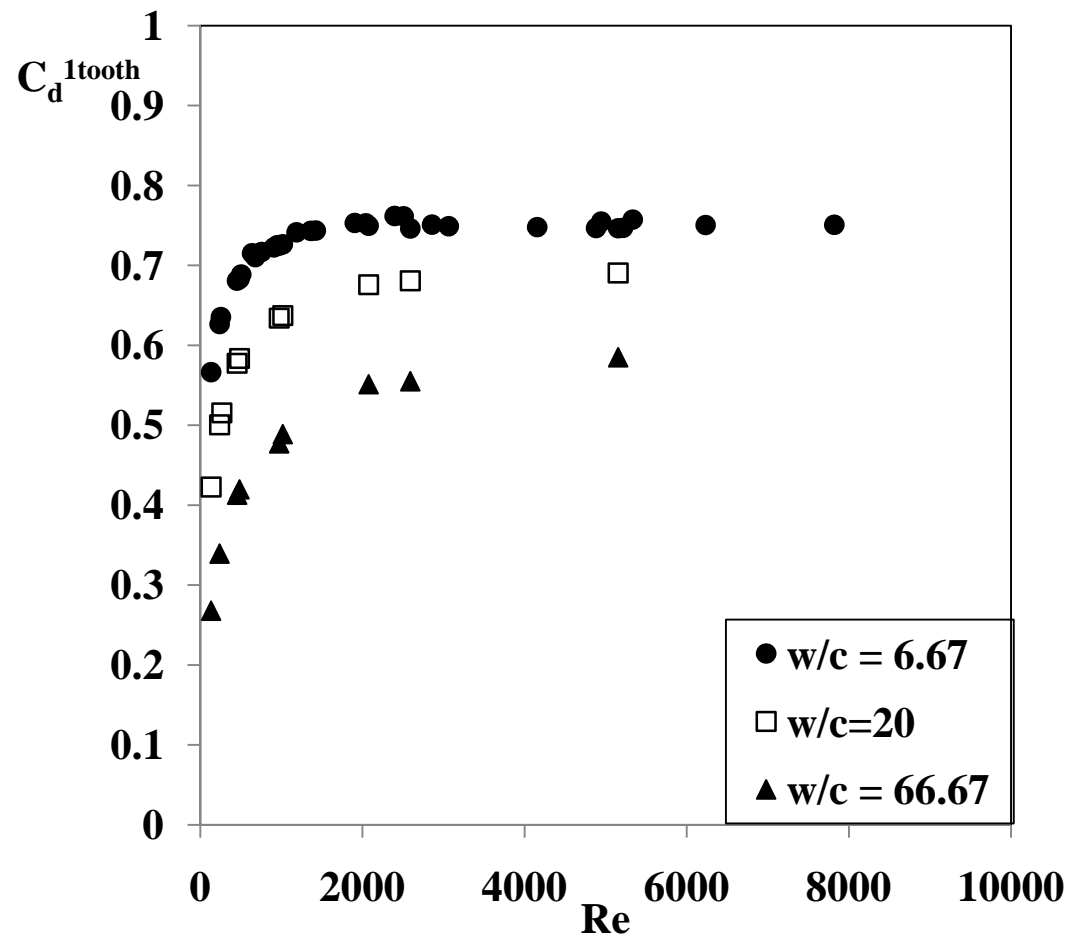


**Figure 6.4. Discharge coefficient of a seal with single tooth with different w/c ratio.**

EFFECT OF TOOTH HEIGHT
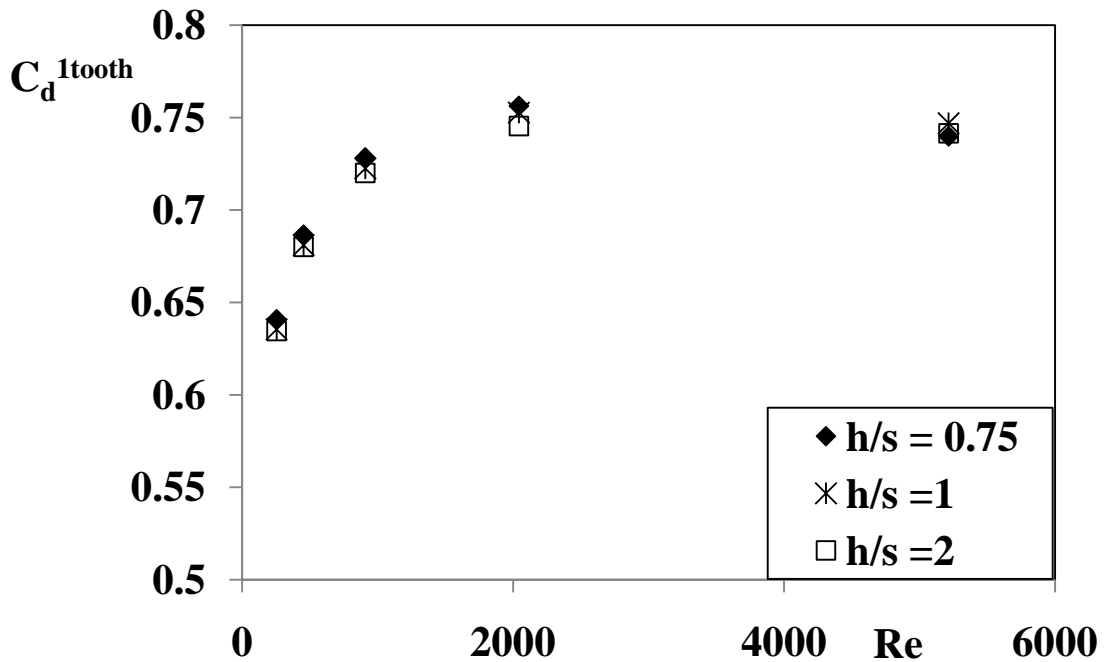


**Figure 6.5. Effect of tooth height on discharge coefficient of seal with single tooth.**

In order to examine the effects of tooth height, simulations are performed for 3 different tooth heights while holding the other geometric parameters constant. Ratios of $h/s$ for the 3 cases are 0.75, 1 and 2 (cases 32, 23 and 33 in Appendix B). It has to be noted that the aspect ratio of cavities of most real world labyrinth seals is around 1 and rarely ever exceeds 2. Each case is simulated for the same range of Reynolds numbers. The results are shown in Figure 6.5. It can be observed that tooth height has almost no effect on the discharge coefficient of seal with single tooth for incompressible flow.

EFFECT OF SHAFT DIAMETER
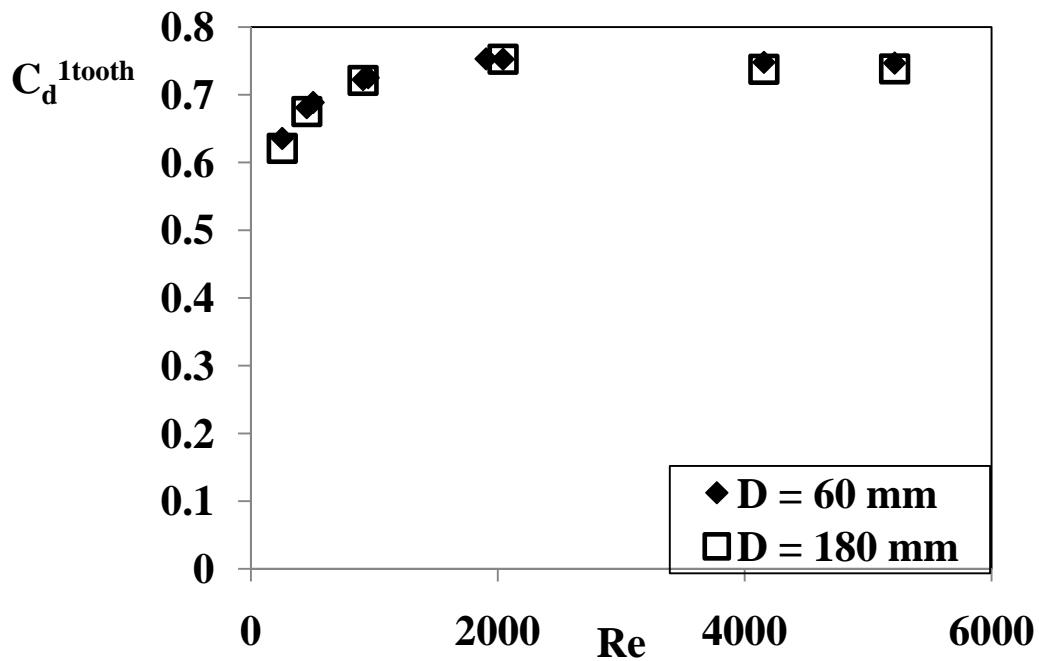


**Figure 6.6. Variation of discharge coefficient of seal with single tooth (cases 23 and 34 in Appendix B, Re = 909) with shaft diameter.**

It can be observed from Figure 6.6 that the discharge coefficient of seal with a single tooth does not change, even after increasing the shaft diameter to 3 times the initial value. Hence it can be concluded that the shaft diameter does not influence the value of $c_d^{1tooth}$.

EFFECT OF SHAFT ROTATION

Earlier studies [23] show that shaft rotation has a negligible effect on labyrinth seal leakage provided the axial Reynolds number is not very low. The CFD simulations using axisymmetric swirl are performed for case 22 in Appendix B for different shaft RPM and Reynolds numbers. The results are shown in Figure 6.7. It can be seen that the

discharge coefficient decreases with increase in RPM and the effect is maximum at low Reynolds numbers. There is a 4% reduction in the discharge coefficient at Reynolds number of at 20000 RPM for Reynolds number of 239. Since most flows encountered in turbomachinery have are at a much higher Reynolds numbers, the effect of shaft RPM is neglected and is not incorporated in the model. A detailed investigation of low Reynolds number- shaft speed interaction is considered to be beyond the scope of this thesis, but is recommended for future work if leakage predictions are required for applications that involve low Reynolds numbers and high shaft speeds.
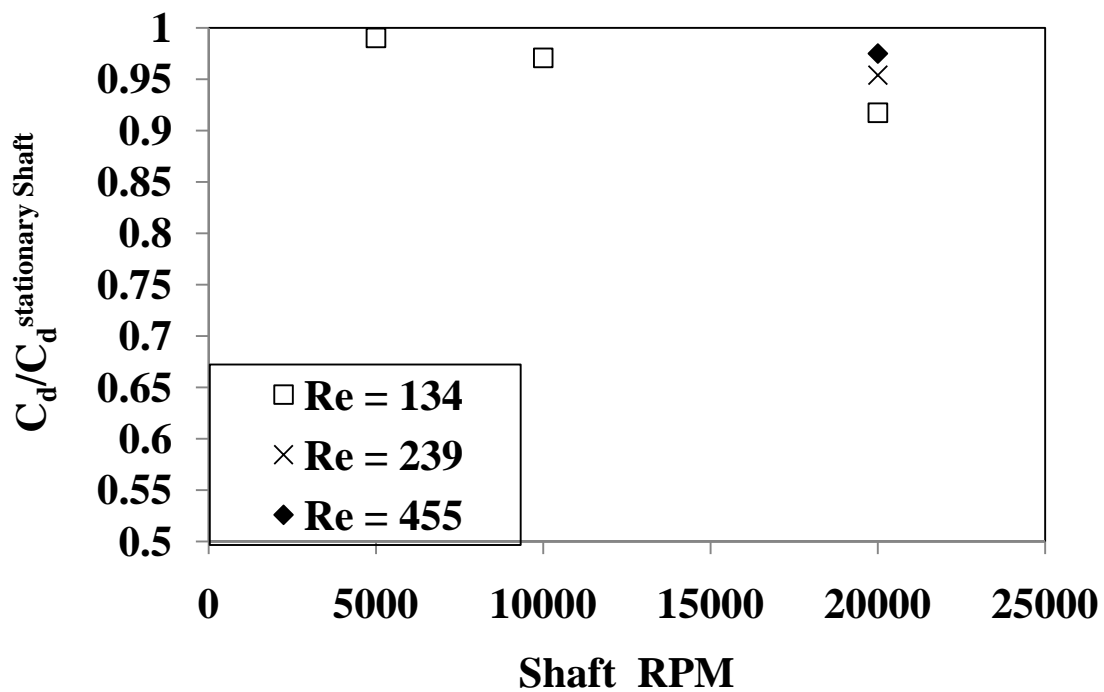


**Figure 6.7. Variation of $C_d$ of seal with single tooth (c = 0.00003m, s = 0.004m, w =0.0002m) with shaft RPM.**

EMPIRICAL MODEL

Since this research ultimately aims to develop an equation that can predict flow rate, an empirical formula that represents the single tooth discharge coefficient based on Reynolds number and w/c ratio is sought. The same is achieved by exploring various curve fits on the computational data matrix using Table Curve and MS Excel. The equation of the form described in 6.2 is chosen. The constants in the equation have been optimized to best fit data across w/c ratios from 2.67 to 66.67 (cases 22-31, 34 in Appendix B). It has to be noted that for values of w/c less than 2.67, an equation of this form does not provide a good fit. But since most labyrinth seals have w/c ratios higher than this value, w/c lower than this limit is not considered for this study. The following formula is proposed to compute the discharge coefficient of a seal with a single tooth for incompressible flow. The only inputs required are the tooth width to radial clearance ratio and the Reynolds number based on clearance.

$$c_d^{1\ tooth} = \frac{\left(0.7757 - 0.002051\left(\frac{w}{c}\right)\right)}{\left(1 + \frac{44.86\left(\frac{w}{c}\right)}{Re}\right)^{0.2157}} \tag{6.3}$$

The equation has been developed from the CFD data of nearly 100 simulations with Reynolds number ranging from 254 to 26800. The standard deviation of the fit is 1.42% and the maximum error is 4.38%. The CFD data and model prediction for the entire data set is compared in Figure 6.8.
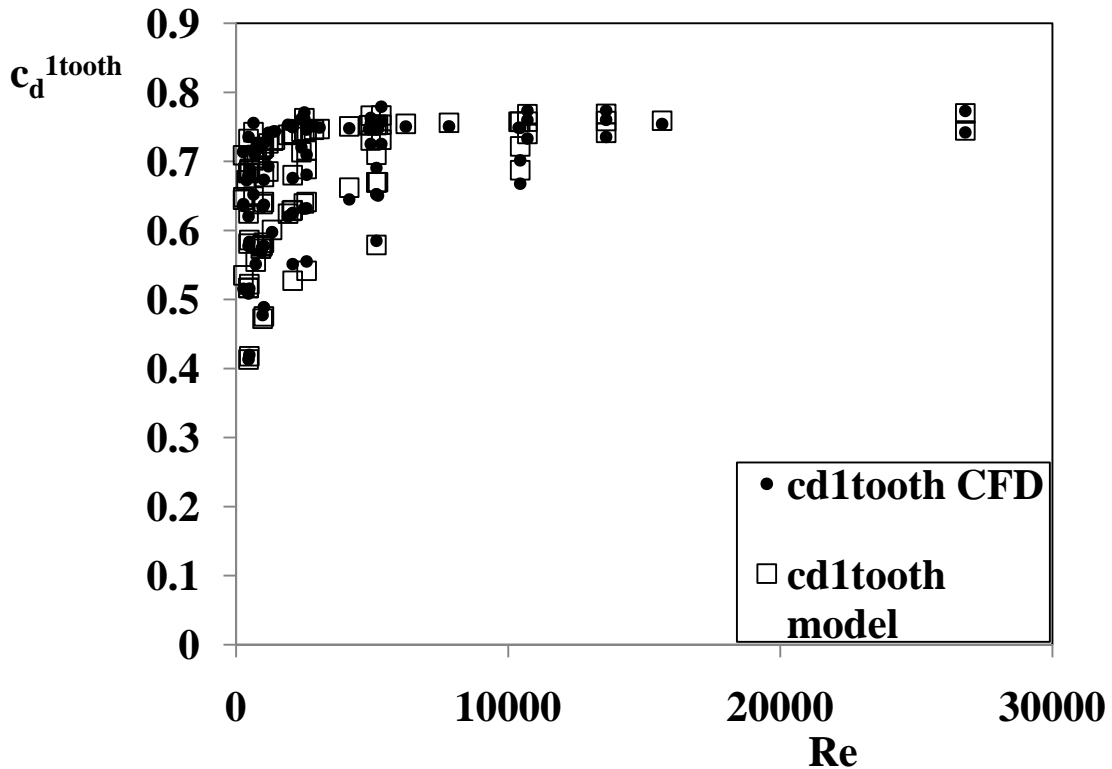
**Figure 6.8. Discharge coefficient of single tooth seals – CFD and model prediction (cases 22-31, 34 in Appendix B).**

## DISCHARGE COEFFICIENT OF FIRST TOOTH

It was felt that the discharge coefficient of the first tooth of a multiple tooth labyrinth seal would be the same as that of the seal with a single tooth, as it has no preceding cavity. However it might be possible that the downstream flow may affect the discharge coefficient. Figure 6.9 compares the streamlines of the flow through a seal with a single tooth with a labyrinth seal with 2 teeth in the vicinity of the first tooth.
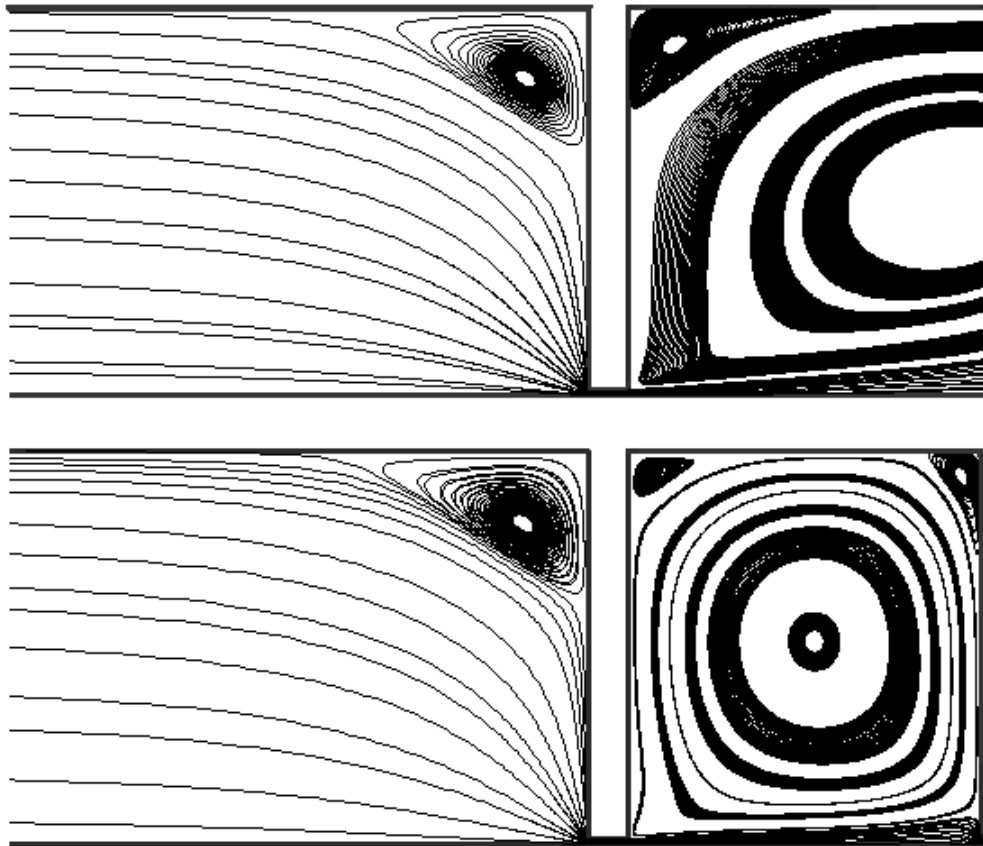
**Figure 6.9. Comparison of streamlines at entrance to seal with single tooth and to the first tooth of a multiple teeth labyrinth seal (cases 23 and 11, Re = 909).**

The Reynolds number and the tooth dimensions of the two cases considered are identical. It can be observed that the flow pattern upstream of the single tooth and the flow pattern upstream of the first tooth of a multiple tooth labyrinth seal are very similar. Thus simulations were performed for labyrinth seals with two and four teeth that have the same tooth width and radial clearance (cases 13 and 37 in Appendix B). These simulations were also performed for the same set of Reynolds numbers. It was found that the $C_d$ of the first tooth of the multiple tooth labyrinth seals is independent of the number

of downstream teeth and is very similar to those of the single tooth seals for any given Reynolds number for incompressible flow. Figure 6.10 illustrates how the discharge coefficients of single tooth and first tooth of seal with two teeth for one specific geometry vary for different Reynolds numbers.
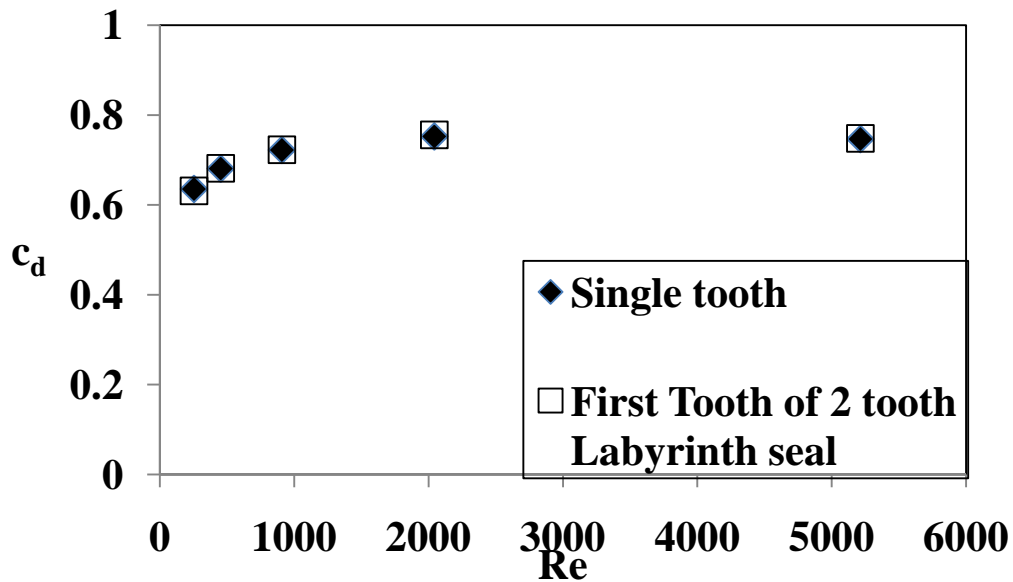


**Figure 6.10. Comparison of discharge coefficients of single tooth seal and the first tooth of a labyrinth seal with two teeth (cases 11 and 23 in Appendix B).**

Hence the model for the discharge coefficient of a single tooth seal developed in the earlier section (equation 6.3) has been verified to describe the $C_d$ of the first tooth of a multiple tooth labyrinth seal.

**DISCHARGE COEFFICIENT OF DOWNSTREAM TEETH**

It is expected that the discharge coefficients of the subsequent teeth may be different from that of the first tooth as the velocity profile at the inlet of the teeth following a cavity is different to that of the first tooth as seen in Figure 6.11. Incompressible simulations are performed on labyrinth seals with multiple teeth and the discharge coefficients of downstream teeth are calculated from the CFD predicted pressure distribution (cases 10 - 20, 35 - 40 in Appendix B). It can be seen from Figure 6.12, that the $C_d$ of a downstream tooth is a function of clearance, pitch, width and Reynolds number. Unlike the case of the first tooth, holding w/c as constant does not collapse the $C_d$ – Re relationship to a single relation. However, as seen in Figure 6.13., the influence of tooth height on the discharge coefficient of the second tooth is negligible for h/s > 0.75 as in case of the first tooth and carry over coefficient. The simulations also show that the discharge coefficient for all downstream teeth in a given seal for a given Reynolds number remains the same for incompressible flow.

It becomes more difficult to directly model the discharge coefficient of the downstream tooth as it is a function of more than two variables. Physically, the discharge coefficient of the downstream tooth is determined by the combined effect of the kinetic energy carry over and the frictional losses that occur under the tooth. Hence it becomes essential to consider the carry over coefficient while modeling the discharge coefficient of subsequent teeth.
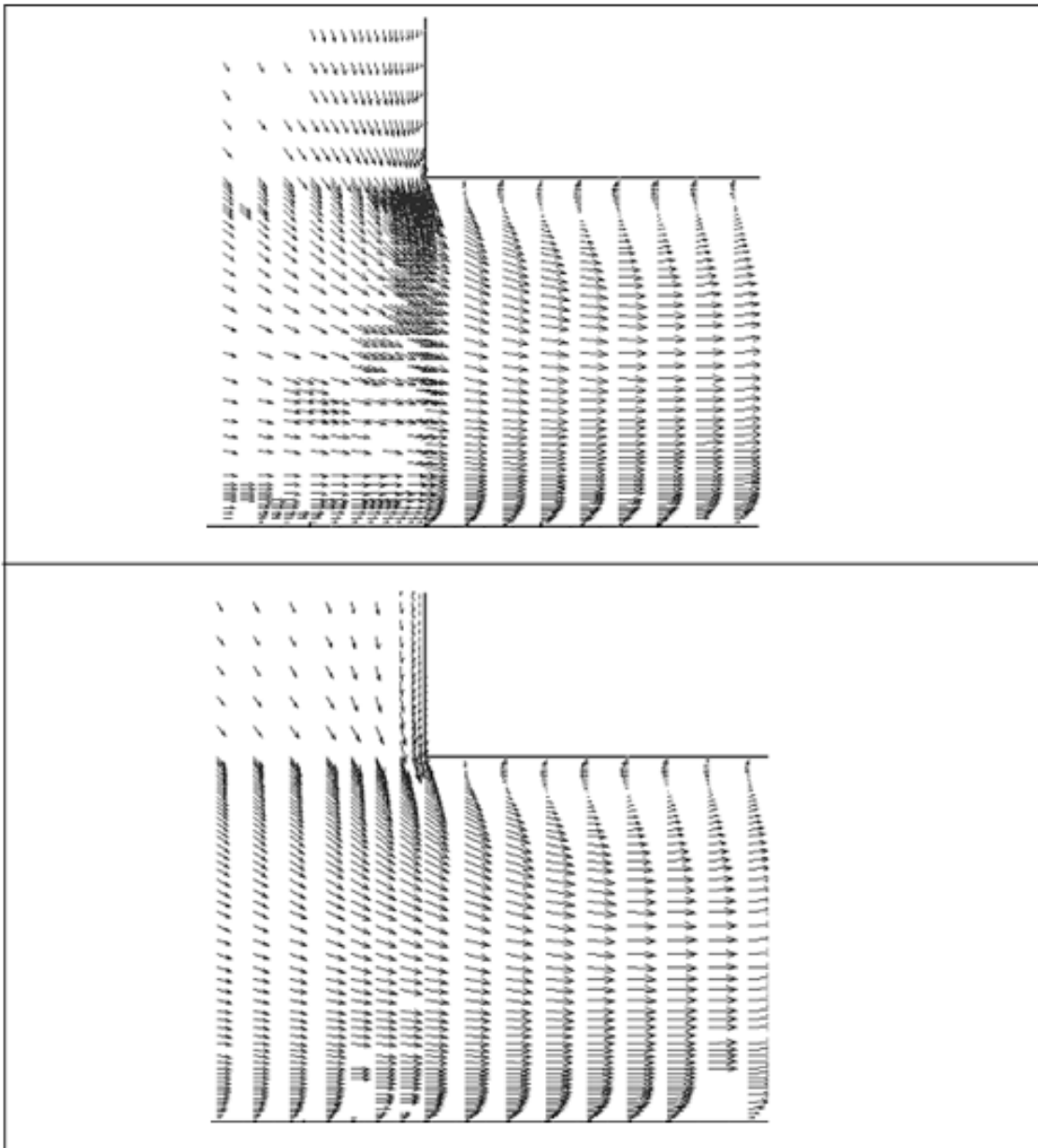
**Figure 6.11. Comparison of velocity profiles upstream of first (top) and second tooth (bottom) of incompressible flow ( Re = 909) through two tooth labyrinth seal (case 11 in Appendix B).**
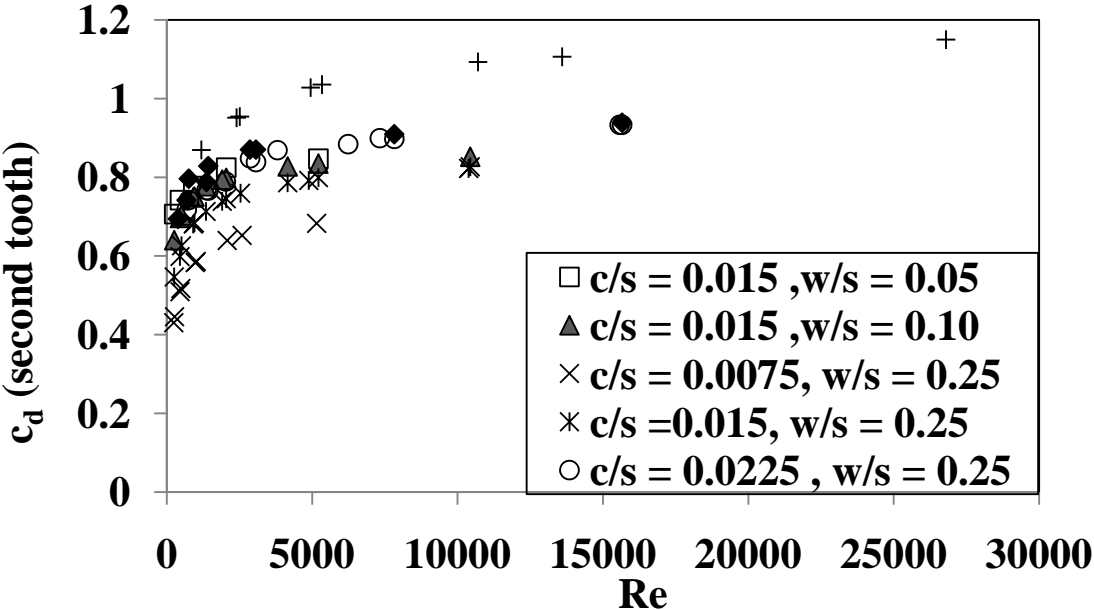
**Figure 6.12. Influence of clearance, pitch and tooth width of discharge coefficient of second tooth (cases 10, 11, 13, 15-17 in Appendix B).**
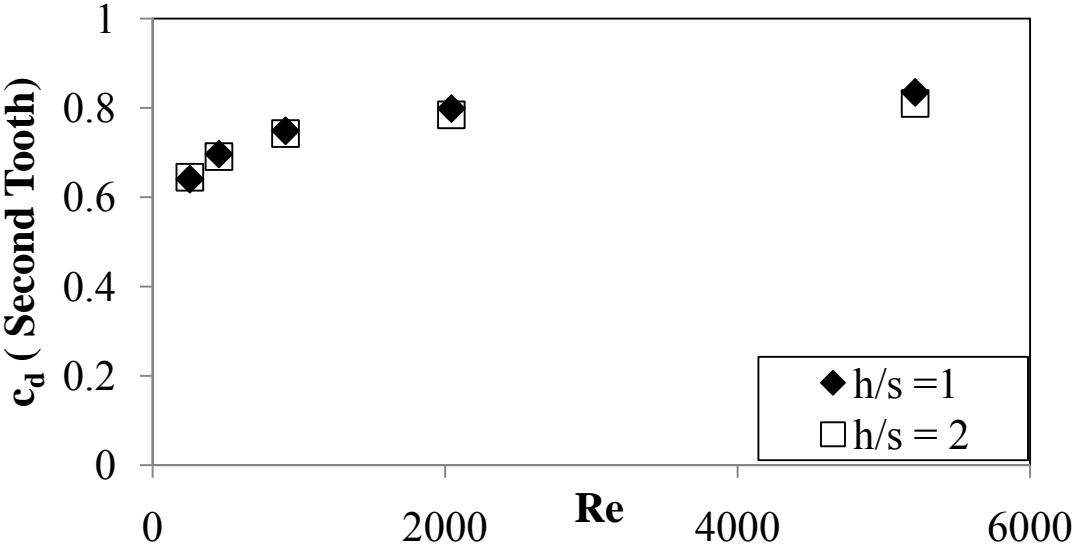


**Figure 6.13. Influence of tooth height of discharge coefficient of second tooth (cases 11 and 38 in Appendix B).**

Figure 6.14 compares the discharge coefficients of the first with the second tooth of a two tooth labyrinth seal (case 11 in Appendix B). It can be observed that the discharge coefficient of the second tooth is higher than the first due to the effects of the kinetic energy carry over. It can also be observed that the deviation in the discharge coefficient of the second tooth from that of the first tooth is higher at higher Reynolds number. The respective carry over coefficient is also shown in the same plot for comparison. The deviation of the discharge coefficient appears to be related to the carry over coefficient.
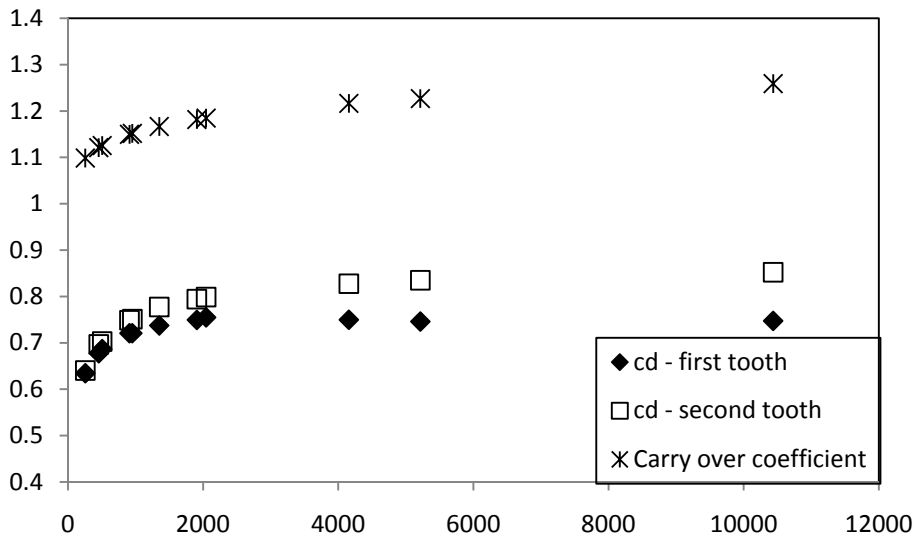


**Figure 6.14. Discharge coefficients of first and second teeth of a two teeth labyrinth seal and respective carry over coefficient.**

Many of the existing leakage models [3, 7, 8, and 10] model this relationship of the discharge coefficient of the downstream teeth and the carry over coefficient by establishing a linear relationship between the mass flow rate and the carry over

coefficient. Based on the earlier literature, it was attempted to establish a linear relationship between the carry over coefficient and the discharge coefficient of the second tooth. The CFD simulations predict, as it can be seen from Figure 6.15, the discharge coefficient is not a linear function of the carry over coefficient. Further, the relationship between $C_d$ and $\gamma$ seems to be different for different tooth geometries.
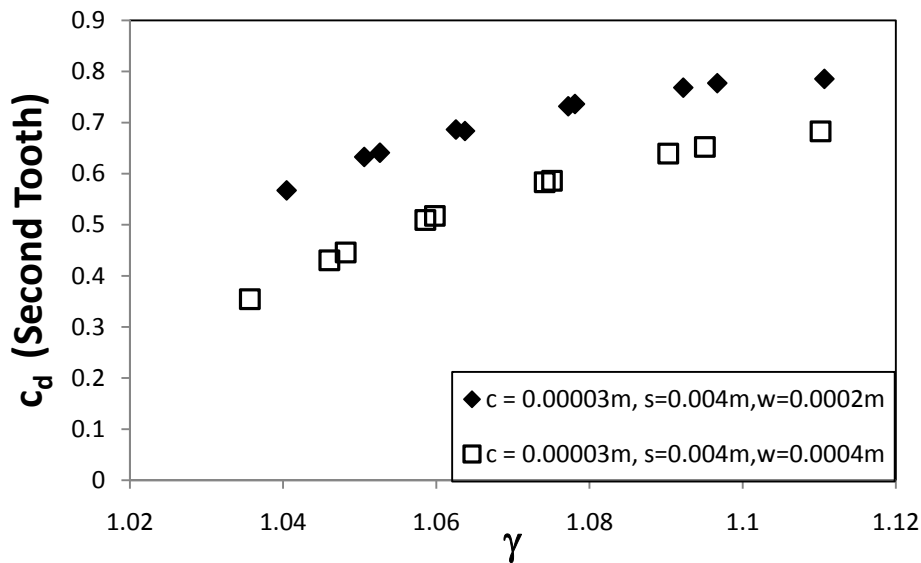


**Figure 6.15. Relationship between discharge coefficient of second tooth of a two teeth labyrinth seal and respective carry over coefficient (cases 35 and 39).**

It has to be noted that this non-linearity and the dependence on geometry were addressed by some of the earlier investigators [7] by incorporating an experimentally determined flow coefficient, $\alpha$ (which also is to account for various other effects like the $C_d$ of the first tooth being different from subsequent teeth). It could be possible that this flow coefficient could be related to the discharge coefficient of the equivalent single tooth labyrinth seal (which is also the $C_d$ of the first tooth).

The discharge coefficients of subsequent teeth seem to depend on both the respective first tooth discharge coefficient and the carry over coefficient. It is thus aimed to establish

$$C_d = f ( C_d^{\text{first tooth}} , \gamma) \tag{6.4}$$

It was assumed that $C_d$ of subsequent teeth should be linearly proportional to the $C_d$ of the first tooth. Defining z as the ratio of the discharge coefficient of the second tooth to that of the first tooth (or discharge coefficient of equivalent seal with single tooth), z should be a function of the carry over coefficient.

$$z = \frac{C_d}{C_d^{\text{first tooth}}} = f(\gamma) \tag{6.5}$$

Hence z was calculated and its functional dependence upon $\gamma$ was investigated. Figure 6.16 shows the dependence of z upon $\gamma$ for different c/s ratios (when all other geometry is fixed) while Figure 6.17 considers how w/s changes the relationship. It can be concluded that the z - $\gamma$ relationship is independent of geometry or flow.
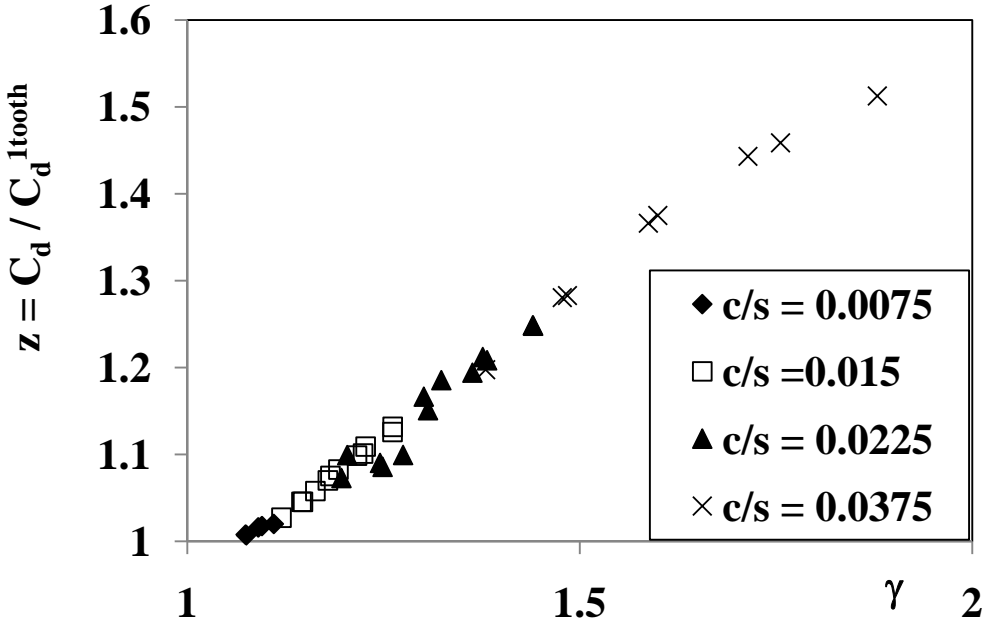
**Figure 6.16. Relationship between z and γ for different c/s ratios (cases 13, 15-17).**
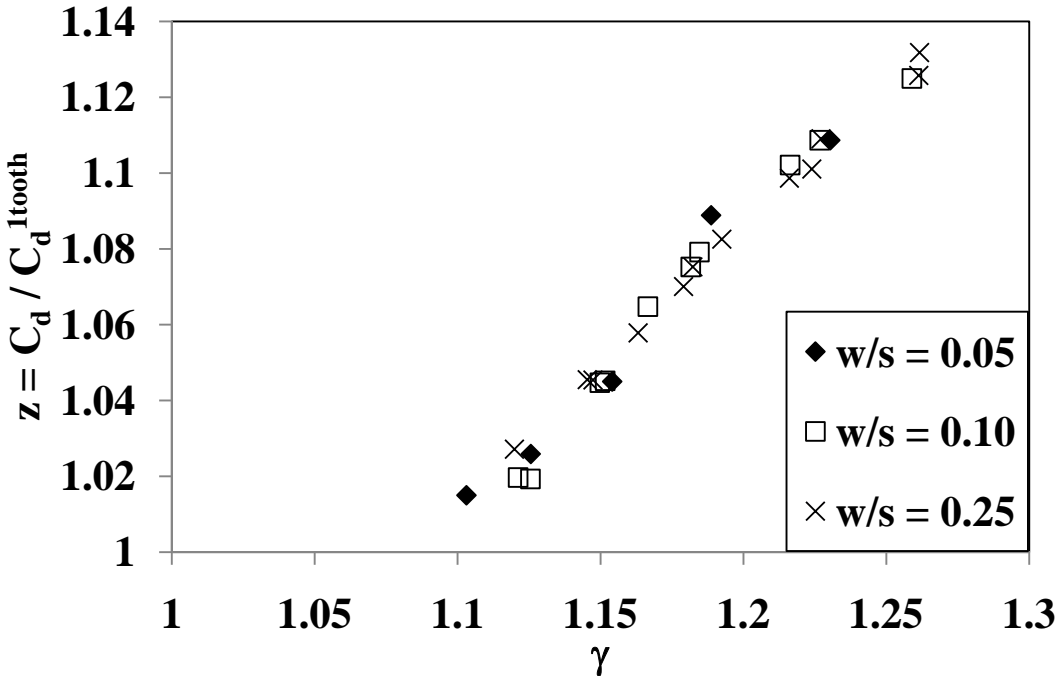


**Figure 6.17. Relationship between z and γ for different w/s ratios (cases 10, 11, 13).**

**MODEL FOR DISCHARGE COEFFICIENT FOR SUBSEQUENT TEETH**

When z is calculated for all incompressible data consisting of simulations of seals with different clearances, pitch, tooth width (all cases in Appendix B except 1-8, 19-21 which have very thin teeth), tooth height, number of teeth (for each subsequent tooth) and shaft diameter and plotted as a function of the respective carry over coefficients in Figure 6.18, a very important relationship is evident.

It is essential to note that the data set consists of different inlet and exit pressures, pressure ratios and Reynolds numbers. It can be seen that there is a reasonable collapse of all the data onto a single relationship. The scatter that is observed at higher $\gamma$ is possibly due to the characteristic scatter that was observed in carry over coefficient.
It has to be noted that the predicted values of $C_d$ for first tooth (based on equation 6.3) and $\gamma$ (based on equation 5.9) are employed instead of the actual measured values. This is done so that the errors associated with the respective prediction algorithms may be corrected/compensated while developing this final model for incompressible flow.
The equation

$$z = 0.925\gamma^{0.861} \tag{6.6}$$

is used to fit the data and is valid for all geometries and operating conditions (provided $c/s < 0.05$, $h/s > 0.75$, $w/c > 2.67$, $w/s < 0.5$, $250 < Re < 15000$). The standard deviation is 1.93% and the maximum error is 5.7%.

It has to be noted that these errors represent the net errors (including the errors in the prediction algorithms of carry over coefficient and discharge coefficient of 1st tooth) for the prediction of discharge coefficient for incompressible flow.

The figure shows a scatter plot with the y-axis labeled $z = C_d / C_d^{1tooth}$ ranging from 0 to 1.8, and the x-axis labeled $\gamma$ ranging from 0 to 2.5. The data points follow the curve fit equation $z = 0.925\gamma^{0.861}$.
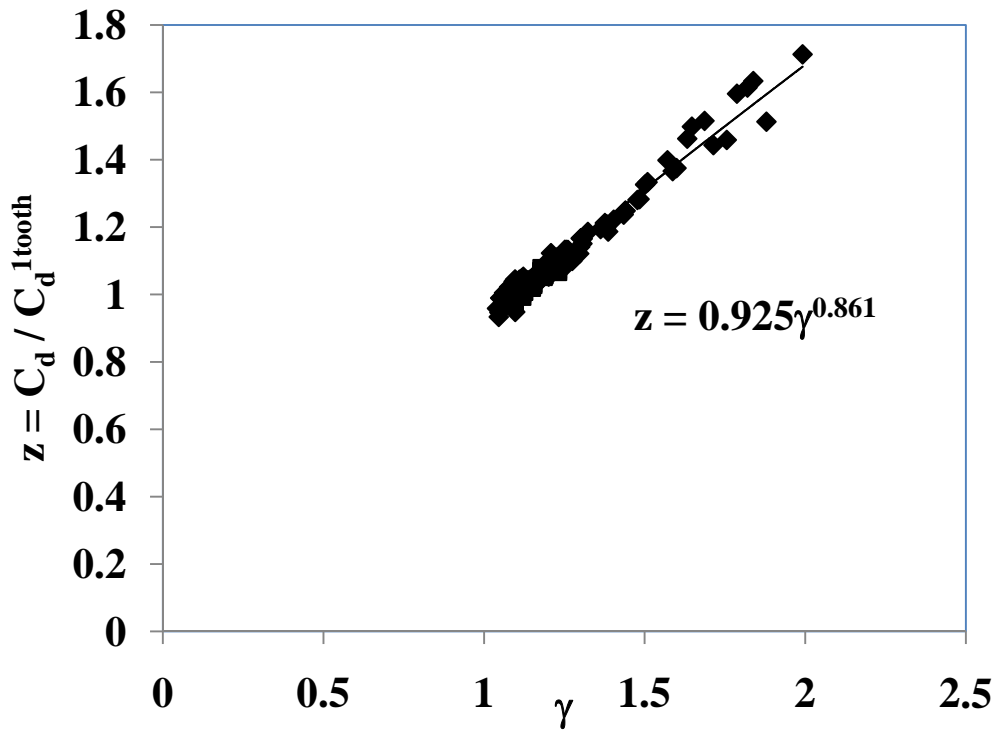
**Figure 6.18. Relationship between Z and $\gamma$ for entire incompressible dataset with employed curve fit.**

Thus, by employing the models developed for discharge coefficient and carry over coefficient, an algorithm can be developed to not only predict leakage for incompressible flow but also the pressure distribution across the seal provided the inlet and exit pressures are known. This model can also be used for gases, provided $Pr > 0.7$ (as shown in the next chapter). For such cases, the density for each cavity is calculated based on the cavity pressure (using ideal gas equation) and the pressure and density of the fluid upstream of a tooth is used to calculate the pressure drops across the tooth. A program for such a case is also included.

The equations are summarized as:

$$\dot{m} = C_{d_n} A \sqrt{2\rho_n (p_n - p_{n+1})} \qquad\qquad (\,1 \geq n \geq N) \qquad\qquad (6.7)$$

For $0.0075 < c/s < 0.0375$, $0.0075 < w/s < 0.5$, $2.67 < w/c < 66.67$ and $0.75 < h/s < 4$, $250 < Re < 15000$.

Where

$$C_{d_n} = \begin{cases} C_d^{1tooth} \text{ for first constriction} & (n = 1) \\ C_d^{1tooth}(0.925\ \gamma^{0.861}) \text{ for subsequent teeth} & (n > 1) \end{cases}$$

$$C_d^{1\ tooth} = \frac{\left(0.7757 - 0.002051\left(\frac{w}{c}\right)\right)}{\left(1 + \frac{44.86\left(\frac{w}{c}\right)}{Re}\right)^{0.2157}}$$

$$\gamma = \left(1 - 6.5\ \left(\frac{c}{s}\right) - 8.638\ \left(\frac{c}{s}\right)\left(\frac{w}{s}\right)\right)(Re + R_0)^{\left(2.454\left(\frac{c}{s}\right) + 2.268\left(\frac{c}{s}\right)\left(\frac{w}{s}\right)^{1.673}\right)},$$

$$R_0 = \left(1 - 6.5\ \left(\frac{c}{s}\right) - 8.638\left(\frac{c}{s}\right)\left(\frac{w}{s}\right)\right)^{\left(-\frac{1}{2.454\left(\frac{c}{s}\right) + 2.268\left(\frac{c}{s}\right)\left(\frac{w}{s}\right)^{1.673}}\right)}$$

$$Re = \frac{\dot{m}}{\pi D \mu}$$

When $p_1$ and $p_{N+1}$ are known, the above models result in a system N equations and N variables ($\dot{m}$, $p_2$, $p_3$,.. $p_N$) . Even though the system is non-linear, it can be solved easily using MS Excel's Solver or using the MATLAB code presented in Appendix C. The time required to compute the results is less than a second.

The program solves the set of equations by Newton's method of successive iteration. Martin's equation is used to initialize the mass flow rate, based on which the Reynolds number, the carry over coefficient and discharge coefficient are computed. The pressures in the seal cavities are calculated. Then, the mass flow rate is recalculated based on the

discharge coefficient for the final constriction, since the exit pressure is known. This new mass flow rate is used to correct the one used in the previous iteration using a relaxation factor in order to increase the stability. The process is repeated until convergence. This algorithm is explained in the flowchart in Figure 6.19. The variables used in the program and the corresponding physical quantities and symbols used in the thesis text are listed in Table 6.1

**Table. 6.1. List of variables used in program to compute leakage.**

| VARIABLE NAME | QUANTITY | UNIT | SYMBOL USED IN TEXT |
|---|---|---|---|
| c | Radial clearance | m | c |
| s | Tooth pitch | m | s |
| w | Tooth width | m | w |
| D | Shaft diameter | m | D |
| Pi | Seal inlet pressure | Pa | $P_i$ |
| Pe | Seal exit pressure | Pa | $P_e$ |
| j | Index for Tooth number | | |
| p(j) | Pressure upstream of $j^{th}$ tooth | Pa | $p_j$ |
| rho | Density for liquids | kg/m3 | $\rho$ |
| rho(j) | Density upstream of $j^{th}$ tooth (gases) | kg/m3 | $\rho_j$ |
| mdot | Leakage mass flow rate | kg/s | $\dot{m}$ |
| | | | |
| i | count for number of iterations | | |
| Re | Reynolds number based on clearance | | Re |
| gamma | Carry over coefficient | | $\gamma$ |
| cd1 | Discharge coefficient for equivalent seal with single tooth ( also discharge coefficient of first tooth) | | $C_d^{1tooth}$ |
| tdc | Discharge coefficient for subsequent tooth | | $C_d$ |
| mdot1 | | kg/s | |
| Error | Relative error between mdot computed between two iterations | | |
| imax | Maximum number of iterations (default value =10000) | | |
| E | Error to achieve Convergence (default value = 0.0001) | | |
| omg | Relaxation factor (default value = 0.1) | | |
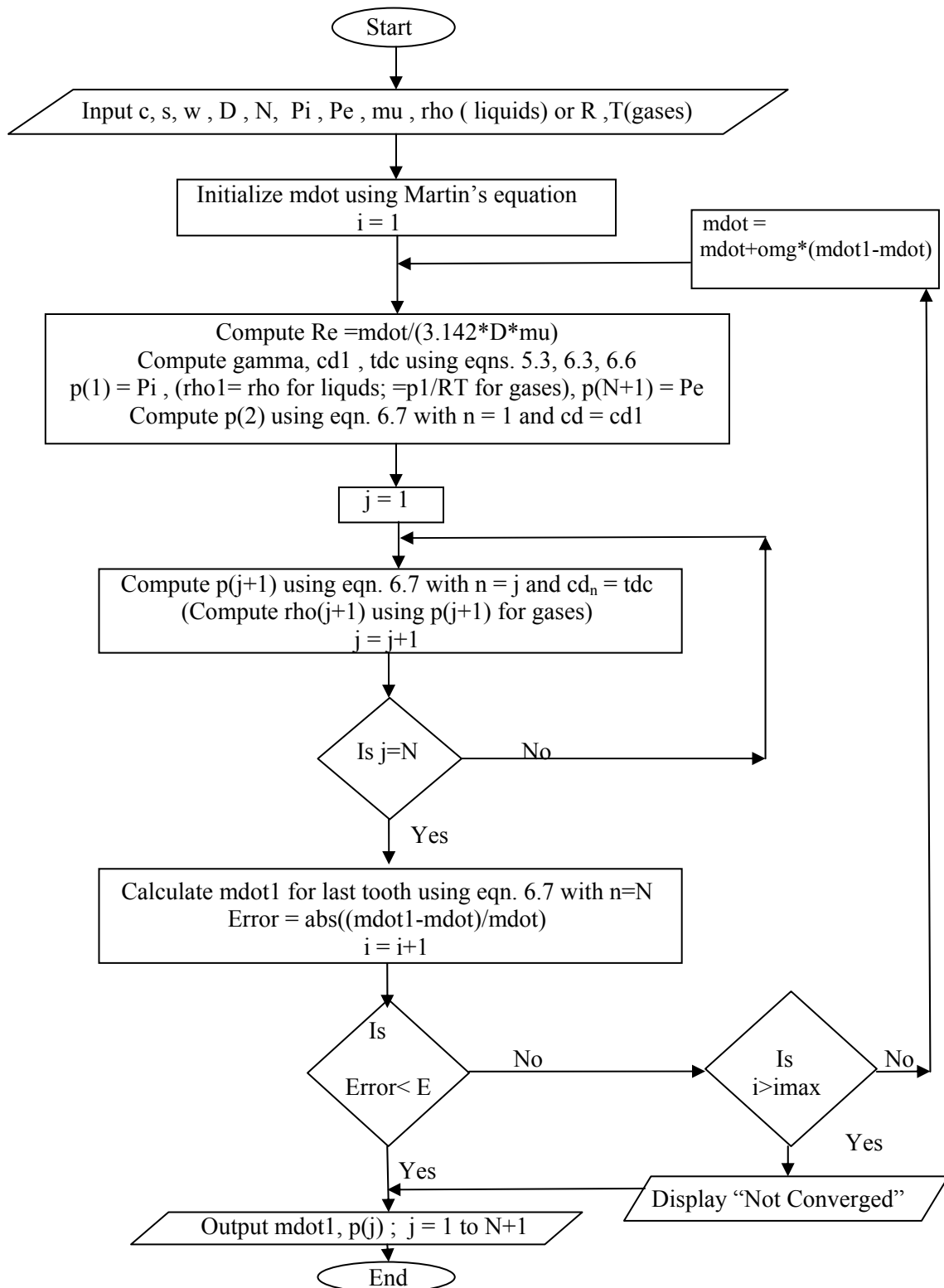
**Figure 6.19. Flow chart for leakage prediction for incompressible flow.**

## CHAPTER VII

## EFFECT OF COMPRESSIBILITY

The earlier sections dealt with incompressible flow through labyrinth seals. A model for carry over coefficient was developed for incompressible flow and its effect on labyrinth seal leakage was analyzed and modeled. A complete equation for predicting leakage for incompressible flow was developed by using CFD simulations that use water as the working fluid.

Labyrinth seals are used in all kinds of turbomachinery utilizing compressible fluids. Hence, there was a need to develop a model that provides accurate leakage prediction for compressible fluids. This section emphasizes using air as the working medium. As seen in Figure 7.1, the model developed in the earlier section, can be used to arrive at reasonably accurate estimation of leakage and pressure distribution for air as long as the individual tooth pressure ratios are greater than 0.7. However at lower pressure ratios, the incompressible model deviates from the CFD results. This is expected as at lower pressure ratios, effects of compressibility become marked and hence an expansion factor, $\psi$, needs to be incorporated into the model.
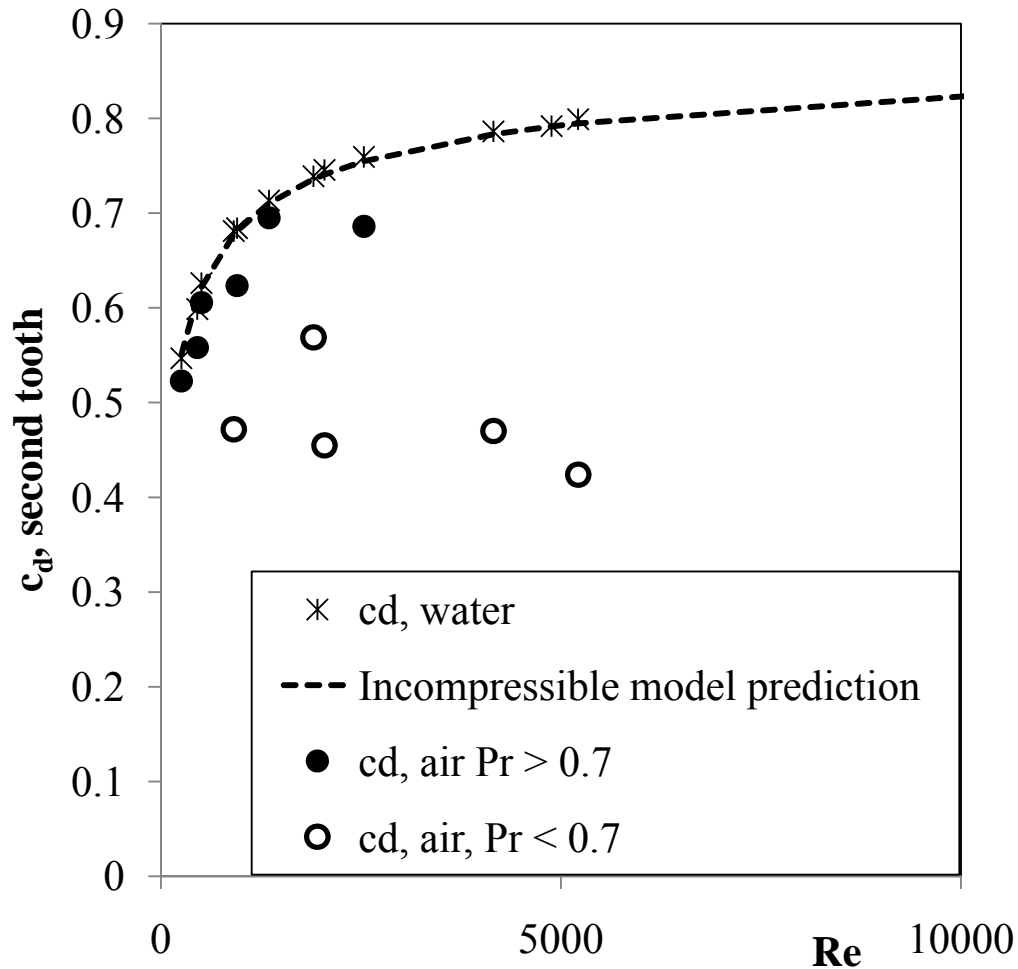
**Figure 7.1. Comparison of discharge coefficients of incompressible and compressible flow (for the second tooth of two tooth labyrinth seal, case 13 in Appendix B).**

Martin's equation [4], which has also formed the basis for models given by Egli [7] and Hodkinson [8] and Vermes [9] has the term $\sqrt{\dfrac{\left(1-\left(\frac{p_e}{p_i}\right)^2\right)}{N-\ln\left(\frac{p_e}{p_i}\right)}}$ to compensate for compressibility effects.

**EXPANSION FACTOR – DEFINITION**

   This thesis defines the expansion factor, $\psi$, as the ratio of the discharge coefficient of a tooth (that includes effect of kinetic energy carry over) for compressible flow to that for incompressible flow through a seal with same geometry and at same Reynolds number. Further, this thesis compares the discharge coefficients computed from CFD simulations of compressible flow with the incompressible discharge coefficient predicted by the model presented in chapter VI.

$$\dot{m} = \psi\, c_d A \sqrt{2\rho_i (p_i - p_e)} \tag{7.1}$$

 Where

$$c_d = c_d^{1tooth} \qquad\qquad\qquad \text{for first constriction.}$$

$$c_d = c_d^{1tooth}(0.925\,\gamma^{0.861}) \quad \text{for subsequent teeth.}$$

$$c_d^{1\,tooth} = \frac{\left(0.7757 - 0.002051\left(\frac{w}{c}\right)\right)}{\left(1 + \frac{44.86\left(\frac{w}{c}\right)}{Re}\right)^{0.2157}}$$

$$\gamma = \left(1 - 6.5\left(\frac{c}{s}\right) - 8.638\left(\frac{c}{s}\right)\left(\frac{w}{s}\right)\right)(Re + R_0)^{\left(2.454\left(\frac{c}{s}\right)+2.268\left(\frac{c}{s}\right)\left(\frac{w}{s}\right)^{1.673}\right)},$$

$$R_0 = \left(1 - 6.5\left(\frac{c}{s}\right) - 8.638\left(\frac{c}{s}\right)\left(\frac{w}{s}\right)\right)^{\left(-\frac{1}{2.454\left(\frac{c}{s}\right)+2.268\left(\frac{c}{s}\right)\left(\frac{w}{s}\right)^{1.673}}\right)}$$

   Therefore it has to be noted that this 'expansion factor' accounts for the effects of compressibility on the kinetic energy carry over, discharge coefficient and also on the relationship between $\gamma$ and $C_d$. Thus, in this study, the expansion factor, $\psi$, is evaluated by dividing the discharge coefficient obtained from the FLUENT CFD simulation with

air as working medium (ideal gas assumption) and by the discharge coefficient (of incompressible flow) predicted by equation 6.6 and 6.3.

The effect of flow parameters, seal geometry, shaft RPM, the number and position of teeth on the expansion factor for air is analyzed and discussed in the following sections. Following this approach, the study of the effect of gas properties will be taken into account.

**EFFECT OF FLOW PARAMETERS ON EXPANSION FACTOR**
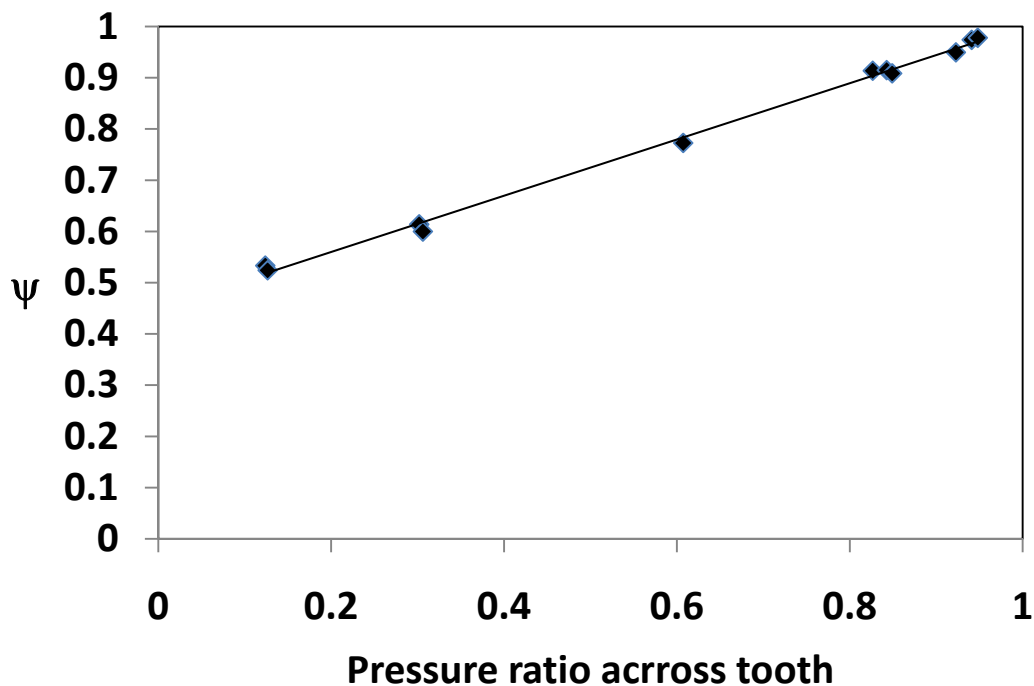


**Figure 7.2. $\psi$ for second tooth of a single cavity labyrinth seal (case 13 in Appendix B) at different backpressures and Reynolds numbers.**

The effects of compressibility are generally quantified by pressure ratio. In Martin's equation, the expansion factor is expressed as a function of overall pressure ratio and

number of teeth. In order to verify this idea of modeling expansion factor purely based on pressure ratio, CFD simulations are performed for different backpressures (1 bar, 2 bar and 5 bar) and Reynolds numbers (ranging from 250 to 10500) for a labyrinth seal with two teeth with c = 0.00006 m , s = 0.004 m and w = 0.001 m. The expansion factor is evaluated for the second tooth in each case and is plotted against the respective tooth pressure ratio (in this case, the ratio of seal exit pressure to the mean pressure in the cavity) in Figure 7.2. It can be observed that regardless of exit pressure or Reynolds number, the $\psi - $ Pr collapses into a single relationship. While there is a possibility that this relationship may depend upon geometric parameters (which will be analyzed in the forthcoming sections), it is clear from Figure 7.2 that pressure ratio across the tooth (not overall pressure ratio) is the only flow parameter that determines the expansion factor.

**EXPANSION FACTOR FOR FIRST AND DOWNSTREAM TOOTH**
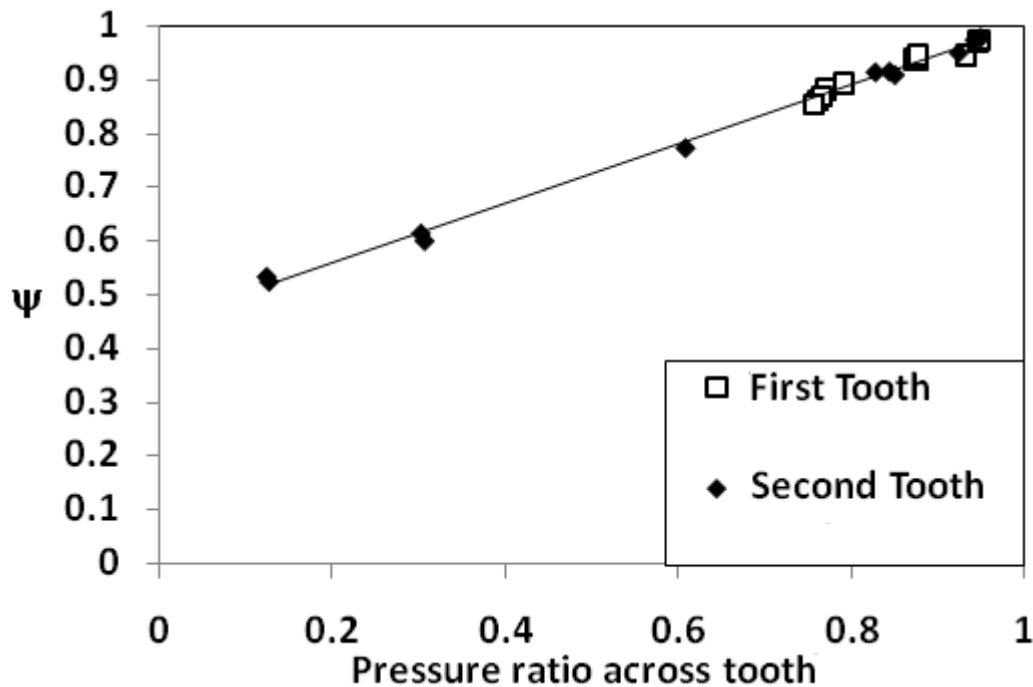


**Figure 7.3. Comparison of ψ for first and second tooth of a single cavity labyrinth seal (case 13 in Appendix B).**

Since the $C_d$ of the first tooth is different from the rest of the teeth due to the absence of a preceding cavity, there was a need to verify whether the expansion factor of the first tooth can be expressed by the same model as that of the subsequent teeth. It can be seen from Figure 7.3. that the expansion factor for the first tooth (evaluation based on ratio of the discharge coefficient of the first tooth for compressible flow to the $c_d^{1tooth}$ model developed for incompressible flow) does indeed bear the same relationship with pressure ratio as the expansion factor for the second tooth for the geometry and flow conditions considered in Figure 7.3.

**EFFECT OF SEAL GEOMETRY ON EXPANSION FACTOR**

In order to investigate whether seal geometry influences expansion factor, simulations are performed on seals with different clearances and tooth widths. The results are plotted in Figure 7.4 (for cases 10, 13 and 16 in Appendix B; Re ranges from 254 to 10437; back pressures of 1, 2 and 5 bar). It was found that $\psi$ is fairly independent of seal geometry within the limits considered. It has to be noted that clearance may have a small effect upon $\psi$, as it can be observed that as there is an increase in clearance, there is as slight increase in $\psi$. However since the change in $\psi$ is around 5% when clearance is increased by 50%, it is considered minimal and this effect was not incorporated into the model.
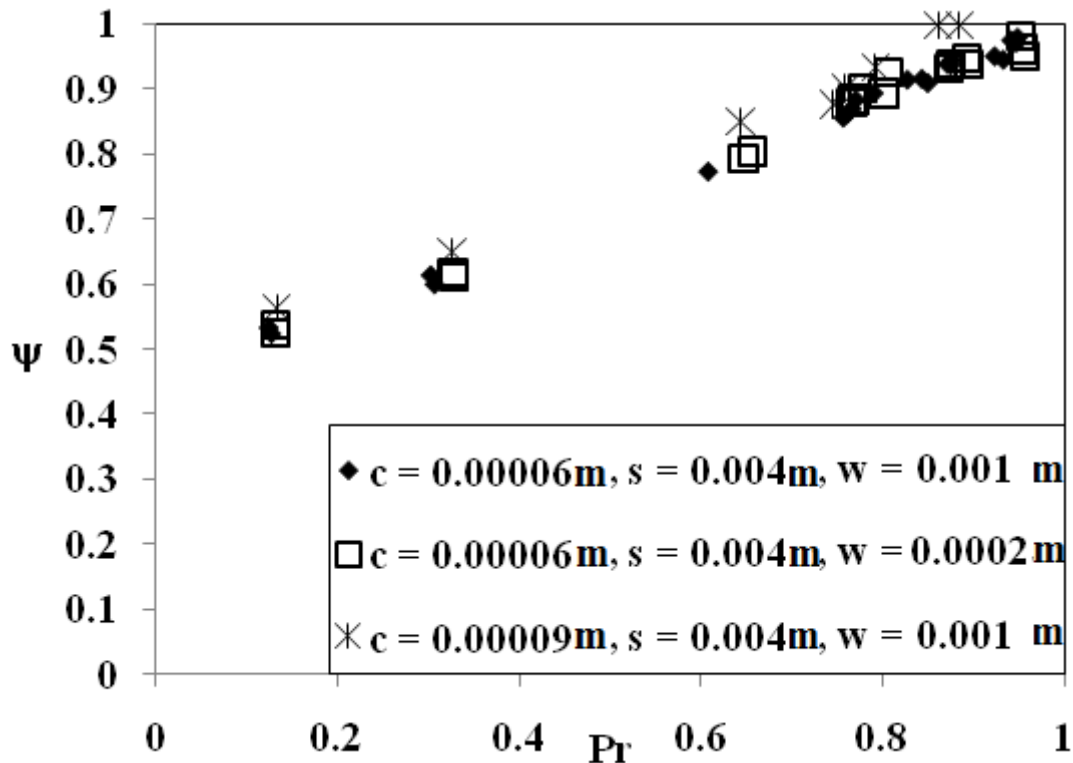


**Figure 7.4. Effect of seal geometry on expansion factor (cases 10, 13 and 16).**

**EFFECT OF POSITION AND NUMBER OF TEETH ON EXPANSION FACTOR**



The graph shows $\psi$ on the vertical axis (from 0 to 1) versus Pr on the horizontal axis (from 0 to 1).

Equation shown on the plot:
$$\psi = 0.558\ Pr + 0.442$$
$$R^2 = 0.9903$$

Legend:
- △ Tooth 1, 4 tooth seal
- ✕ Tooth 2, 4 tooth seal
- ✶ Tooth 3, 4 tooth seal
- ● Tooth 4, 4 tooth seal
- ◇ 2 tooth seal
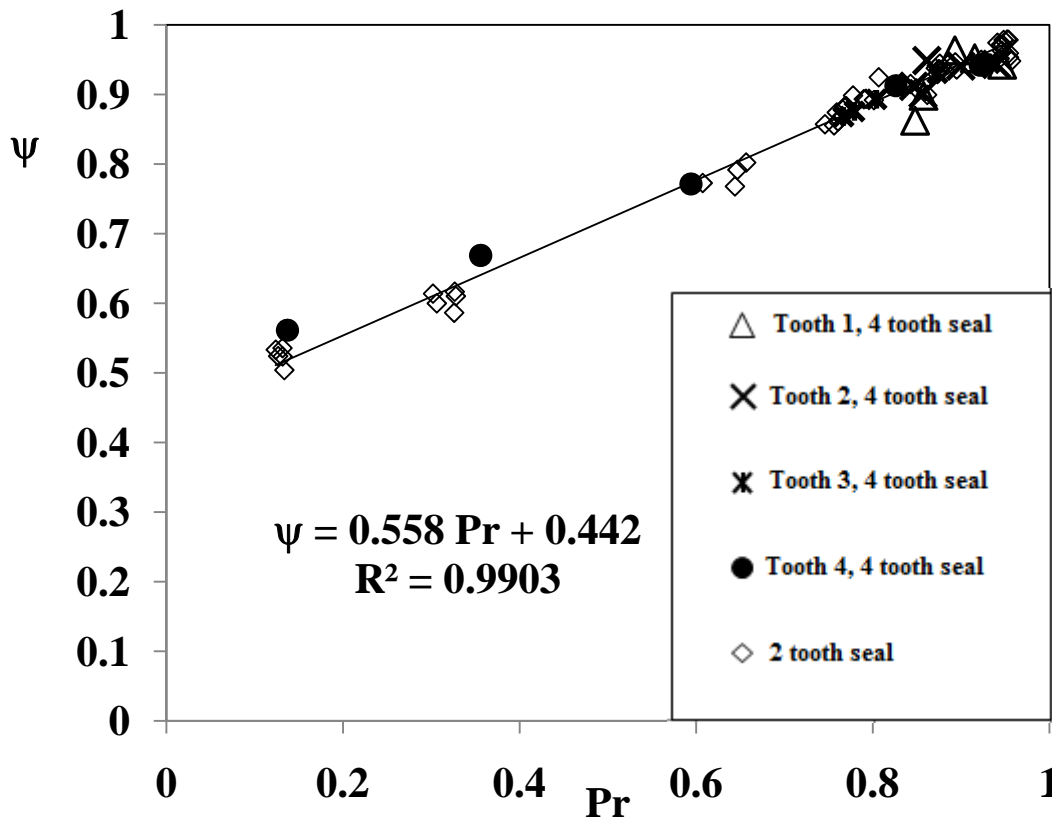
**Figure 7.5. Comparison of expansion factors for different teeth in a 4 tooth seal.**

The conclusions drawn in the above sections were based upon compressible simulations performed on labyrinth seal with a single cavity (two teeth). In order to extend the understanding to real world labyrinth seals which have multiple cavities, simulations are performed on a four tooth seal. The expansion factor is calculated for flow under each tooth. Figure 7.5 compares the expansion factor across different teeth of the multiple cavity seal (case 37 in Appendix B). It can be seen that the $\psi$ – Pr relationship is independent of the position of the tooth. The data for the two tooth seal (case 13 in Appendix B) is also included in Figure 7.5. It can be seen that $\psi$ across

different teeth in the four tooth seal follows the same relationship with pressure ratio as the two tooth seal. Hence it can be concluded that the expansion factor is independent of the number of teeth and only depends on the pressure ratio across a given tooth.

It has to be noted that these results do not necessarily contradict earlier models which contain the information on the number of teeth, as they are based on overall pressure ratio across the seal. The current work models the expansion coefficient across a tooth based on the tooth pressure ratio using the linear relationship shown below.

$$\psi = 0.558 \, Pr + 0.442 \tag{7.2}$$

It is interesting to note that the expansion factor for orifice flow meters behaves in a similar manner.

**EFFECT OF RATIO OF SPECIFIC HEATS ON EXPANSION FACTOR**
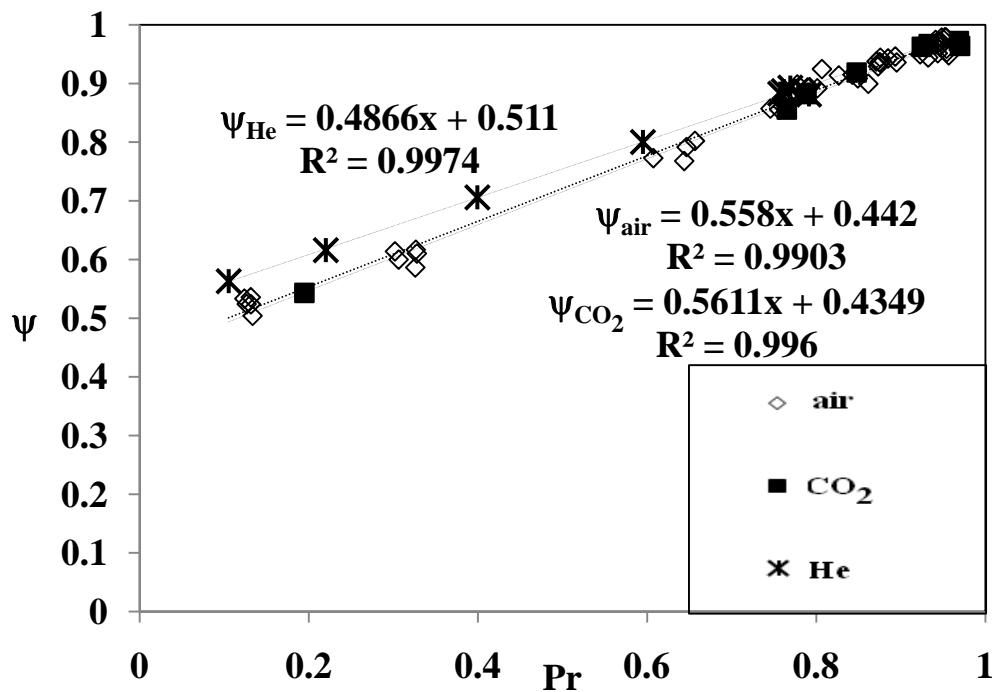


**Figure 7.6. Effect of ratio of specific heats on expansion factor.**

According to Martin's formula, leakage is independent of k (ratio of specific heats). But from the actual derivation, it can be seen that one of the terms contains the expression 2/k, which is rounded off to 1. In Neumann's model [10], the flow coefficient is a function of $\left(\left(\frac{p_i}{p_{i+1}}\right)^{\frac{k-1}{k}} - 1\right)$. The effect of k on the expansion factor requires further investigation as k is a significant parameter in the study of compressible flow. Thus the leakage rate may have a weak dependence upon k, which this section investigates.

The study carried out in the earlier section with air as working medium is extended for Carbon Dioxide and Helium, gases having extreme values of k. Carbon dioxide, being a triatomic molecule has k =1.3 , while Helium being a monatomic gas has k = 1.67.  Both Carbon dioxide and Helium may be encountered in real world labyrinth seals. The same geometric and flow conditions considered in Figure 7.3 are utilized for the Carbon Dioxide and Helium study.

From the results plotted in Figure 7.6 (case 13 in Appendix B), it can be seen that the expansion factor (which incorporates all effects of K) for $CO_2$ has a negligible deviation from that of air and hence this model may be used for leakage prediction of $CO_2$ over the entire range of conditions considered. However, it must be noted that this study assumes ideal gas behavior and the real gas behavior of $CO_2$ may deviate from the prediction significantly at elevated pressures. A study considering the effects of real gas models is beyond the scope of this thesis but is recommended for future work.

The effects of k are more marked in case of Helium, whose expansion factor has a greater deviation from that of air. However, it can be observed that the effects of

compressibility for Helium can still be modeled as a linear function of the pressure ratio, albeit with a smaller slope.

## ALGORITHM FOR LEAKAGE PREDICTION FOR COMPRESSIBLE FLOW

The algorithm for leakage prediction for incompressible flow presented in the last chapter is extended to predicting leakage for compressible flow by allowing for the variation of density based on pressure and ideal gas law and by incorporating the expansion factor. The model given by eqn. 7.2 is used to compute $\psi$ for every tooth. $\psi$ is initially set to 1 for all teeth. After the each iteration, $\psi$ is calculated for every tooth based on the computed pressures and is used for the next iteration. The variable Y[n] is used to represent $\psi$ of the $n^{th}$ tooth.

The algorithm is explained in the flow chart shown in Figure 7.7 and the corresponding MATLAB code is included in APPENDIX C.
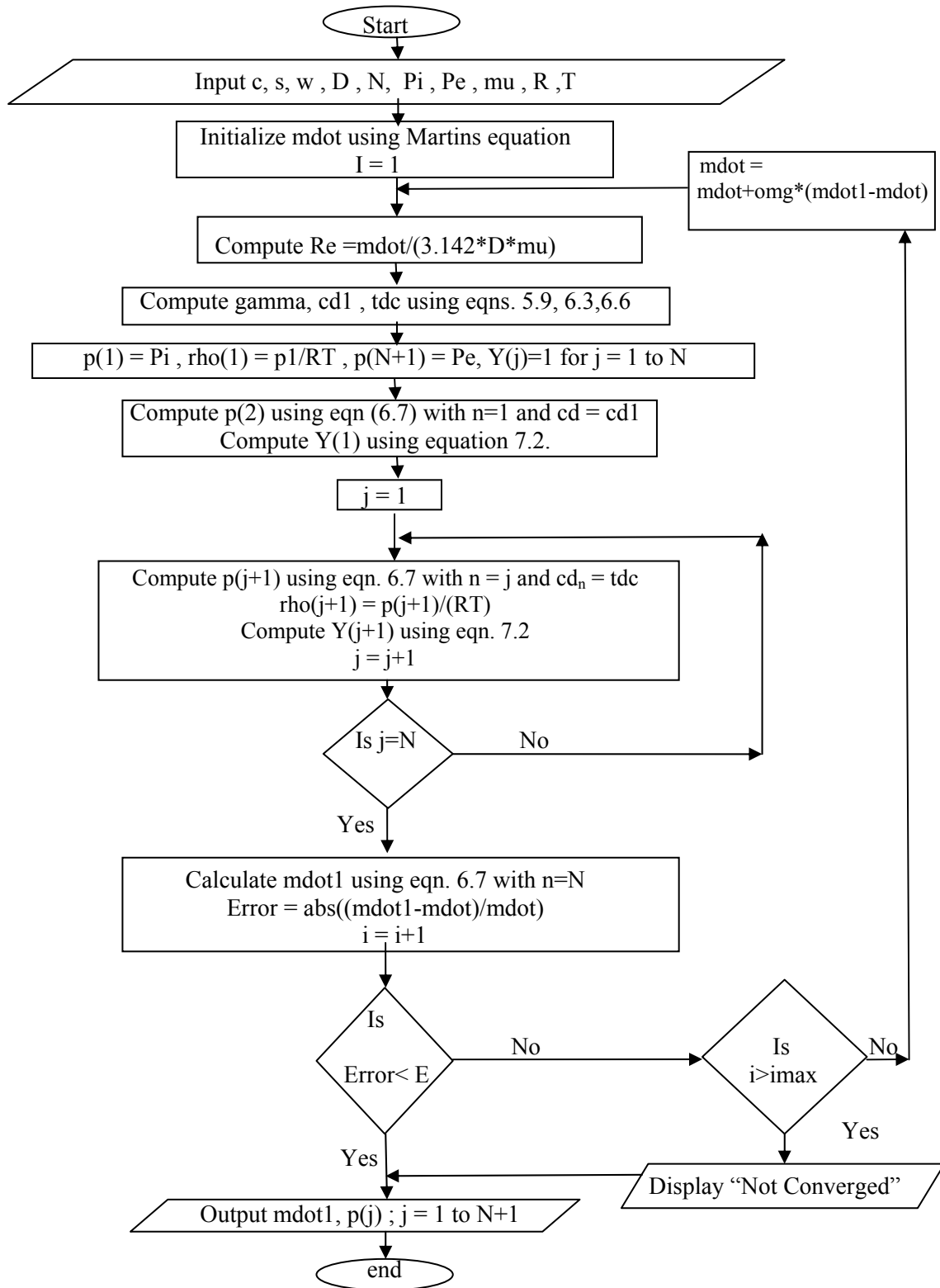
**Figure 7.7.** **Flow chart for leakage prediction incorporating model for ψ.**

# CHAPTER VIII

# VALIDATION

In this chapter, the models developed in this thesis are evaluated against prior experiments conducted by other researchers. While the models themselves have been developed from CFD simulations which employ turbulence models and numerical schemes that have been validated against experiments for similar geometries, it was felt necessary to apply the model to independent experiments and carry out a direct comparison of the model predictions against the experimental results. This study will indicate the accuracy of the leakage prediction algorithm developed in this thesis and also indicate the range of geometries and flow conditions for which the model provides accurate prediction. The data for this section is taken from two sources, namely, Cogan's thesis [2] and Gamal's dissertation [3].

Cogan did not perform experiments of his own, but developed a program to predict leakage for incompressible flow through labyrinth seals by interpolation of experimental data collected from published results. For all the experimental data he considered, Cogan, non-dimensionalized leakage in terms of flow coefficient as

$$\alpha = \frac{\dot{m}}{\gamma\,A}\sqrt{\frac{n-\ln\left(\frac{P_e}{P_i}\right)}{1-\left(\frac{P_e}{P_i}\right)^2}}$$ , where $\gamma$ is the carry over coefficient used by Hodkinson.

Therefore $\alpha$ represents the ratio of mass flow rate to the mass flow rate predicted by Hodkinson's equation. It has to be noted that the current study directly takes data from Cogan's thesis as it is presented in a more usable table format.

**VALIDATION AGAINST EXPERIMENTS PERFORMED BY YAMADA**

Yamada [24] in 1962 performed experiments with incompressible flow through labyrinth seals. His study involved a number of experiments where he determined the influence of various flow and geometrical parameters on leakage. He expressed his results in terms of friction coefficient.

The detailed geometry and test conditions of Yamada are included in Appendix D. Figures 8.1 – 8.4 compare the flow coefficient based on Yamada's experiments and predictions obtained using program 1 in Appendix C, which is based on the leakage prediction algorithm of incompressible flow covered in Chapter VI. This algorithm was developed for $0.0075 < c/s < 0.0375$, $0.0075 < w/s < 0.5$, $2.67 < w/c < 66.67$ and $0.75 < h/s < 4$.

Figures 8.1 – 8.3 plot the flow coefficient against pressure ratio (essentially mass flow rate as a function of inlet pressure, as exit pressure is kept constant) for different clearance to pitch ratios (clearance is varied while pitch is fixed). It can be observed that reasonably accurate predictions are obtained for c/s of 0.0433 (Figure 8.1). The RMS of the percentage error is 12.5% for this clearance to pitch ratio which is approximately 20% more than the maximum c/s for which the algorithm has been developed. This can be considered as a significant improvement over Hodkinson's model, which when used without any experimentally determined 'correction', results in $\alpha = 1$ in the plots, as mass flow rate is non-dimensionalized by Hodkinson's predictions (resulting in RMS of 49.7% for Figure 8.1). (It has to be noted that Hodkinson's equation was developed for gases).

The model under predicts leakage by a larger percentage for higher clearances as seen in Figures 8.2 and 8.3. This is due to the model for γ, which has been developed for smaller c/s ratios. The RMS of % errors are 16.5% for c/s ratio of 0.062 and 40.2% for c/s of 0.0925, both of which are much larger than the maximum c/s of 0.0375 of the simulations from which the model was developed. Hence, the error encountered when increasing c/s above 0.0375 is not unexpected.
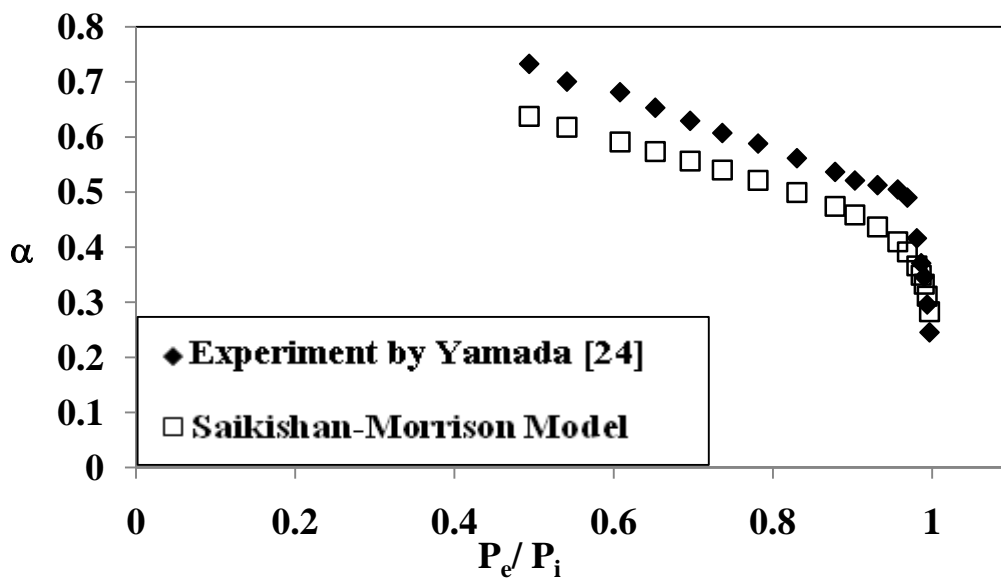


**Figure 8.1. Comparison of predicted and Yamada's experimentally determined flow coefficient for c/s = 0.0433 (w/s = 0.2487, $P_e$ = 101320 Pa, N = 20).**

82
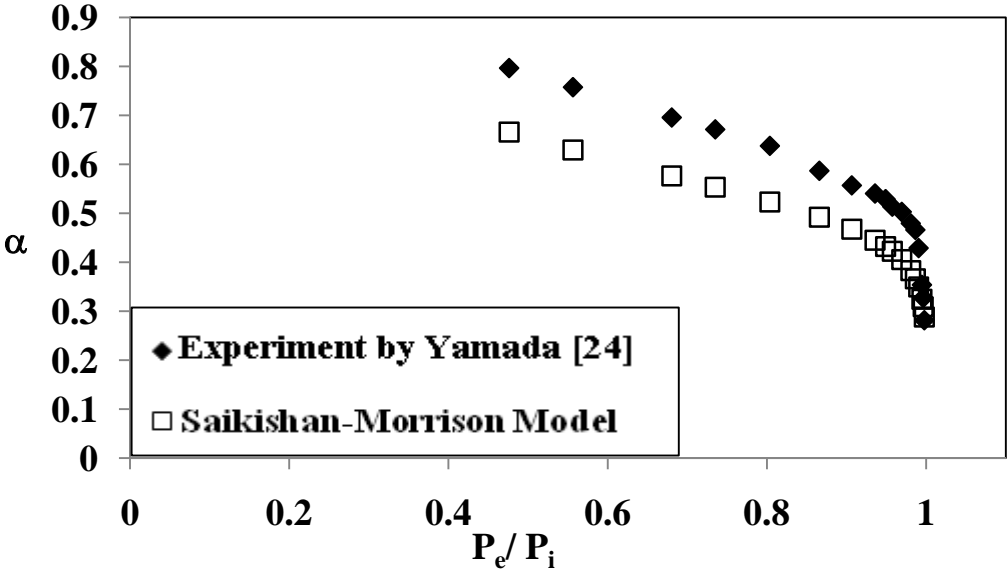


**Figure 8.2. Comparison of predicted and Yamada's experimentally determined flow coefficient for c/s = 0.062 (w/s = 0.2487, $P_e$ = 101320 Pa, N = 20).**
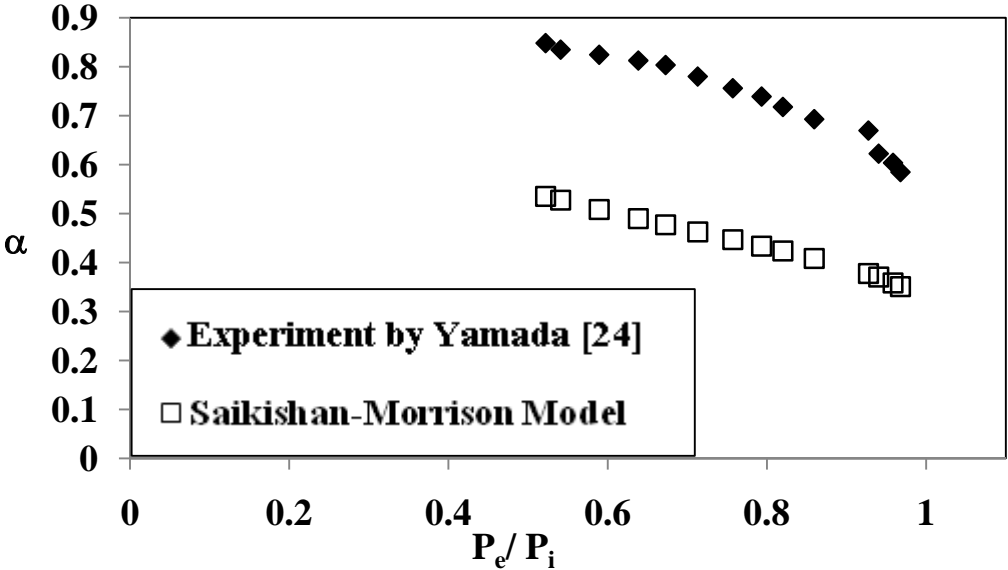


**Figure 8.3. Comparison of predicted and Yamada's experimentally determined flow coefficient for c/s = 0.0925 (w/s = 0.2487, $P_e$ = 101320 Pa, N = 20).**
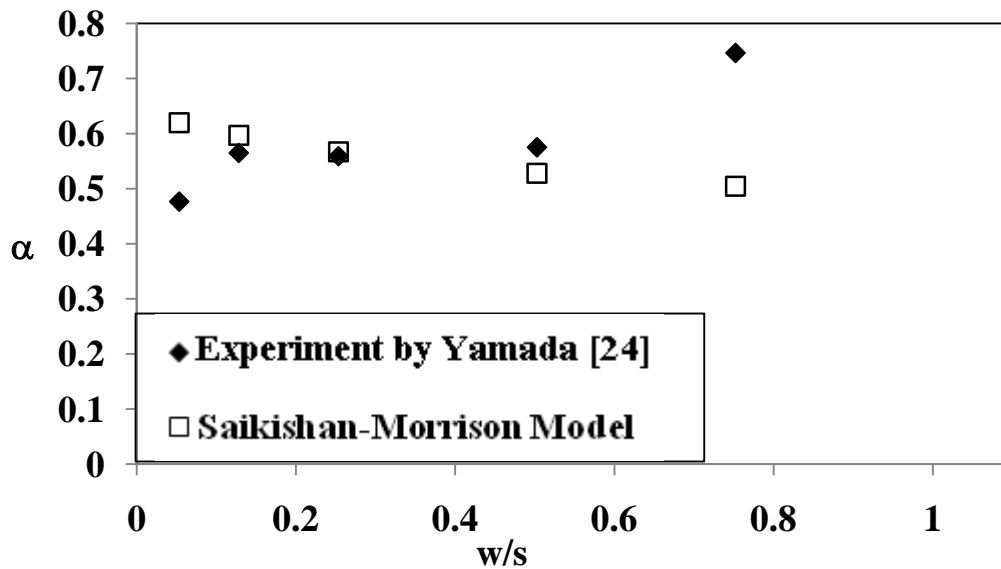
**Figure 8.4. Comparison of predicted and Yamada's experimentally determined flow coefficient for different w/s (c/s = 0.04574, $P_i$ = 111341 Pa, $P_e$ = 101320 Pa).**

In Figure 8.4, the variation of Yamada's experimental leakage rate with tooth width is compared to the values predicted by the model developed in this thesis. It can be seen that the predicted flow coefficients are very close to the experimental values (error < 10%) except for the first and last data points. The model over predicts the leakage by 30% for the first data point (w/s = 0.05). This deviation is due to the fact the w/c ratio for this case is 1.165 which is below the lower limit of 2.67 for which the model for the $C_d^{1tooth}$ (eqn. 6.3) term can be used. The model under predicts leakage by 32% for w/s = 0.752 which is outside the w/s range for the model for $\gamma$ (eqn. 5.9) where the maximum w/s is 0.5.

**VALIDATION AGAINST EXPERIMENTS BY NIKITIN AND IPATOV**
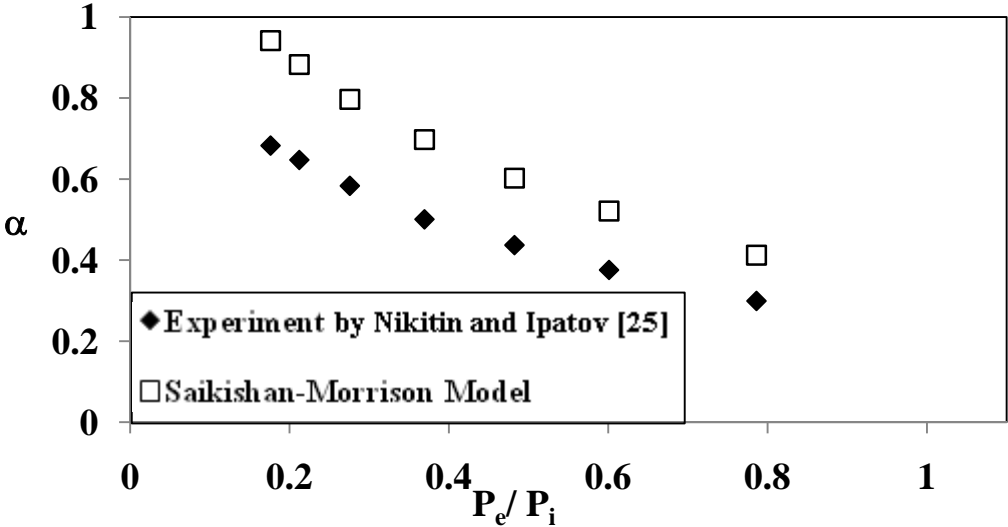


**Figure 8.5. Comparison of model predicted flow coefficients with Nikitin and Ipatov's experimental data for 2 throttles (Refer Appendix D for geometry and operating conditions).**
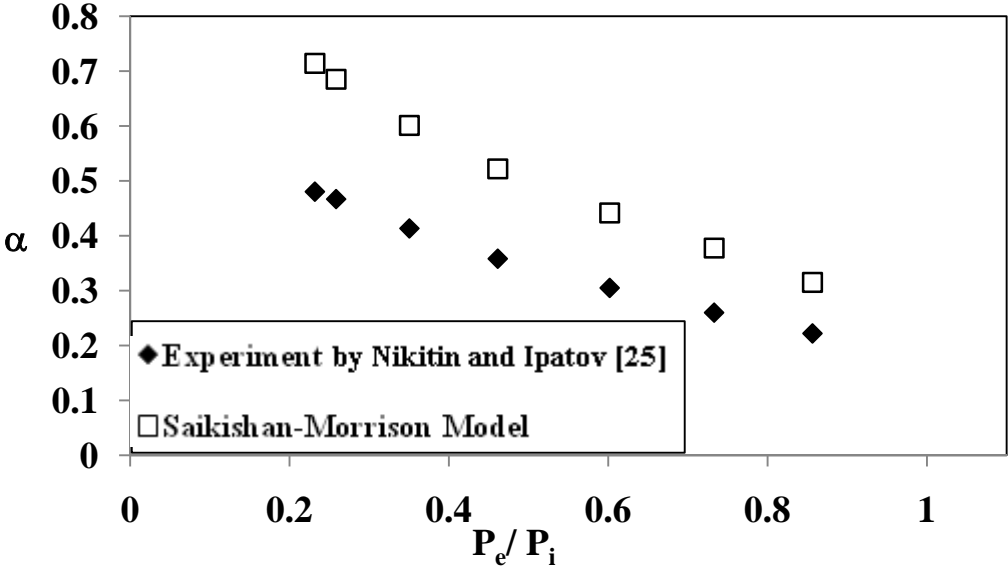


**Figure 8.6. Comparison of model predicted flow coefficients with Nikitin and Ipatov's experimental data for 3 throttles.**
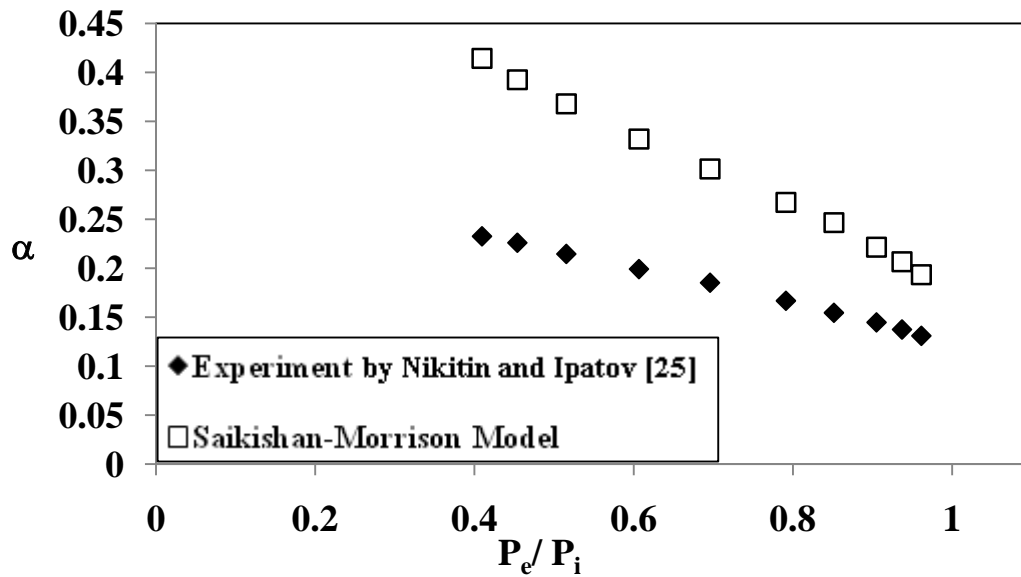
**Figure 8.7. Comparison of model predicted flow coefficients with Nikitin and Ipatov's experimental data for 7 throttles.**

Figures 8.5, 8.6 and 8.7 compare the flow coefficients experimentally determined by Nikitin and Ipatov [25] and corresponding flow coefficients obtained by using the incompressible model developed in this thesis. It can be seen that the model over predicts the leakage rate. This is perhaps due to the fact the h/s ratio used was 0.34 which is well below the 0.75 limit imposed by the model for carry over coefficient. This would indicate shallow cavities may be more efficient at reducing leakage. It is recommended that further studies are performed for shallow cavities.

**VALIDATION AGAINST GAMAL'S EXPERIMENTAL DATA**

Gamal conducted leakage tests on labyrinth seals with air as working medium. His data was organized into two sets A and B. 'Set A' consists of retrofitted seals which is not used for validation in this work.

The seal design for 'Set B' consisted of a seal holder, a set of blades, three sets of spacers, a set of cavity inserts, and a seal holder cap, allowing for a number of geometrical configurations. The matrix of data from his 'Set B' (included in Appendix D) consists of a number of seal geometries with different pitches, tooth widths and cavity depths tested for different inlet pressures. The leakage predictions based on algorithms developed in this work for compressible flow with and without the use of the expansion factor (allowing density change based on pressure but neglecting effect of compressibility on discharge coefficients) are compared to Gamal's experimental data `for 'Set B' in Figures 8.8 – 8.18. The details of the dimensions for each seal case are provided in Appendix D.
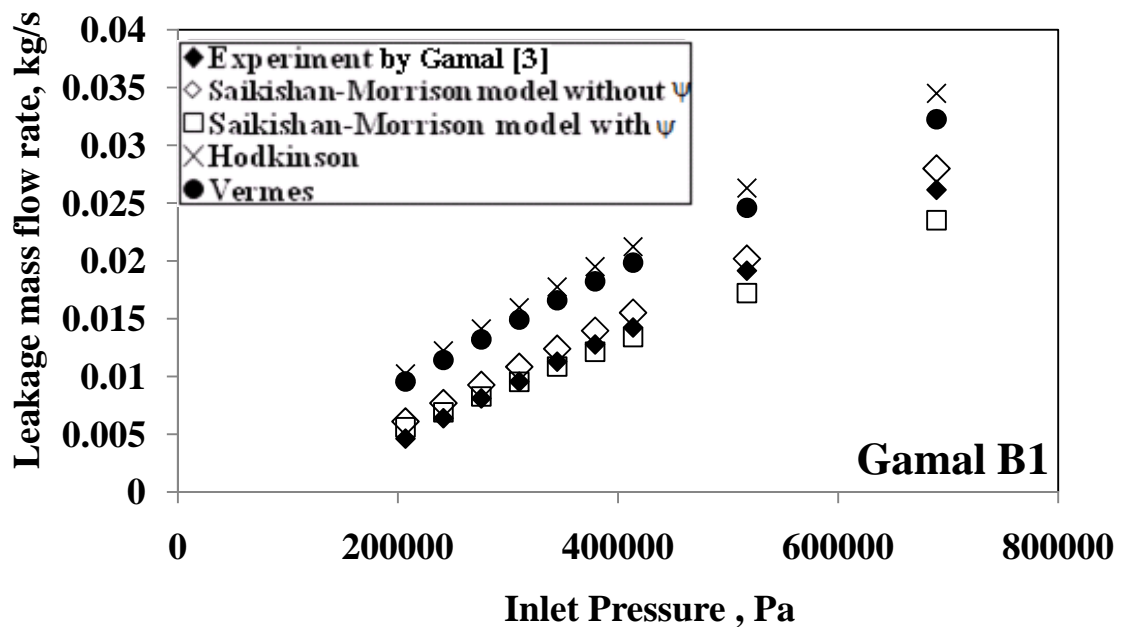


**Figure 8.8. Comparison of predicted leakage rates with Gamal's experimental data for seal B1 (c/s = 0.0064; w/s = 0.2013; h/s = 0.7987 ; N = 4).**
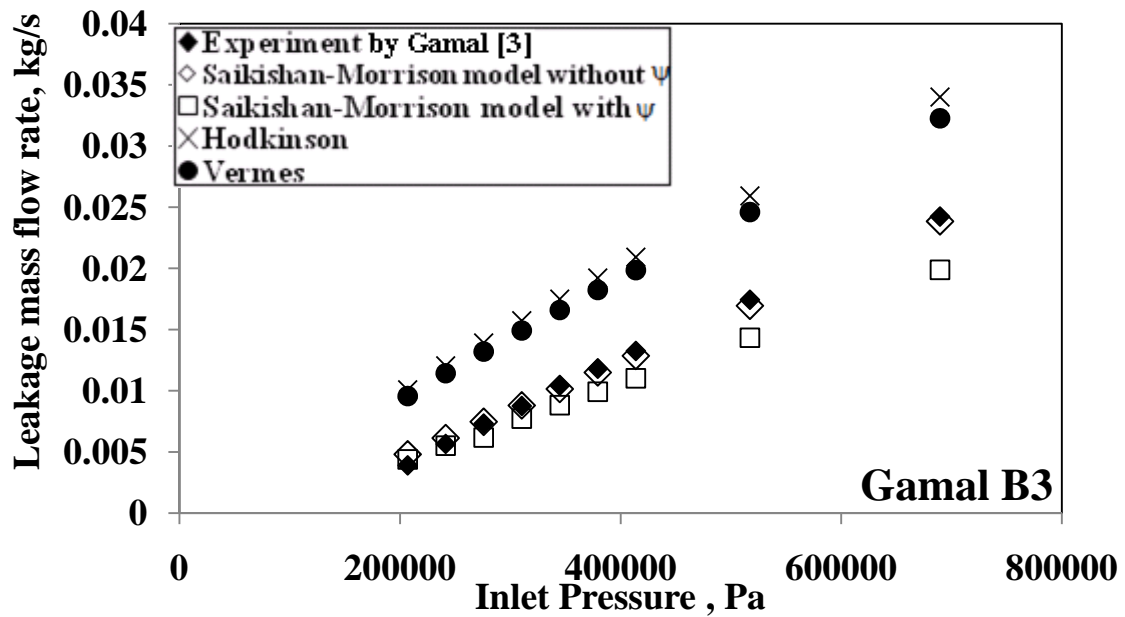
**Figure 8.9. Comparison of predicted leakage rates with Gamal's experimental data for seal B3 (c/s = 0.0053; w/s = 0.3351; h/s = 0.6649; N = 4).**
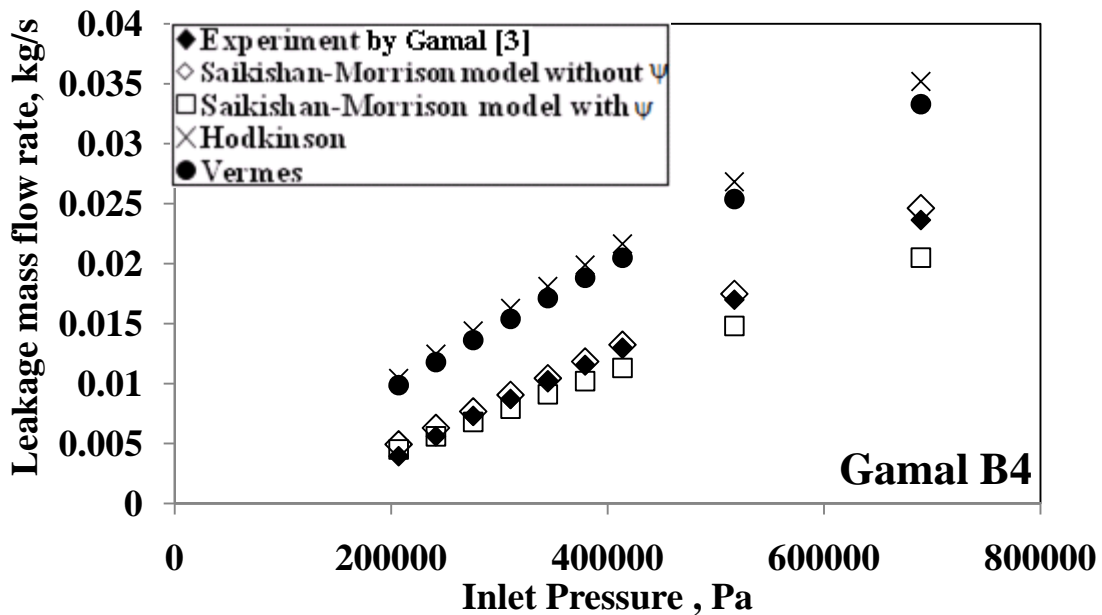


**Figure 8.10. Comparison of predicted leakage rates with Gamal's experimental data for seal B4 (c/s = 0.0080; w/s = 0.5; h/s = 0.99; N = 4).**

88
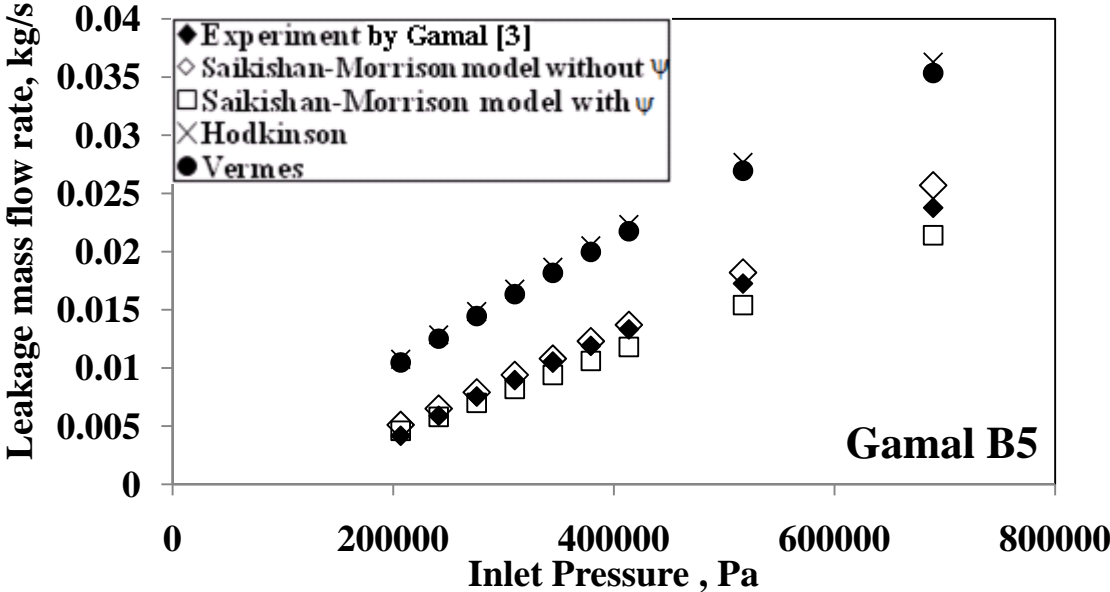


**Figure 8.11. Comparison of predicted leakage rates with Gamal's experimental data for seal B5 (c/s = 0.0106; w/s = 0.6667; h/s = 1.3229; N = 4).**
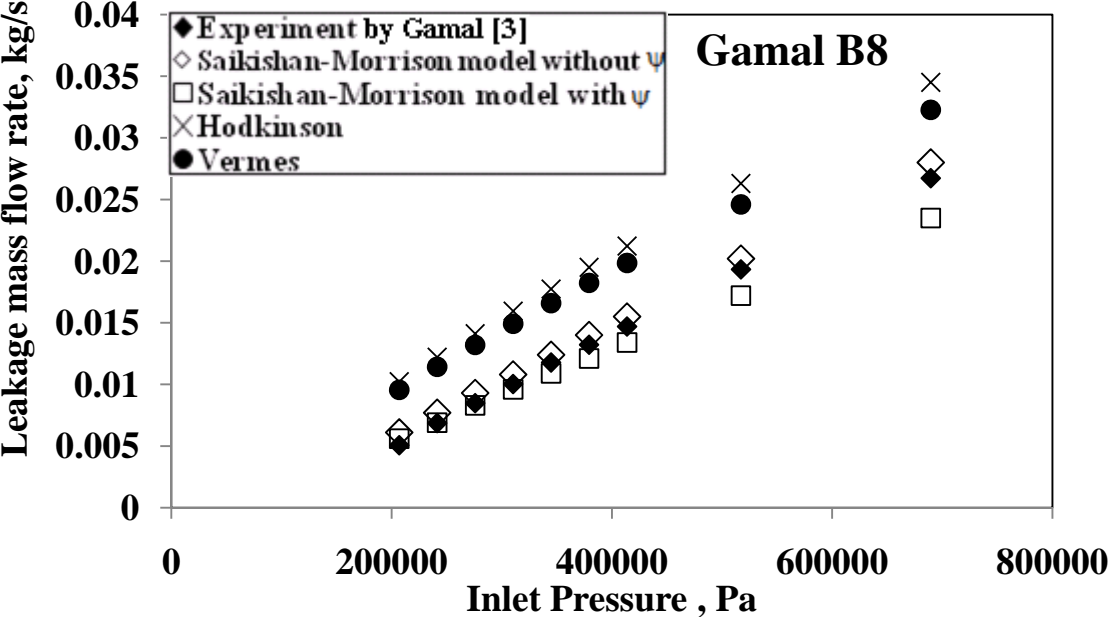


**Figure 8.12. Comparison of predicted leakage rates with Gamal's experimental data for seal B8 (c/s = 0.0064; w/s = 0.2013; h/s = 0.1572; N = 4).**
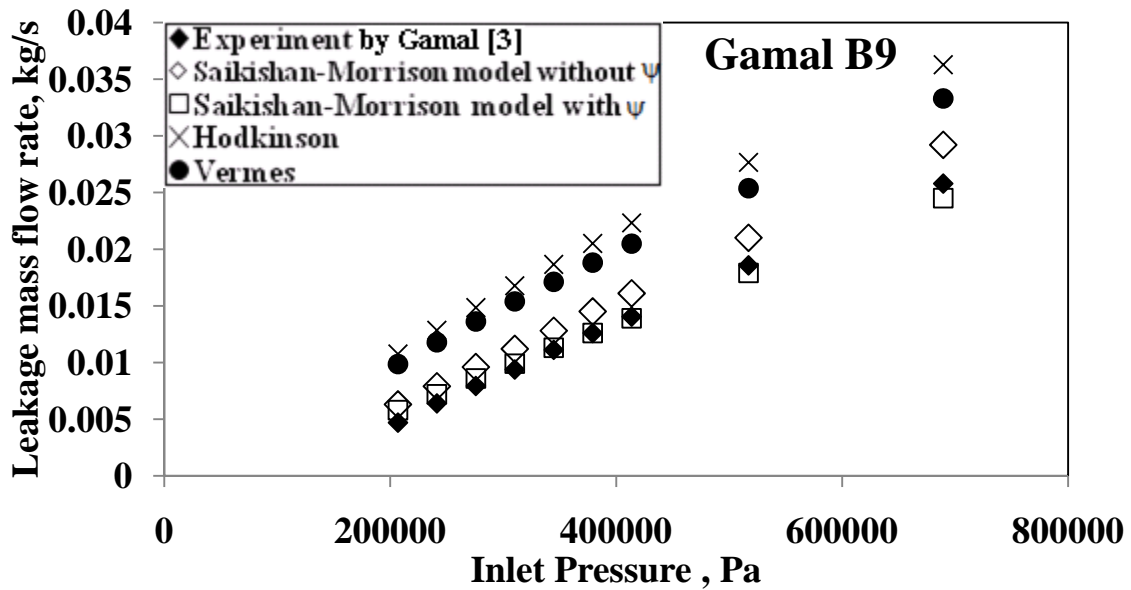
**Figure 8.13. Comparison of predicted leakage rates with Gamal's experimental data for seal B9 (c/s = 0.0106; w/s = 0.3333; h/s = 0.2604; N = 4).**
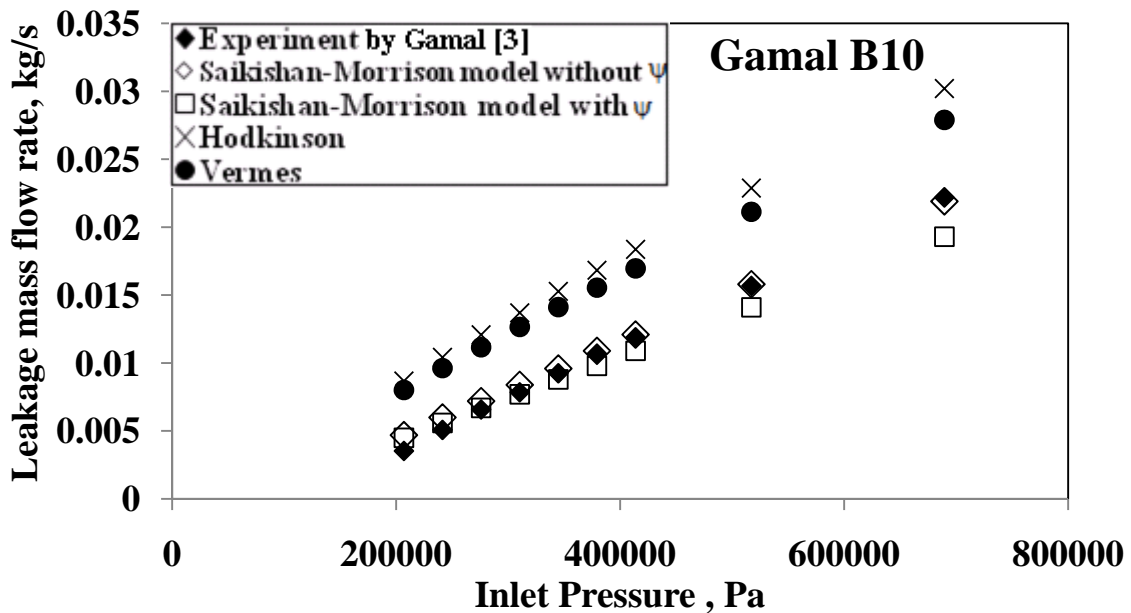


**Figure 8.14. Comparison of predicted leakage rates with Gamal's experimental data for seal B10 (c/s = 0.0064; w/s = 0.2013; h/s = 0.7987; N =6).**

90
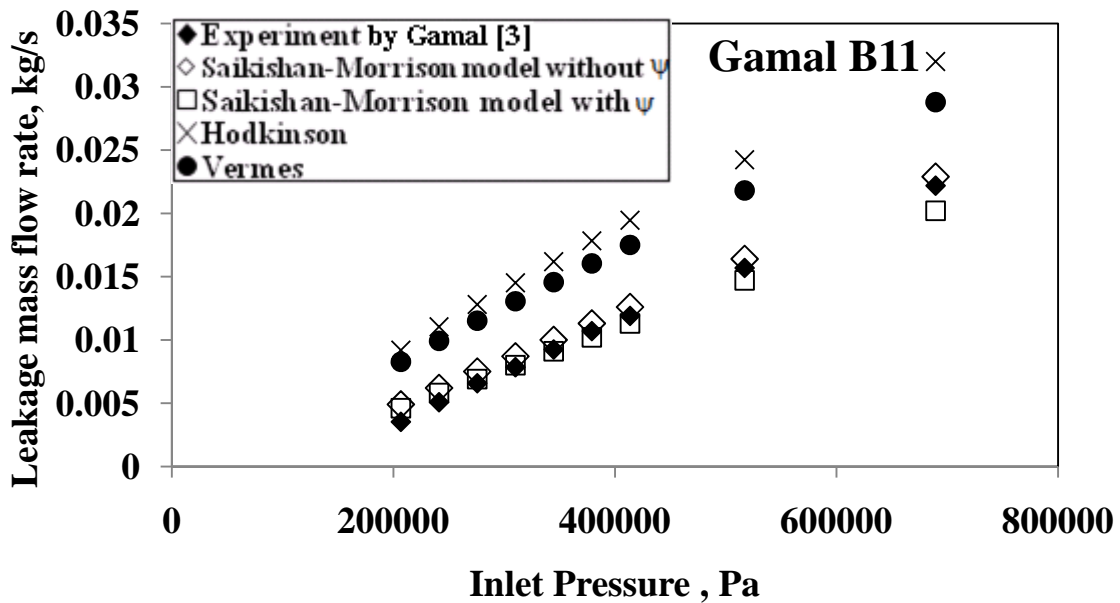


**Figure 8.15. Comparison of predicted leakage rates with Gamal's experimental data for seal B11 (c/s = 0.0106; w/s = 0.3333; h/s = 1.3229; N =6).**
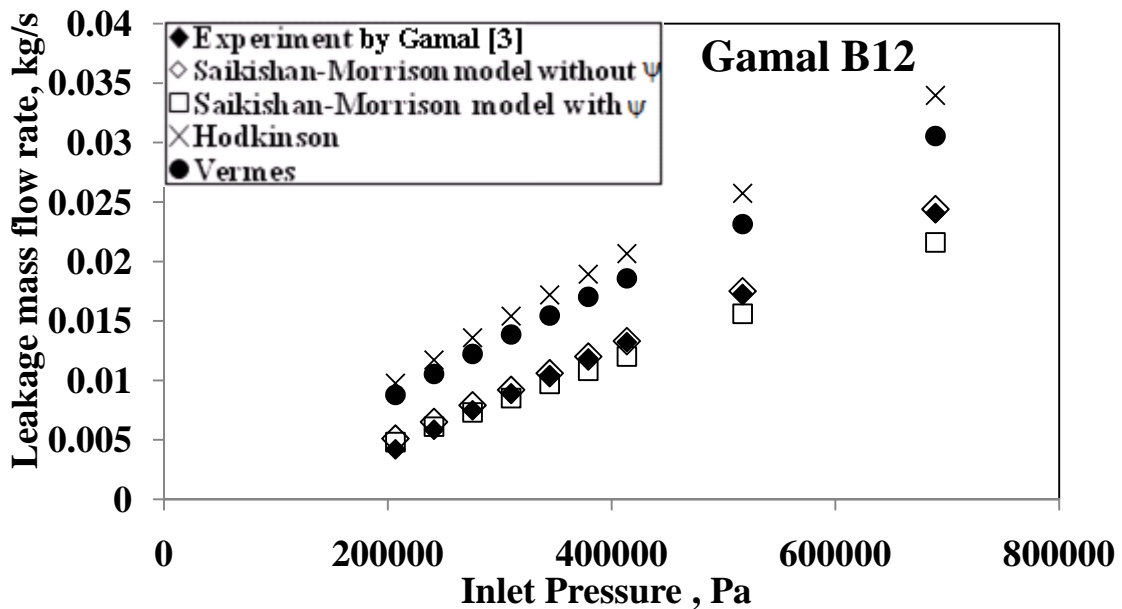


**Figure 8.16. Comparison of predicted leakage rates with Gamal's experimental data for seal B12 (c/s = 0.0159; w/s = 0.5000; h/s = 1.9844; N =6).**
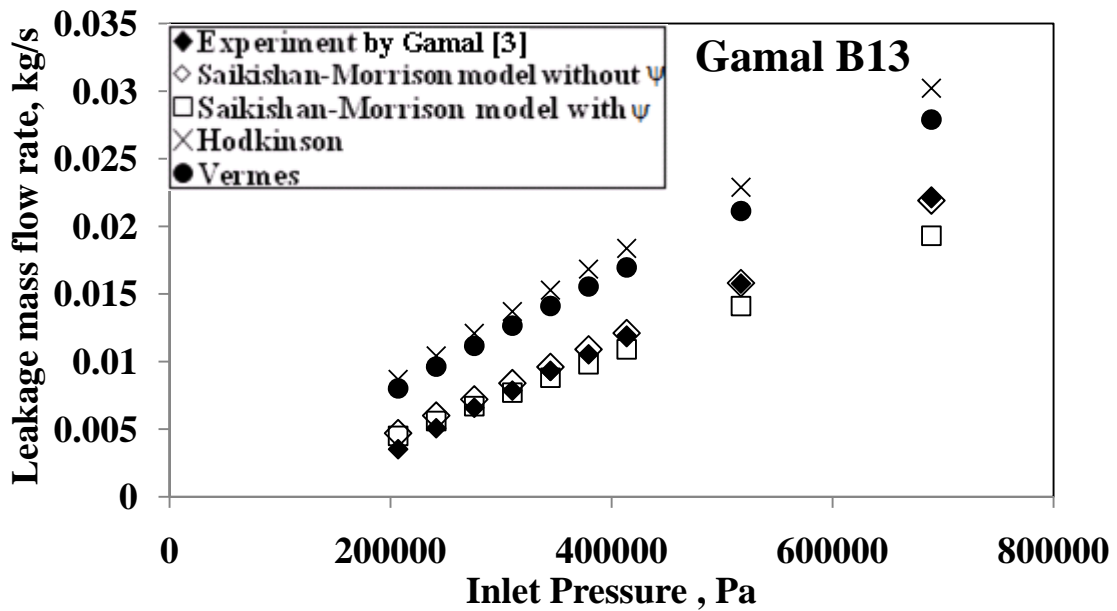
**Figure 8.17. Comparison of predicted leakage rates with Gamal's experimental data for seal B13 (c/s = 0.0064; w/s = 0.2013; h/s = 0.1572; N =6).**
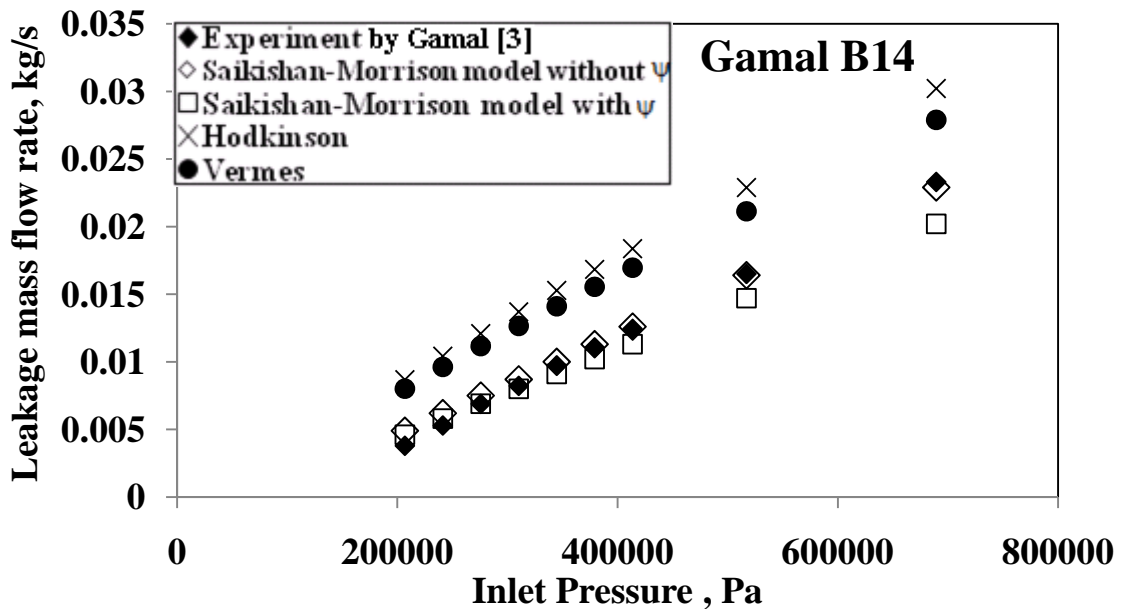


**Figure 8.18. Comparison of predicted leakage rates with Gamal's experimental data for seal B14 (c/s = 0.0106; w/s = 0.3333; h/s = 0.2604; N =6).**

These data fall within the operational range of the developed model, except for h/s ratios in a few cases. It can be observed from the above figures that the algorithm developed in this work has a higher accuracy of leakage prediction compared to the models given by Hodkinson and Vermes. However, the results show that the algorithm that does not incorporate the expansion factor ($\psi = 1$, but still allows for change in density with pressure), fits the experimental data better especially in case of the six tooth labyrinth seals (B10-B14). This could be due to the fact that the inlet pressures used were not high enough to cause sufficiently pressure ratios across individual teeth. It could also be an indication that the linear model for $\psi$ is not accurate at pressure ratios close to 1 and hence it is recommended to use the model with $\psi = 1$ for higher pressure ratios.

**VALIDATION AGAINST PICARDO'S EXPERIMENTAL DATA**

Picardo [26] conducted leakage tests on labyrinth seals with air at high pressure. His experiments were performed on two seals which had different clearances. Their respective c/s ratios were 0.0439 and 0.022 (detailed geometry provided in Appendix D). The inlet pressure for all the tests were 70 bar while overall pressure ratios ranged from 0.1 to 0.5. The Reynolds number range for seal A was 62500-69500, while that of seal B was 31700 – 36400, well outside the maximum Reynolds number used to develop the current model.

Gamal [3] performed a detailed evaluation of a number of existing leakage equations by comparing their prediction to Picardo's experimentally measured mass flow rate.

This section extends Gamal's analysis by adding the model developed in this thesis. Figure 8.19 compares the prediction error of various leakage equations for each of the different tests conducted by Picardo.
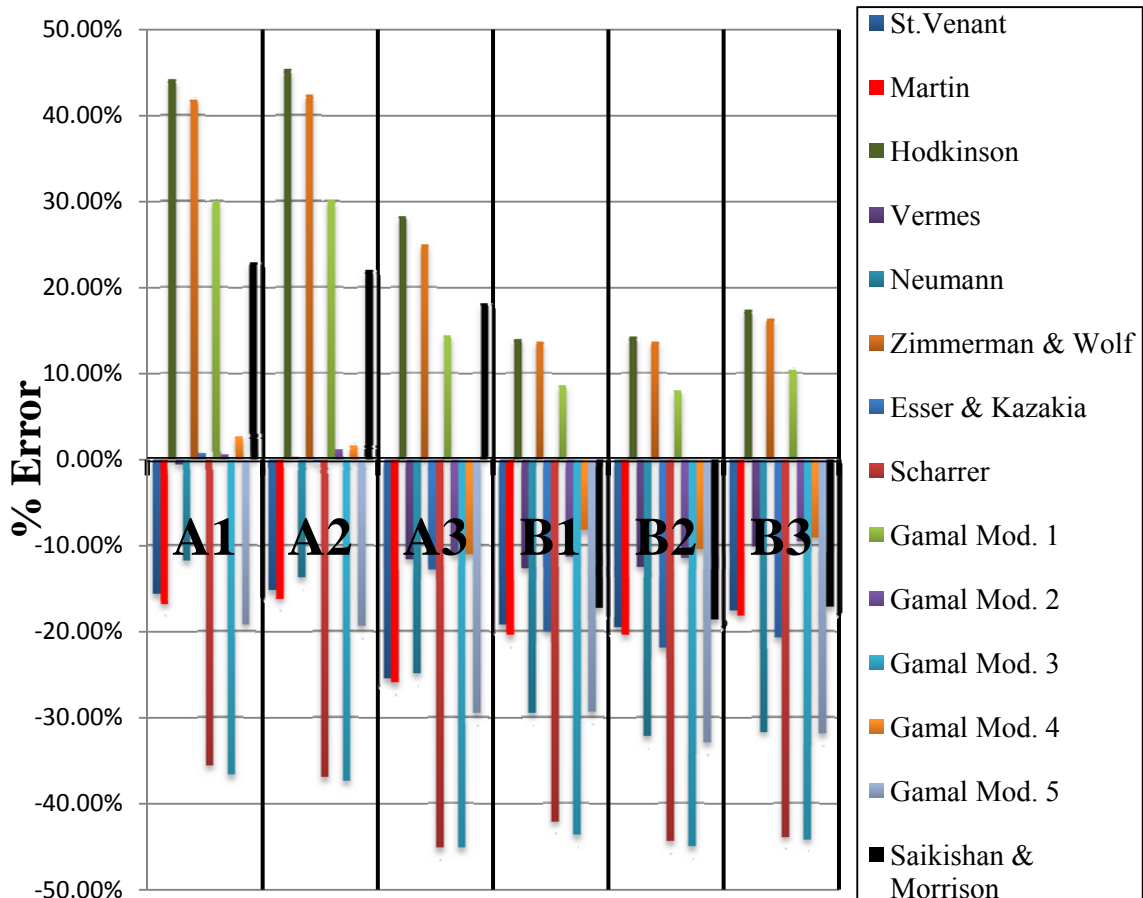


**Figure 8.19. Comparison of accuracy of leakage prediction of different models for Picardo's experimental data [26].**

It can be seen that the prediction of the model presented in this thesis is within 25% of the experimental value. While it is outperformed by some models like the Vermes' model and Gamal's Mod 4 for this specific set of conditions, it is more accurate than many of the other leakage models.  It has to be noted that w/c is 1.27 for A1, A2

and A3 and 2.54 for B1, B2 and B3. This is less than 2.67, which is the minimum of the range for which this model has been developed. The c/s for A1, A2 and A3 is 0.0439, which is also marginally outside the desired range for this model. The Reynolds numbers encountered in this data are also much higher than the maximum Reynolds number used in the simulations.

# CHAPTER IX

# SUMMARY AND RECOMMENDED FUTURE STUDY

The following section summarizes the motivation, methodology and findings of this Thesis

## MOTIVATION

Accurate determination of leakage rate through labyrinth seals is essential for performance and rotodynamic study of turbomachinery. An earlier study conducted by Morrison and Adnan Al-Ghasem [1] on windback seals showed a possibility of flow dependence of kinetic energy carry over. This finding led to the question whether the kinetic energy coefficient for labyrinth seals is a function of flow conditions. This question is the motivation behind this research, as none of the widely used leakage models accounted for this effect. The inability of the existing models to provide accurate leakage prediction for all operating conditions and the expense of running a CFD code for leakage prediction for every geometry and flow condition necessitates a model that can provide accurate leakage prediction which this study attempts to develop.

## METHODOLOGY

Simulations performed using the commercial CFD code FLUENT were used to generate data for this study. The Standard k-ε model with enhanced wall function was employed in accordance with evaluations performed by earlier studies. A number of simulations were performed on flow through rectangular cavities (representing tooth on

stator straight through labyrinth seals with flat teeth) by changing geometry and operating conditions. Tecplot 360 was used to analyze the flow field within the cavity.

**FINDINGS**

CARRY OVER COEFFICIENT

The carry over coefficient based on the jet divergence angle was found to change with flow parameters, when seal geometry was fixed, contradicting earlier models, which express the carry over coefficient purely as a function of seal geometry. It was found that, for incompressible flow, the Reynolds number based on clearance was the only flow parameter that influenced the carry over coefficient. $\gamma$ was found to remain constant with respect to changes in operating pressures, density or viscosity of the fluid as long as the Reynolds number was fixed. Based on the simulations for various seal geometries and operating conditions, it was found that the $\gamma$-Re relationship was mainly a function of clearance to pitch ratio of the seal and a model was developed using a power law curve fit.  Tooth height (provided the cavity depth is greater than three-fourths of the tooth pitch), shaft diameter, number of teeth and shaft rotation had no influence on the $\gamma$-Re relationship, while tooth width had a secondary effect which was incorporated into the model.

DISCHARGE COEFFICIENT

The discharge coefficient for incompressible flow through a seal with single tooth (no cavity), $C_d^{1tooth}$, was found to depend only on Reynolds number (based on clearance) and tooth width to clearance ratio and a model for the same was developed.

The discharge coefficient of the first tooth in a multiple tooth labyrinth seal was found to be identical to the discharge coefficient of a seal with single tooth implying that flow downstream had negligible effect on the discharge coefficient. While the discharge coefficients of subsequent teeth were identical to each other, they were found to be different to that of the first tooth as they were affected by the kinetic energy carry over. It was found that, $C_d$, the discharge coefficient of a downstream tooth, can be expressed as a function of only the carry over coefficient of the preceding cavity and the discharge coefficient of the equivalent seal with single tooth. Expressing $C_d/C_d^{1tooth}$ as a function of $\gamma$, collapses the data into a single relationship for all geometry and flow conditions. This is perhaps the most significant finding of this research. Using the models developed for $\gamma$ and $C_d$, an algorithm and a MATLAB code based on the same for leakage prediction for incompressible flow through straight through labyrinth seals with flat tooth was developed.

## EFFECT OF COMPRESSIBILITY

The expansion factor, $\psi$, which is the ratio of the discharge coefficient of flow of an ideal gas to the discharge coefficient for an incompressible fluid for the same tooth at the same Reynolds number, was found to be a linear function of pressure ratio across the tooth. Further, the expansion factor was found to be independent of Reynolds number, seal dimensions, inlet and exit pressures for a given ideal gas and for a given pressure ratio across the tooth. The expansion factor had a mild dependence on the ratio of specific heats, k. While the $\psi$- Pr relationship for $CO_2$ (k = 1.3) was very similar to that

of air (k = 1.4), a slight deviation in the slope was observed for He (k = 1.67). However this effect is not included in the model. By incorporating the model for $\psi$, a leakage prediction algorithm for compressible flows and a MATLAB code for the same were developed.

VALIDATION

The algorithm for leakage prediction was validated against prior experimental data. The incompressible model was used to predict the mass flow rates for experiments conducted by Yamada [24] as well as for the leakage tests performed by Nikitin and Ipatov [25]. The model performed reasonably well within its limits of c/s, w/s, w/c and h/s ratios.

The compressible algorithms, with and without the model for $\psi$, were compared with data from Gamal's experiments [3] which contain a matrix of pitches, tooth widths, heights and inlet pressures. It was found that the algorithm without the expansion factor performs better than the one with $\psi$, mainly due to the low tooth pressure ratios. The model is significantly more accurate than the models proposed by Hodkinson [8] and Vermes [9]. The model predicted the leakage for Picardo's seals [26] with maximum deviation within 25%. The geometries in this case were marginally outside the range of geometries used in the simulation from which the model was developed, while the Reynolds numbers exceeded the model's maximum value by factors of two and three.

**RECOMMENDED FUTURE WORK**

1. There are certain limits of dimensions for which the model developed in this thesis can provide accurate prediction. The major limits are: c/s ratio should be less than 0.05 and h/s ratio should be close to or greater than 1. While these limits apply to most labyrinth seals used today, seals used for some large turbomachinery have a higher operating clearance and this model is not applicable to such cases. Developing a new model or modifying the model developed in this work to accommodate larger clearances and shallower cavities would require many more simulations and was considered beyond the scope of the current study. The same can be said about higher Reynolds numbers. However, this could be a probable future work.

2. The ideal gas model used in this work for the study of effects of compressibility might not be valid at high operating pressures. In certain applications, like $CO_2$ compressors, labyrinth seals are subjected to such high operating pressures. Therefore it is recommended to study the validity of, and if required modification of the current model, using a real gas equation of state and at high pressures.

3. This model is limited to tooth on stator, straight through labyrinth seals with rectangular cavities and unbeveled teeth. It is recommended to study the effects of cavity shapes, beveled teeth, staggered and tooth on rotor designs using a similar approach as presented in this thesis.

4.  This model has been validated against some of the experimental data with reasonably good results. However more experimental studies and exhaustive validation is recommended.

# REFERENCES

1. Morrison, G.L. and Al-Ghasem, A., 2007, "Experimental and Computational Analysis of a Gas Compressor Windback Seal," GT2007-27986, *Proceedings of ASME Turbo Expo 2007*, Montreal, Canada, May 14-17.

2. Cogan, K.C., 1982, " Leakage Prediction of Incompressible Fluids in Labyrinth Seals," M.S. thesis. Texas A&M University, College Station.

3. Gamal, A.M., 2007, " Leakage and Rotodynamic Effects of Pocket Damper Seals and See-Through Labyrinth Seals," Ph.D. dissertation. Texas A&M University, College Station.

4. Martin, H., 1908, "Labyrinth Packings," Engineering, pp. 35-36.

5. Stodola, A. ,1927, *Steam and Gas Turbines*, 6$^{th}$ ed., The McGraw-Hill Book Company, New York.

6. Gercke, M., 1934, "Flow through Labyrinth Packing," Mechanical Engineer, **56**, pp. 678-680.

7. Egli, A. , 1935, "The leakage of Steam through Labyrinth Seals,", Trans. ASME, **57**, pp 115-122.

8. Hodkinson, B., 1939, "Estimation of the Leakage through a Labyrinth Gland," Proceedings of the Institution of Mechanical Engineers **141**, pp. 283–288.

9. Vermes, G., 1961, "A Fluid Mechanics Approach to the Labyrinth Seal Leakage Problem," ASME Transactions - Journal of Engineering for Power, **83** (2), pp. 161-169.

10. Childs, D. W., 1993, *Turbomachinery Rotordynamics – Phenomena, Modeling, and Analysis*, John Wiley & Sons, New York.

11. Gurevich, M. I., 1965, *Theory of Jets in an Ideal Fluid*, Translated by Street, R. L. and Zagustin, K., Academic Press, New York.

12. Zimmerman, H. and Wolff, K. H., 1987, "Comparison between Empirical and Numerical Labyrinth Flow Correlations," ASME 87-GT-86.

13. Vennard, J. K. and Street, R. L., 1982, *Elementary Fluid Mechanics*, John Wiley & Sons, New York.

14. Scharrer, J., 1988, "Theory Versus Experiment for the Rotordynamic Coefficient of Labyrinth Gas Seals: Part I – A Two Control Volume Model," Journal of Vibration, Acoustics, Stress and Reliability in Design, **110**, pp. 270-280.

15. Esser, D. and Kazakia, J. Y., 1995, "Air Flow in Cavities of Labyrinth Seals," International Journal of Engineering Science, **33** (15), pp. 2309-2326.

16. FLUENT 6.3.26 User's Guide, Fluent Inc., Lebanon, NH, USA.

17. Johnson M.C., 1989, "Development of a 3-D Laser Doppler Anemometry System With Measurements in Annular and Labyrinth Seals," Ph.D. dissertation. Texas A&M University, College Station.

18. Rhode, D.L. and Hibbs,R.I., 1993, " Clearance Effects on Corresponding Annular and Labyrinth Seal Flow Leakage Characteristics," Journal of Tribology, **115**, pp 699 – 704.

19. Moore, J. J., 2003, "Three-Dimensional CFD Rotordynamic Analysis of Gas Labyrinth Seals," Journal of Vibration and Acoustics, **125** (4), pp. 427-433.

20. Vakili, A.D., Meganathan, A.J., Michaud, M.A., Radhakrishnan, S., 2005, "An Experimental and Numerical Study of Labyrinth Seal Flow", GT2005-68224, *Proceedings of ASME Turbo Expo 2005*, Reno-Tahoe, Nevada, USA , June 6-9.

21. Wittig S., Schelling, U., Kim, S., and Jacobsen, K., 1987, "Numerical Predictions and Measurements of Discharge Coefficients in Labyrinth Seals," ASME 87-GT-188.

22. Kearton, W. J. and Keh, T. H., 1952, "Leakage of Air through Labyrinth Glands of Staggered Type," Institution of Mechanical Engineers Proceedings, **166** (2), pp. 180-188.

23. Waschka W., Wittig S., Kim  S., 1992, "Influence of High Rotational Speeds on the Heat Transfer and Discharge Coefficients in Labyrinth Seals", ASME Journal of Turbomachinery, **114**, pp. 462–468.

24. Yamada, Y., 1962, "On the Pressure Loss of Flow between Rotating Co-Axial Cylinders with Rectangular Grooves", Bulletin of the JSME, **5** (20),  pp 642-651.

25. Nikitin, G.A., and Ipatov, A.M., 1973, " Design of Labyrinth Seals in Hydraulic Equipment, " Russian Engineering Journal, **53** (10),  pp. 26-30.

26. Picardo, A. M., 2003, "High Pressure Testing of See-Through Labyrinth Seals," M.S. thesis, Mechanical Engineering Department, Texas A&M University, College Station.

27. Pope, S.B., 2000, *Turbulent Flows*, Cambridge University Press, Cambridge, U.K.

## APPENDIX A

**STANDARD k – ε TURBULENCE MODEL**

A detailed discussion on fundamentals of turbulent flows and turbulence modeling can be found in many standard textbooks [27]. Turbulent flows have fluctuating velocity fields. Transition of laminar flow to turbulence occurs when the Reynolds number, which is a bifurcation parameter, exceeds a critical value (which depends on geometry). The non-linearity of the Navier Stokes equations, which describe fluid flow, causes the disturbances in the flow field to grow, when the Reynolds number exceeds the critical value. This can be understood from the Orr- Sommerfeld equation and the stability diagram. The instability results in chaos, which is physically represented by fluctuating fields of velocity, pressure and temperature.

One of the ways of dealing with the issue of simulating turbulent flows is to consider the Reynolds Averaged Navier Stokes (RANS), which separate the velocity field into 'mean' and 'fluctuating' components, as Direct Numerical Simulation (DNS), in which all length and time scales are resolved, is too expensive for solving any practical problem with today's computational resources. The RANS equation (when the mean flow is steady) is shown in Cartesian index notation in equation A.1. $\overline{U}$ and $u'$ represent the mean and fluctuating part of velocity.

$$\overline{U_k}\frac{\partial \overline{\rho U_1}}{\partial x_k} = -\frac{\partial \overline{P}}{\partial x_i} + \mu\,\frac{\partial^2 \overline{U_1}}{\partial x_k\,\partial x_k} - \frac{\partial\,\overline{(\rho u_1' u_k')}}{\partial x_k} \tag{A.1}$$

The mean flow equations can be solved, provided the influence of the fluctuating component on the mean flow can be modeled. The Reynolds 'stress' tensor, expressed

by $\overline{\rho u_i' u_k'}$ , is a term that appears in the mean flow equations due to the effect of fluctuations and originates from the convective term. The mean flow of the turbulent flow behaves in a similar manner to the laminar flow of a fluid with a strain dependent viscosity. Hence the Reynolds 'stresses' can be modeled using a 'turbulent viscosity' , $\mu_t$ , as to arrive at equation A.2.

$$\overline{U_k}\frac{\partial \overline{\rho U_i}}{\partial x_k} = -\frac{\partial \overline{P}}{\partial x_i} + (\mu + \mu_t)\frac{\partial^2 \overline{U_i}}{\partial x_k\, \partial x_k} \tag{A.2}$$

The k-ε model is a two equation model in which the turbulent viscosity is expressed as a function of the turbulent kinetic energy, κ and dissipation, ε

$$\mu_t = \rho C_\mu \frac{\kappa^2}{\varepsilon} \tag{A.3}$$

Where the turbulent kinetic energy and dissipation are statistics of the fluctuating component of the velocity and are defined as

$$\kappa = \frac{1}{2}\overline{u_i' u_i'} \tag{A.4}$$

$$\varepsilon = \frac{\mu}{\rho}\overline{\left(\frac{\partial u_i'}{\partial x_k}\frac{\partial u_i'}{\partial x_k}\right)} \tag{A.5}$$

and $C_\mu$ is a constant with a standard value of 0.09.

But since the exact closure equations for κ and ε are not known, the standard k-ε model utilizes the following model transport equations. The model for κ (A.6) is based on the exact equation, while the model for ε (A.7) is purely empirical. While, it is possible to derive the exact equation for dissipation, it is not considered useful as explained by Pope [27].

$$\frac{\partial(\rho\kappa)}{\partial t} + \frac{\partial(\rho\kappa u_j)}{\partial x_j} = \frac{\partial}{\partial x_j}\left[\left(\mu + \frac{\mu_t}{\sigma_k}\right)\frac{\partial\kappa}{\partial x_j}\right] + G_k + G_b - \rho\varepsilon - Y_M + S_k \tag{A.6}$$

$$\frac{\partial(\rho\varepsilon)}{\partial t} + \frac{\partial(\rho\varepsilon u_j)}{\partial x_j} = \frac{\partial}{\partial x_j}\left[\left(\mu + \frac{\mu_t}{\sigma_\varepsilon}\right)\frac{\partial\varepsilon}{\partial x_j}\right] + C_{1\varepsilon}\frac{\varepsilon}{k}(G_k + C_{3\varepsilon}G_b) - C_{2\varepsilon}\,\rho\frac{\varepsilon^2}{k} + S_\varepsilon \tag{A.7}$$

Where

$G_k$ is the production of $\kappa$ and is modeled as $2\mu_t\frac{\partial\overline{U_1}}{\partial x_j}\frac{\partial\overline{U_1}}{\partial x_j}$.

$G_b$ represents generation of $\kappa$ due to buoyancy.

$Y_M$ represents compressibility effects on turbulence and is modeled as $2\rho\varepsilon\frac{\kappa}{kRT}$.

$S_k$ and $S_\varepsilon$ are user defined source terms.

$\sigma_k$ and $\sigma_\varepsilon$ are the turbulent Prandtl numbers for $\kappa$ and $\varepsilon$, and have default values of 1.0 and 1.3 respectively.

$C_{1\varepsilon}$ and $C_{2\varepsilon}$ are constants with default values of 1.44 and 1.92.

In this thesis, the default values are used.

The k-ε can be used only for modeling turbulence away from the wall. Hence to model wall bounded turbulent flows as in the case of simulating labyrinth seals, wall functions must be employed near the wall.

**FINITE VOLUME METHOD**

The Finite Volume Method is a numerical technique for solving partial differential equations. As with other discretization techniques like finite difference and finite element methods, it reduces partial differential equations with a set of boundary conditions into a system of algebraic equations that can be solved by a computer to provide an approximate solution. It works by dividing the computational domain into a number of finite control volumes and by solving the conservation equations for each control volume. The control volumes are constructed around each node point in the grid. Discretization using the finite volume method can be illustrated by considering the unsteady 2-D transport equation for a scalar quantity, $\phi$

$$\int_V \frac{\partial \rho \phi}{\partial t}\, dV + \oint \rho \phi \vec{v} \cdot d\vec{A} = \oint \Gamma_\phi \nabla \phi \cdot d\vec{A} + \int_V S_\phi\, dV \qquad \text{(A.8)}$$

where

| | | |
|---|---|---|
| $\rho$ | = | density |
| $\vec{v}$ | = | velocity vector |
| $\vec{A}$ | = | surface area vector |
| $\Gamma_\phi$ | = | diffusion coefficient for $\phi$ |
| $\nabla \phi$ | = | gradient of $\phi$ |
| $S_\phi$ | = | source of per unit volume of $\phi$ |

$$\frac{\partial \rho \phi}{\partial t} V + \sum_{f}^{N_{\text{faces}}} \rho_f \vec{v}_f \phi_f \cdot \vec{A}_f = \sum_{f}^{N_{\text{faces}}} \Gamma_\phi \nabla \phi_f \cdot \vec{A}_f + S_\phi V \qquad \text{(A.9)}$$

where

| | | |
|---|---|---|
| $N_{\text{faces}}$ | = | number of faces enclosing cell |
| $\phi_f$ | = | value of $\phi$ convected through face f |
| $\rho_f \vec{v}_f \cdot \vec{A}_f$ | = | mass flux through the face f |
| $\vec{A}_f$ | = | area of face f |
| $\nabla \phi_f$ | = | gradient of $\phi$ at face f |
| $V$ | = | cell volume |

Equation A.9 is applied to every face in the computational domain and is solved iteratively.

# APPENDIX B

**Table.B.1. Seal geometries used for simulation**

| Case # | No. of Teeth | Clearance (mm) | Pitch (mm) | Tooth Width (mm) | Tooth Height (mm) | Shaft Diameter (mm) |
|--------|--------------|----------------|------------|------------------|-------------------|---------------------|
| 1 | 2 | 0.03 | 4 | 0.03 | 4 | 60 |
| 2 | 2 | 0.06 | 4 | 0.03 | 4 | 60 |
| 3 | 2 | 0.09 | 4 | 0.03 | 4 | 60 |
| 4 | 2 | 0.15 | 4 | 0.03 | 4 | 60 |
| 5 | 2 | 0.06 | 8 | 0.03 | 8 | 60 |
| 6 | 2 | 0.06 | 4 | 0.03 | 3 | 60 |
| 7 | 2 | 0.06 | 4 | 0.03 | 8 | 60 |
| 8 | 2 | 0.06 | 4 | 0.03 | 16 | 60 |
| 10 | 2 | 0.06 | 4 | 0.2 | 4 | 60 |
| 11 | 2 | 0.06 | 4 | 0.4 | 4 | 60 |
| 12 | 2 | 0.06 | 4 | 0.6 | 4 | 60 |
| 13 | 2 | 0.06 | 4 | 1 | 4 | 60 |
| 14 | 2 | 0.06 | 4 | 2 | 4 | 60 |
| 15 | 2 | 0.03 | 4 | 1 | 4 | 60 |
| 16 | 2 | 0.09 | 4 | 1 | 4 | 60 |
| 17 | 2 | 0.15 | 4 | 1 | 4 | 60 |
| 18 | 2 | 0.15 | 4 | 2 | 4 | 60 |
| 19 | 2 | 0.06 | 4 | 0.03 | 4 | 180 |
| 20 | 2 | 0.06 | 4 | 0.03 | 4 | 300 |
| 21 | 8 | 0.06 | 4 | 0.03 | 4 | 60 |
| 22 | 1 | 0.03 | - | 0.2 | 4 | 60 |
| 23 | 1 | 0.06 | - | 0.4 | 4 | 60 |
| 24 | 1 | 0.09 | - | 0.6 | 4 | 60 |
| 25 | 1 | 0.15 | - | 1 | 4 | 60 |
| 26 | 1 | 0.03 | - | 0.4 | 4 | 60 |
| 27 | 1 | 0.15 | - | 2 | 4 | 60 |
| 28 | 1 | 0.03 | - | 0.6 | 4 | 60 |
| 29 | 1 | 0.03 | - | 1 | 4 | 60 |
| 30 | 1 | 0.06 | - | 2 | 4 | 60 |
| 31 | 1 | 0.03 | - | 2 | 4 | 60 |
| 32 | 1 | 0.06 | - | 0.4 | 3 | 60 |
| 33 | 1 | 0.06 | - | 0.4 | 8 | 60 |
| 34 | 1 | 0.06 | - | 0.4 | 4 | 180 |

| Case # | No. of Teeth | Clearance (mm) | Pitch (mm) | Tooth Width (mm) | Tooth Height (mm) | Shaft Diameter (mm) |
|--------|--------------|----------------|------------|------------------|-------------------|---------------------|
| 35 | 2 | 0.03 | 4 | 0.2 | 4 | 60 |
| 36 | 2 | 0.09 | 4 | 0.6 | 4 | 60 |
| 37 | 4 | 0.06 | 4 | 1 | 4 | 60 |
| 38 | 2 | 0.06 | 4 | 0.4 | 8 | 60 |
| 39 | 2 | 0.03 | 4 | 0.4 | 4 | 60 |
| 40 | 2 | 0.06 | 4 | 0.4 | 4 | 180 |

## APPENDIX C

**MATLAB CODE FOR LEAKAGE PREDICTION (for incompressible flow)**

```
c = input('Enter radial clearance in m : ');
s = input('Enter tooth pitch in m: ');
w = input('Enter tooth width in m: ');
R = input('Enter shaft radius in m: ');
N = input('Enter number of teeth : ');
Pi = input('Enter seal inlet pressure in Pa: ');
Pe = input('Enter seal exit pressure in Pa: ');
rho= input('Enter density in kg/m^3 : ');
mu = input('Enter dynamic viscosity in PaS : ');;
A = 2*3.142*R*c;
p = ones(1,N+1); p(1) = Pi; p(N+1) = Pe;
mdot = 0.1*A*sqrt((Pi-Pe)*rho);
error=1;
for i=1:10000
   Re = mdot/(3.142*2*R*mu);
   gamma =((1-6.5*(c/s))- 8.638*(c/s) *(w/s))*(Re+((1-6.5*(c/s))- 8.638*(c/s) *(w/s))^(-
1/(2.454*(c/s)+2.258*(c/s)*(w/s)^1.673)))^(2.454*(c/s)+2.258*(c/s)*(w/s)^1.673);
   cd1  =(1.097-0.0029*w/c)*(1+(44.86*w/c)/Re)^(-0.2157)/sqrt(2);
   tdc  =cd1*0.925*gamma^.861;
   p(2) = p(1)-(mdot/A)^2/(2*cd1^2*rho);

      for j = 2:N-1
      p(j+1) =p(j)-(mdot/A)^2/(2*tdc^2*rho);
      end
   mdot1 = A* tdc*sqrt(2*(rho*(p(N)-p(N+1))));
   error = abs((mdot1-mdot)/mdot);
   mdot=(mdot1-mdot)*0.1+mdot;
   if(error<0.0001)
      break;
   end
end
display('leakage rate in kg/s is : ');
mdot
display('The pressure distribution is (in Pa) : ');
p
```

**MATLAB CODE FOR LEAKAGE PREDICTION (for air; without ψ)**

```
c = input('Enter radial clearance in m : ');
s = input('Enter tooth pitch in m: ');
w = input('Enter tooth width in m: ');
R = input('Enter shaft radius in m: ');
N = input('Enter number of teeth : ');
Pi = input('Enter seal inlet pressure in Pa: ');
Pe = input('Enter seal exit pressure in Pa: ');
T= input('Enter exit temperature in K : ');
mu =0.0000179; Rg=287;
A = 2*3.142*R*c;
p = ones(1,N+1); p(1) = Pi; p(N+1) = Pe; rho(1)=p(1)/(Rg*T);
mdot = 0.1*A*sqrt((Pi-Pe)*rho(1));
error=1;
for i=1:10000
   Re = mdot/(3.142*2*R*mu);
   gamma =((1-6.5*(c/s))- 8.638*(c/s) *(w/s))*(Re+((1-6.5*(c/s))- 8.638*(c/s) *(w/s))^(-
1/(2.454*(c/s)+2.258*(c/s)*(w/s)^1.673)))^(2.454*(c/s)+2.258*(c/s)*(w/s)^1.673);
   cd1  =(1.097-0.0029*w/c)*(1+(44.86*w/c)/Re)^(-0.2157)/sqrt(2);
   tdc  =cd1*0.925*gamma^.861;
   p(2) = p(1)-(mdot/A)^2/(2*cd1^2*rho(1));
   rho(2)=p(2)/(Rg*T);
   for j = 2:N-1
      p(j+1) =p(j)-(mdot/A)^2/(2*tdc^2*rho(j));
      rho(j+1)=p(j+1)/(Rg*T);
   end
   mdot1 = A*tdc*sqrt(2*(rho(N)*(p(N)-p(N+1))));
   error = abs((mdot1-mdot)/mdot);
   mdot=(mdot1-mdot)*0.1+mdot;
   if(error<0.0001)
      break;
   end
end
display('leakage rate in kg/s is : ');
mdot
display('The pressure distribution is (in Pa) : ');
p
```

**MATLAB CODE FOR LEAKAGE PREDICTION (for air)**

```
c = input('Enter radial clearance in m : ');
s = input('Enter tooth pitch in m: ');
w = input('Enter tooth width in m: ');
R = input('Enter shaft radius in m: ');
N = input('Enter number of teeth : ');
Pi = input('Enter seal inlet pressure in Pa: ');
Pe = input('Enter seal exit pressure in Pa: ');
T= input('Enter exit temperature in K : ');
mu =0.0000179; Rg=287;
A = 2*3.142*R*c;
p = ones(1,N+1); p(1) = Pi; p(N+1) = Pe; rho(1)=p(1)/(Rg*T);
mdot = 0.1*A*sqrt((Pi-Pe)*rho(1));
error=1;
Y=ones(1,N);
for i=1:10000
   Re = mdot/(3.142*2*R*mu);
   gamma =((1-6.5*(c/s))- 8.638*(c/s) *(w/s))*(Re+((1-6.5*(c/s))- 8.638*(c/s) *(w/s))^(-
1/(2.454*(c/s)+2.258*(c/s)*(w/s)^1.673)))^(2.454*(c/s)+2.258*(c/s)*(w/s)^1.673);
   cd1  =(1.097-0.0029*w/c)*(1+(44.86*w/c)/Re)^(-0.2157)/sqrt(2);
   tdc  =cd1*0.925*gamma^.861;
   p(2) = p(1)-(mdot/A)^2/(2*Y(1)^2*cd1^2*rho(1));
   Y(1)=0.558+0.442*(p(2)/p(1));
   rho(2)=p(2)/(Rg*T);
   for j = 2:N-1
      p(j+1) =p(j)-(mdot/A)^2/(2*Y(j)^2*tdc^2*rho(j));
      rho(j+1)=p(j+1)/(Rg*T);
      Y(j)= 0.558+0.442*(p(j+1)/p(j));
   end
   Y(N)= 0.558+0.442*(p(N+1)/p(N));
   mdot1 = A*Y(N)*tdc*sqrt(2*(rho(N)*(p(N)-p(N+1))));
   error = abs((mdot1-mdot)/mdot);
   mdot=(mdot1-mdot)*0.1+mdot;
   if(error<0.0001)
      break;
   end
end
display('leakage rate in kg/s is : ');
mdot
display('The pressure distribution is (in Pa) : ');
p
```

**MATLAB CODE FOR LEAKAGE PREDICTION (for any ideal gas with k ~ 1.4)**

```
c = input('Enter radial clearance in m : ');
s = input('Enter tooth pitch in m: ');
w = input('Enter tooth width in m: ');
R = input('Enter shaft radius in m: ');
N = input('Enter number of teeth : ');
Pi = input('Enter seal inlet pressure in Pa: ');
Pe = input('Enter seal exit pressure in Pa: ');
T= input('Enter exit temperature in K : ');
mu =0.0000179; Rg=287;
A = 2*3.142*R*c;
p = ones(1,N+1); p(1) = Pi; p(N+1) = Pe; rho(1)=p(1)/(Rg*T);
mdot = 0.1*A*sqrt((Pi-Pe)*rho(1));
error=1;
Y=ones(1,N);
for i=1:10000
   Re = mdot/(3.142*2*R*mu);
   gamma =((1-6.5*(c/s))- 8.638*(c/s) *(w/s))*(Re+((1-6.5*(c/s))- 8.638*(c/s) *(w/s))^(-
1/(2.454*(c/s)+2.258*(c/s)*(w/s)^1.673)))^(2.454*(c/s)+2.258*(c/s)*(w/s)^1.673);
   cd1 =(1.097-0.0029*w/c)*(1+(44.86*w/c)/Re)^(-0.2157)/sqrt(2);
   tdc =cd1*0.925*gamma^.861;
   p(2) = p(1)-(mdot/A)^2/(2*Y(1)^2*cd1^2*rho(1));
   Y(1)=0.558+0.442*(p(2)/p(1));
   rho(2)=p(2)/(Rg*T);
   for j = 2:N-1
      p(j+1) =p(j)-(mdot/A)^2/(2*Y(j)^2*tdc^2*rho(j));
      rho(j+1)=p(j+1)/(Rg*T);
      Y(j)= 0.558+0.442*(p(j+1)/p(j));
   end
   Y(N)= 0.558+0.442*(p(N+1)/p(N));
   mdot1 = A*Y(N)*tdc*sqrt(2*(rho(N)*(p(N)-p(N+1))));
   error = abs((mdot1-mdot)/mdot);
   mdot=(mdot1-mdot)*0.1+mdot;
   if(error<0.0001)
      break;
   end
end
display('leakage rate in kg/s is : ');
mdot
display('The pressure distribution is (in Pa) : ');
p
```

# APPENDIX D

**Table D.1. Seal geometries used by Yamada [24]**

| Case # | No. of Teeth | Clearance (mm) | Pitch (mm) | Tooth Width (mm) | Tooth Height (mm) |
|--------|--------------|----------------|------------|------------------|-------------------|
| 1 | 20 | 0.433 | 10 | 2.49 | 5 |
| 2 | 20 | 0.62 | 10 | 2.49 | 5 |
| 3 | 20 | 0.926 | 10 | 2.49 | 5 |
| 4 | 10 | 0.9144 | 20 | 15.03723 | 5 |
| 5 | 10 | 0.9144 | 20 | 10.05111 | 5 |
| 6 | 10 | 0.9144 | 20 | 5.066555 | 5 |
| 7 | 10 | 0.9144 | 20 | 2.563032 | 5 |
| 8 | 10 | 0.9144 | 20 | 1.066134 | 5 |

**Table.D.2. Seal geometries used by Nikitin and Ipatov [25]**

| Case # | No. of Teeth | Clearance (mm) | Pitch (mm) | Tooth Width (mm) | Tooth Height (mm) |
|--------|--------------|----------------|------------|------------------|-------------------|
| 1 | 2 | 0.045 | 1.46 | 1 | 0.5 |
| 2 | 3 | 0.045 | 1.46 | 1 | 0.5 |
| 3 | 7 | 0.045 | 1.46 | 1 | 0.5 |

**Table.D.3. Seal geometries used by Gamal [3]**

| Case # | No. of Teeth | Clearance (mm) | Pitch (mm) | Tooth width (mm) | Tooth height (mm) | Shaft diameter (mm) |
|--------|--------------|----------------|------------|------------------|-------------------|---------------------|
| B1 | 4 | 0.102 | 15.9 | 3.2 | 12.7 | 102 |
| B3 | 4 | 0.102 | 19.1 | 6.4 | 12.7 | 102 |
| B4 | 4 | 0.102 | 12.8 | 6.4 | 12.7 | 102 |
| B5 | 4 | 0.102 | 9.6 | 6.4 | 12.7 | 102 |
| B8 | 4 | 0.102 | 15.9 | 3.2 | 2.5 | 102 |
| B9 | 4 | 0.102 | 9.6 | 3.2 | 2.5 | 102 |
| B10 | 6 | 0.102 | 15.9 | 3.2 | 12.7 | 102 |
| B11 | 6 | 0.102 | 9.6 | 3.2 | 12.7 | 102 |
| B12 | 6 | 0.102 | 6.4 | 3.2 | 12.7 | 102 |
| B13 | 6 | 0.102 | 15.9 | 3.2 | 2.5 | 102 |
| B14 | 6 | 0.102 | 9.6 | 3.2 | 2.5 | 102 |

**Table.D.4. Seal geometries used by Picardo [26]**

| Case # | No. of Teeth | Clearance (mm) | Pitch (mm) | Tooth Width (mm) | Tooth Height (mm) | Shaft Diameter (mm) |
|--------|--------------|----------------|------------|------------------|-------------------|---------------------|
| A1 – A3 | 18 | 0.1 | 4.55 | 0.254 | 4.3 | 115 |
| B1- B3 | 18 | 0.2 | 4.55 | 0.254 | 4.3 | 115 |

# VITA

Saikishan Suryanarayanan is the son of Mr. Balasundaram Suryanarayanan and Mrs. Kodumudi Sugavanam Suryaprabha. He was born and brought up in the beautiful city of Chennai (Madras), Tamil Nadu, India. He completed his Bachelor of Engineering in mechanical engineering at Sri Venkateswara College of Engineering, affiliated with Anna University, Chennai, India in 2007. He came to the United States of America to pursue graduate studies in mechanical engineering at Texas A&M University, College Station, TX, in the fall of 2007. He received a Master of Science in mechanical engineering in May 2009. He wishes to pursue a career of research in fluid dynamics.

Saikishan Suryanarayanan can be contacted through Texas A&M University's Department of Mechanical Engineering at the following address:

Texas A&M University

Department of Mechanical Engineering

3123 TAMU

College Station, TX 77843 – 3123

USA.